# Manipulation of Highly Nonlinear Organic Crystals for Efficient Optical-to-THz Conversion

<u>B. J. Kang</u>[1], S.-H. Lee[2], M. Jazbinsek[3], O-P. Kwon[2], and F. Rotermund[1]

[1]Department of Physics, Korea Advanced Institute of Science and Technology (KAIST), 34141 Daejeon, South Korea,
rotermund@kaist.ac.kr
[2]Department of Molecular Science and Technology, Ajou University, 443-749 Suwon, South Korea
[3]Institute of Computational Physics, Zürich University of Applied Sciences (ZHAW), 8401 Winterthur, Switzerland

In recent years, as table-top intense coherent terahertz (THz) sources are getting more important for advanced THz sciences [1], highly nonlinear organic crystals applicable for efficient optical-to-THz conversion have been intensively investigated [2]. Nonlinear optical organic crystals exhibit great potential for intense broadband THz wave generation thanks to their large optical nonlinearities and advantageous phase-matching characteristics. In addition, compared to inorganic crystals, organic crystals are regarded as a cost-effective solution, and it is easy to fine-tune the nonlinear optical characteristics by modifying its chemical structures. However, strong re-absorption of the generated THz waves due to various phonon resonances in many organic crystals still remains as a bottleneck to be solved [3]. Thus, one key issue for developing new THz generators is not only to promote macroscopic nonlinearity to a higher level but also to suppress phonon absorption of materials located in the THz region. In this work, we present two effective approaches to substantially improve THz spectral properties based on chemical modification and tandem configuration.

In the first approach, strong secondary bonds by increasing electronegativity and mass of molecules are introduced to reduce the change of dipole moment and restrict the vibrational motions which are related to absorption in the THz frequency regime [4]. New HMQ-4TFS crystals exhibit a relatively low absorption coefficient in the THz range of 0.5-4 THz, which is attributed to suppressed molecular vibrations due to strong hydrogen-bonds as shown in Fig. 1(a). In addition, HMQ-4TFS crystals possess a very large macroscopic optical nonlinearity, comparable (or even higher) to benchmark stilbazolium crystals.

Based on the suppressed absorption coefficient and the large macroscopic nonlinearity, HMQ-4TFS crystals show superior characteristics for efficient THz wave generation. Compared to the standard inorganic ZnTe crystal, HMQ-4TFS shows excellent THz generation characteristics; up to 23 times higher peak-to-peak THz electric field and a broader spectral bandwidth (about 7 THz) than ZnTe (see Fig. 1(b)). In order to examine the influence of the strongly electronegative groups on molecular anions, THz generation characteristics are compared between analogous HMQ-4TFS and HMQ-T crystals (see Fig. 1(c) and 1(d)). Compared to a HMQ-T crystal, a HMQ-4TFS crystal exhibits a 50 % higher peak-to-peak THz electric field at the same pump pulse energy. In addition, the generated THz spectra of HMQ-T crystals show many absorption dimples, which are correlated with the position, strength and bandwidth of the phonon modes already shown in Fig. 1(a). Such higher optical-to-THz conversion efficiency with smaller number of dimples in HMQ-4TFS compared to HMQ-T crystals is attributed to the suppressed phonon modes and different phase-matching condition between optical and THz regions by change of the linear optical properties in the crystalline state.
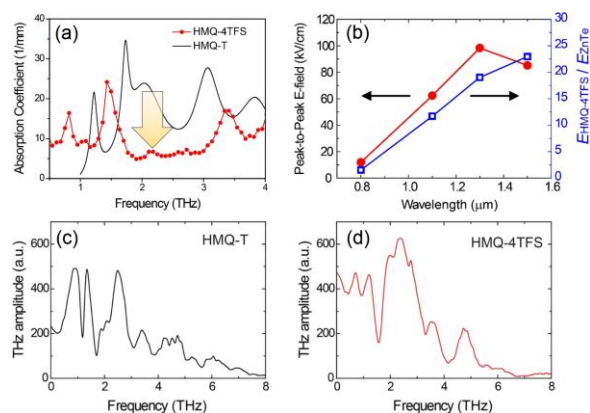


**Fig. 1.** (a) Absorption coefficient along the polar axis of HMQ-4TFS and HMQ-T crystals, (b) Peak-to-peak E-field of HMQ-4TFS crystal and the ratio of peak-to-peak THz E-field of HMQ-4TFS to ZnTe, (c) THz frequency-domain spectra generated from a HMQ-T crystal and (d) HMQ-4TFS crystal at the optical pump wavelength of 1500 nm

Another strategy is the tandem configuration realized by the orientational stacking of two different nonlinear organic crystals [5]. To achieve effective THz spectral filling, we selected two complementary organic crystals. The HMQ-TMS single crystal, which is one of representative nonlinear organic crystal, is used as a front crystal in the proposed tandem configuration, which possesses a large macroscopic nonlinearity and a broad transparency range. The remaining optical pump can further generate THz waves in the subsequent rear crystal. Since the front crystal has a strong phonon mode absorption near 1.7 THz, the rear crystal attached to the front one has to be capable to compensate for this phonon absorption. Fortunately, OH1 crystal is chosen as a suitable candidate, which shows a smooth spectrum with the peak frequency located near the phonon-induced absorption dimple of the HMQ-TMS crystal and different tendency of phase matching condition. Such a tandem structure compensates for the spectral gap of the generated THz waves caused by phonon absorption and phase mismatch.
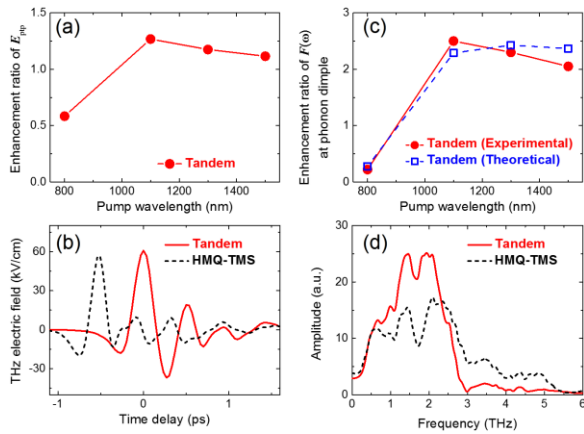
**Fig. 2.** Characteristics of THz waves generated from the organic tandem THz generator. (a) Enhancement ratio of the peak-to-peak E-field in tandem configuration as a function of pump wavelength, (b) time traces of THz E-fields generated in tandem cell and single HMQ-TMS crystal at 1100-nm pumping, (c) experimental and theoretical results of the enhancement ratio of the THz spectral component at a phonon absorption gap depending on the pump wavelength and (d) the corresponding THz spectra at 1100-nm pumping

Since the THz wave generation strongly depends on the optical characteristics of organic crystals, we performed detailed characterization of our tandem cell at different pump wavelengths. Figure 2(a) shows the enhancement ratio of the peak-to-peak electric field generated from the HMQ-TMS/OH1 tandem configuration as a function of the pump wavelength. The field enhancement compared to the single HMQ-TMS is estimated for the pump wavelength range of 1100-1500 nm. The maximum enhancement ratio is 1.3 when pumped at 1100 nm. The time traces of the THz electric field of the tandem cell and the single HMQ-TMS crystal at 1100-nm pumping are shown in Fig. 2(b). Figure 2(c) shows the spectral enhancement ratio of tandem configuration at phonon absorption region of the HMQ-TMS single crystal. At 800-nm pumping, the overall performance becomes worse and is also lower than that of the HMQ-TMS single crystal in every respect due to the large velocity mismatch that originated from the refractive index dispersion, particularly in the OH1 crystal. In the 1100-1500 nm

range, the amplitude at the phonon absorption dimple is enhanced with a considerable spectral improvement near 1.7 THz. The spectral component at the phonon mode resonance of HMQ-TMS increases by more than 2 times. The maximum enhancement ratio is 2.5 at 1100 nm and the corresponding THz spectrum is depicted in Fig. 2(d). The results agree well with the theoretical prediction. The THz spectral bandwidth of the tandem cell is slightly narrowed compared to the single HMQ-TMS crystals due to the absorption peak of the rear OH1 crystal near 3 THz.

To summarize, chemical modification and tandem configuration of organic crystals provide a very promising design strategy to manipulate optical-to-THz conversion. Conversion efficiency and spectral property can be further improved by proper combination to suppress various phonon absorptions as well as optimized phase-matching condition. As a powerful design tool, the proposed methods will contribute to development of intense broadband coherent THz sources.

### References

1. *Tonouchi, M.* Cutting-edge THz technology // Nat. Photonics 2007. V. 1, No. 2. P. 97-105.

2. *Shalaby, M., Hauri, C. P.* Demonstration of a low-frequency three-dimensional terahertz bullet with extreme brightness // Nat. Commun. 2015. V. 6, P. 5976.

3. *Lee, S.-H., Jazbinsek, M., Hauri, C. P., Kwon, O. P.* Recent progress in acentric core structures for highly efficient nonlinear optical crystals and their supramolecular interactions and terahertz applications // CrystEngComm 2016. V. 18, No. 38. P. 7180-7203.

4. *Lee, S.-H., Kang, B. J., Yoo, B.-W., Lee, S.-C., Lee, S.-J., Jazbinsek, M., Yun, H., Rotermund, F., Kwon, O.-P.* Terahertz phonon mode engineering of highly efficient organic terahertz generators // Adv. Funct. Mater. 2017. V. 27, No. 14. P. 1605583.

5. *Kang, B. J., Lee, S.-H., Kim, W. T., Lee, S.-C., Lee, K., Benacchio, G., Montemezzani, G., Jazbinsek, M., Kwon, O-P., Rotermund, F.* New class of efficient terahertz generators: Effective terahertz spectral filling by complementary tandem configuration of nonlinear organic crystals // Adv. Funct. Mater. 2018. V. 28, No. 15. P. 1707195.

# Broadband THz generation and detection

Matteo Clerici[1], Alessandro Tomasino[2,3], Anna Mazhorova[2], Marco Peccianti[4],
Alessia Pasquazi[4], Sze-Phing Ho[2,5], Xin Jin[2], Riccardo Piccoli[2], Sebastien Delprat[2],
Mohamed Chaker[2], Alessandro Busacca[3], Yoann Jestin[2], Andrey Markov[2], Luca Razzari[2],
Jalil Ali[5], Roberto Morandotti[2,6,7]

[1]School of Engineering, University of Glasgow, Glasgow, G12 8LT, United Kingdom. Matteo.clerici@glasgow.ac.uk
[2]INRS-EMT, 1650 Boulevard Lionel-Boulet, Varennes, Québec J3X 1S2, Canada
[3]DEIM, University of Palermo, Viale delle Science, Palermo 90128, Italy
[4]Department of Physics and Astronomy, University of Sussex, Brighton BN1 9RH, United Kingdom
[5]Laser Centre, Ibnu Sina ISIR, UTM, 81310 UTM Skudai, Malaysia
[6]National Research University of Information Technologies, Mechanics and Optics, 199034 St. Petersburg, Russia
[7]Institute of Fundamental and Frontier Sciences, University of Electronic Science and Technology of China, Chengdu,
610054 Sichuan, China

We shall report on our results on the terahertz (THz) short pulse generation and detection, focusing on two main aspects: 1) increasing the generation efficiency of broadband sources and 2) developing new tools for the detection of the generated broadband THz radiation.

The first part of the talk will present our results on the generation of intense THz pulses with long wavelengths ω-2ω driven fieldionisationn. Symmetry-broken electric fields compose, e.g. by the sum of the fundamental and second harmonic of a pulsed laser with a proper phase difference are known to generate THz radiation thanks to the onset of transient photocurrents [1].
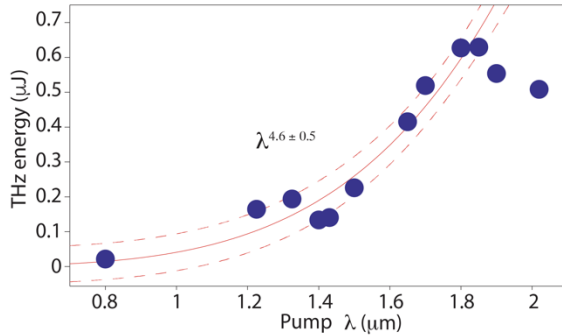


**Fig. 1.** Measured increase in the THz emission energy as a function of the pump wavelength in a two-colour pumping scheme (see [2])

Here we shall review our first experimental result thatleadsd to a demonstrated increase of the THz generation efficiency by increasing the driving pulse wavelength [2], and that is now at thecentrer of further investigations by several other groups and resulted in impressive resultsregardingf conversion efficiency ata longer wavelength.

The intense THz pulse generated by our scheme allowed us to study nonlinear light-matter interaction effects. We shall review these effects which include the counter-propagating frequency mixing with infrared pulses [3], imaging and beam-profiling [4,. and observation of nonlinear scattering events in diamond [5]. We shall also report on the observation of THz driven lasing of N2[+] gas molecules under intense pump condition from NIR laser pulse, as well as our interpretation of the process and potential developments in terms of remote sensing [6].
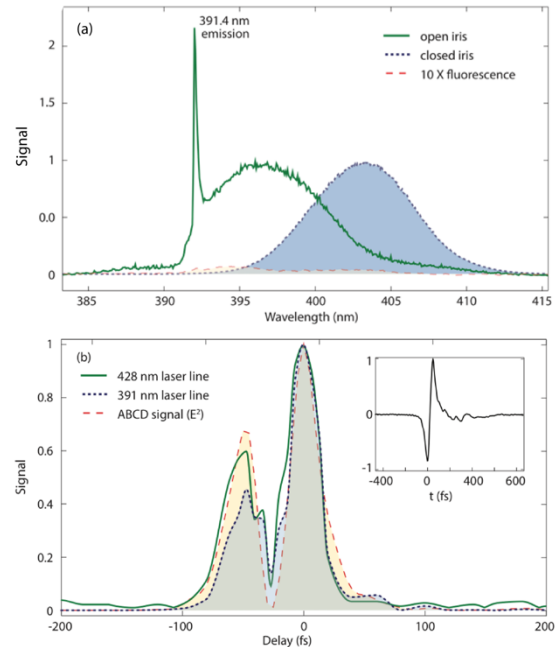


**Fig. 2.** (a) Spectrum of the signal resulting from the nonlinear interaction of THz radiation and the intense 780nm pump pulse when both are temporally overlapped. The open irisreferreds to the case of high 780nm pulse intensities and shown the onset of a coherent signal at ~391nm. The closed iris refers to the case of alow-intensityy pump puls, and the resulting spectrum is what expected froma regulard EFISH interaction. (b) Shows that the coherent emission observed at both 391nm and 428nm (in correspondence of molecular transitions) directly follows the driving electric field strength as a function of the delay between the 780nm pulse and the THz pulse

Finally, we shall review our development in the coherent, time-resolved detection of THz electric field using small devices based on the Electric-Field-Induced Second-Harmonic generation effect (EFISH) [7]. Recently, a broadband detection scheme relying on wave mixing in air between a short optical probe and the investigatedTHzZ pulse has been demonstrated and

3

named Air Biased Coherent Detection (ABCD) [8,9]. In ABCD, the information on the THz electric field is retrieved thanks to a modulating external DCfieldd applied to the region where the optical probe and the THz pulse interacts. Yet this technique required high energy probes, high voltage sources and free space propagation. Furthermore, the finite breakdown filed in air limits the signal strength and signal to noise ratio.
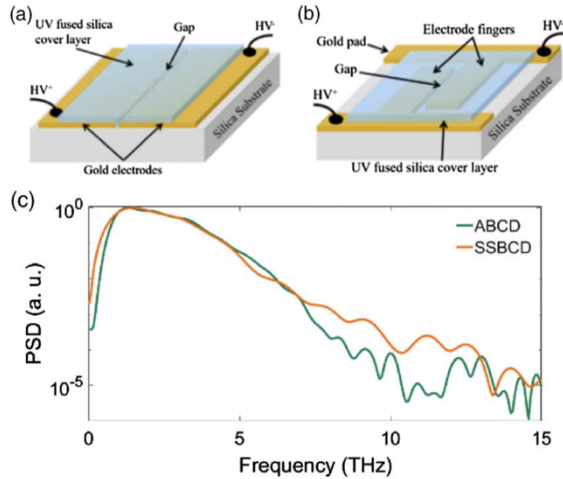


**Fig. 2.** Solid-state biased coherent detection. (a) shows a single slit case while (b) shows the building block of an array. (c) compares the measured spectrum with standard ABCD with what obtained with thenewlyw proposed technique (SSBCD)

We have investigated a novel implementation of the ABCD protocol relying on electric field induced second harmonic generation effect in few microns thick Silica ($SiO_2$) samples that can be easily operated with 200 V level sources, and we named this Solid-Stated

Biased Coherent Detection (SSBCD), see Fig.2. Exploiting the large breakdown voltage and the high non-linearity of the glass we achieve high SNR with < 1µJ probe at moderate bias fields [10]. THz field enhancement insub-micrometress slits based on the Silicon Nitride platform will also be show, and improvements will be reported.

### References

1. Y. Minami, M. Nakajima, T. Suemoto, Effect of preformed plasma on terahertz-wave emission from the plasma generated bytwo-colourr laser pulses. *Phys. Rev. A.* **83**, 023828 (2011).

2. M. Clerici *et al.*, Wavelength Scaling of Terahertz Generation by Gas Ionization. *Phys. Rev. Lett.* **110**, 253901 (2013).

3. M. Clerici *et al.*, Counterpropagating frequency mixing with terahertz waves in diamond. *Opt. Lett.* **38**, 178 (2013).

4. M. Clerici *et al.*, CCD-based imaging and 3D space-time mapping of terahertz fields via Kerr frequency conversion. *Opt. Lett.* **38** (2013).

5. M. Petev et al., Phase-insensitive scattering of Terahertz radiation. Photonics. 4 (2017)

6. M. Clerici et al., Spectrally resolved wave-mixing between near- and far-infrared pulses in gas. New J. Phys. 15, 125011 (2013).

7. A. Nahata, T. F. Heinz, Detection of freely propagating terahertz radiation by use of optical second-harmonic generation. *Opt. Lett.* **23**, 67 (1998).

8. J. Dai, X. Xie, X.-C. C. Zhang, Detection of Broadband Terahertz Waves with a Laser-Induced Plasma in Gases. *Phys. Rev. Lett.* **97**, 103903 (2006).

9. N. Karpowicz *et al.*, Coherent heterodyne time-domain spectrometry covering the entire "terahertz gap." *Appl. Phys. Lett.* **92**, 011131 (2008).

10. A. Tomasino *et al.*, Solid-state-biased coherent detection of ultra-broadband terahertz pulses. *Optica.* **4**, 1358 (2017).

# The dipole mechanism of terahertz waves emission under laser action on clusters

## A. A. Frolov

Joint Institute for High Temperatures RAS, Moscow, 125412, Russia, frolov@ihed.ras.ru

Relatively recently, generation of THz radiation was experimentally observed in the interaction of laser radiation with clusters formed by injection of a high-pressure noble gas jet into a vacuum chamber [1]. In the first theoretical work [2] devoted to analysis of emission of THz waves under laser–cluster interaction, the problem of irradiation of a cluster by two laser pulses with close frequencies was considered. According to [2], ionization and nonlinear interaction of laser pulses in cluster plasma result in the generation of radiation at the difference frequency, which can lie in the THz frequency band. However, the results obtained in [2] cannot be considered quite reliable, because, in that work, the problem of penetration of laser radiation into the supercritical cluster plasma was not considered and the laser field in the cluster was assumed to be the same as in vacuum. The first self-consistent theory of generation of THz waves in the interaction of a femtosecond laser pulse with a spherical cluster was developed in [3], where dense cluster plasma with an electron density significantly exceeding the critical value was considered. Somewhat later, in [4], this theory was extended to the case of an arbitrary density of free electrons in cluster nanoplasma.

In the present paper, the theory developed earlier in [3, 4] for quadrupole radiation of THz waves under laser–cluster interaction is generalized to the case of the dipole mechanism of THz field generation. It is shown that the dipole structure of THz radiation is realized for small-size clusters with a sufficiently high electron collision frequency $\nu_e$ [5].

The problem of penetration of laser radiation with frequency $\omega_0$ and duration $\tau$ into a cluster that is much smaller than the skin depth is considered and the spatial distribution of the laser field inside the cluster of radius $a$ for an arbitrary density of free electrons $N_{0e}$ is found by expansion in powers of the ratio of the radial coordinate to the laser wavelength in vacuum $\lambda_0$. It is shown that the electric field of laser radiation is appreciably amplified in a supercritical cluster plasma if the laser frequency is close to the frequency of the dipole or quadrupole mode of a plasma sphere.

The excitation of low-frequency electromagnetic fields in a cluster under the ponderomotive action of laser radiation on free electrons is considered and the spatial distribution of low-frequency electromagnetic fields in the cluster and vacuum is calculated. The results obtained for vacuum low-frequency fields are analyzed at large distances from the cluster in the wave zone.

The angular, spectral, and energetic characteristics of THz radiation for a laser pulse with a Gaussian time profile are studied. The spectrum of THz radiation is analyzed. It is established that the spectrum depends substantially on the density of free electrons. For a low-density cluster plasma, the emission spectrum has sharp peaks at the frequencies of dipole

$$\omega_d = \omega_p \big/ \sqrt{\varepsilon_0 + 2}, \qquad (1)$$

and quadrupole

$$\omega_q = \omega_p \big/ \sqrt{\varepsilon_0 + 3/2}, \qquad (2)$$

oscillations of the plasma sphere (see Fig. 1), where $\omega_p$ is the electron plasma frequency, $\varepsilon_0$ is the low-frequency permittivity of the cluster with allowance for the contribution of only neutral atoms.
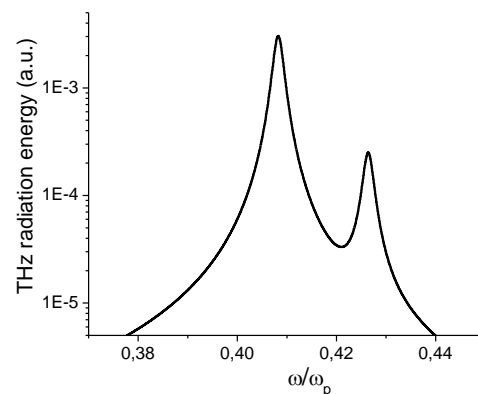


**Fig. 1.** THz radiation energy emitted by spherical cluster as function of frequency for $(\omega_p \tau)^2 = 30$, $\varepsilon_0 = 4$

These peaks are associated with the so-called leaky modes that are excited in the cluster under the action of laser radiation and can be emitted into the ambient medium. With an increase in the density of electrons, these peaks gradually disappear, and instead of them in the case of a supercritical electron density a broad maximum is formed at a frequency comparable to the reciprocal of the laser pulse duration $\omega \approx 2/\tau$ (Fig. 2).
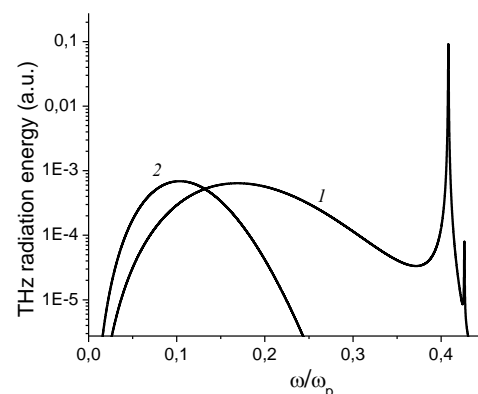


**Fig. 2.** THz radiation energy emitted by spherical cluster as function of frequency for $\varepsilon_0 = 4$ and different values of parameter $\omega_p \tau$: (*1*) 13 and (*2*) 20

It is shown that, for small clusters with sufficiently frequent electron collisions $\nu_e$, the angular energy distribution has a dipole structure and THz waves are emitted mainly at an angle of $\pi/2$ with respect to the propagation direction of the laser pulse (see Fig. 3).
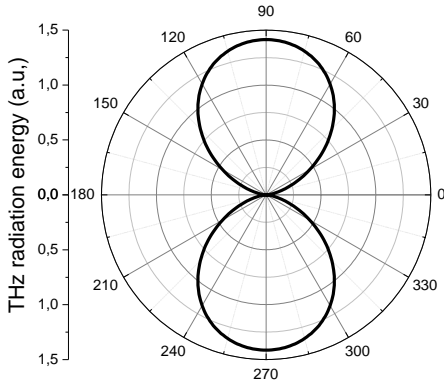


**Fig. 3.** Directional pattern of THz radiation emitted by spherical cluster

The total energy of THz radiation is calculated, and its dependence on the density of free electrons is analyzed. It is shown that the energy of THz radiation is maximal for a overdense cluster plasma under the resonance conditions in which the frequency of laser radiation coincides with the eigenfrequency of a dipole or quadrupole mode of the plasma sphere (see Fig. 4).
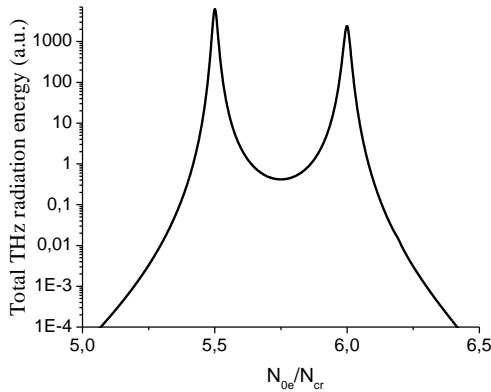


**Fig. 4.** Total energy of THz radiation of a spherical cluster vs. dimensionless density $N_{0e}/N_{cr}$ for $\varepsilon_0=4$, $N_{cr}$ - critical density

It is established that the dipole mechanism of THz emission prevails in small-size clusters with frequent electron collisions, when inequality

$$(\nu_e\lambda_0 c\tau/a^2\omega_0)(\omega_p/\omega_0)^2 >> 0.1\div 0.3 \qquad (3)$$

is fulfilled, where $c$ - speed of light.

The spatiotemporal structure of the electromagnetic field in a THz pulse is studied. It is shown that the profile of the THz signal depends substantially on the density of free electrons. For a low-density cluster plasma, the field of the THz pulse oscillates at the frequencies of the dipole and quadrupole modes of the plasma sphere, and its duration is determined by the damping rate of the corresponding mode and can reach a few picoseconds (Fig.5). For a supercritical electron density, the THz signal contains only two oscillation cycles and its duration is comparable with the duration of the laser pulse (Fig. 6).
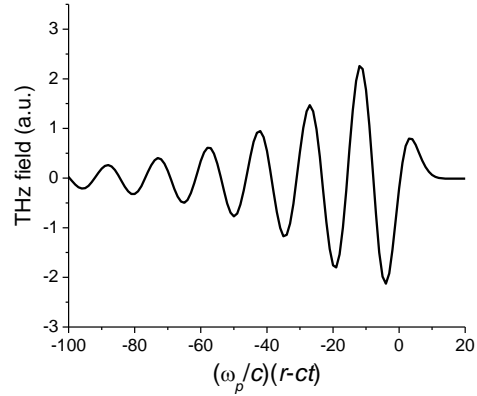


**Fig. 5.** Dimensionless field of terahertz radiation pulse as function of comoving coordinate for $(\omega_p\tau)^2=30$, $\varepsilon_0=4$

Estimates show that, in the interaction of femtosecond laser pulses with clustered gases, high-power THz pulses can be generated with a rather high conversion efficiency.
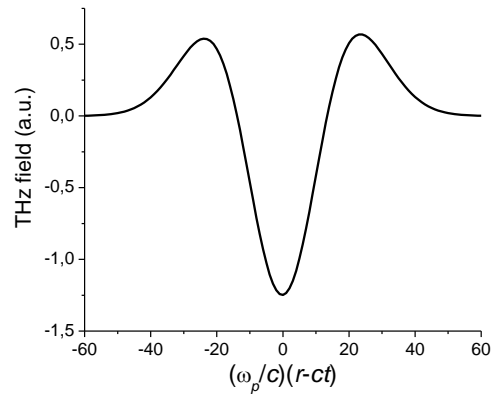


**Fig. 6.** Dimensionless field of terahertz radiation pulse as function of comoving coordinate for $\omega_p\tau=20$, $\varepsilon_0=4$

### References

1. *Nagashima, T., Hirayama, H., Shibuya, K., Hangyo, M., Hashida, M., Tokita, S., Sakabe, S.* Terahertz pulse radiation from argon clusters irradiated with intense femtosecond laser pulses // Opt. Express. 2009. V. 17, No. 11. P. 8807-8812.

2. *Kumar, M., Tripathi, V. K.* Terahertz generation by nonlinear mixing of laser pulses in a clustered gas // Phys. Plasmas. 2011. V. 18, No. 5. P. 053105.

3. *Frolov, A. A.* Emission of terahertz waves in the interaction of a laser pulse with clusters // Plasma Phys. Rep. 2016. V. 42, No. 7. P. 637-646.

4. *Frolov, A. A.* Influence of the Electron Density on the Characteristics of Terahertz Waves Generated under Laser–Cluster Interaction // Plasma Phys. Rep. 2016. V. 42, No. 12. P. 1111-1126.

5. *Frolov, A. A.* Dipole Generation of Terahertz Waves under Laser–Cluster Interaction // Plasma Phys. Rep. 2018. V. 44, No. 1. P. 40-54.

# Multi wavelength injection-seeded THz parametric system

Kosuke Murate, <u>Kodo Kawase</u>

Department of Electronics, Nagoya University, Nagoya, Japan, kawase@nuee.nagoya-u.ac.jp

For several years, we have worked on the development of an injection-seeded terahertz (THz) parametric generator (is-TPG) as a high-power THz-wave source. Recently, the peak output power of is-TPG approached a few tens of kW after introducing a microchip Nd:YAG laser with a shorter pulse width [1].

However, long measurement times are necessary for spectroscopic imaging because is-TPG is a tunable source that emits a single wavelength in each pulse [2-4]. We recently generated multiwavelength THz waves from is-TPG [5]. In multiwavelength generation, the wavelength does not need to be tuned, allowing a spectrum to be acquired in a single pulse. Therefore, the measurement time can be drastically shortened by using this system for spectroscopic imaging. Furthermore, we introduced a new scheme that improved the stability by acquiring reference spectrum at the same time.

When a high-power pump beam and seed beam

imping on a LiNbO$_3$ crystal, a narrow line width and high brightness THz wave is generated by parametric wavelength conversion [1]. Wide tunability of the is-TPG can be achieved by controlling the wavelength of the seed beam and its angle to satisfy the non-collinear phase-matching condition of the LiNbO$_3$ crystal.

In this study, we generated multiwavelength THz waves by injecting multiwavelength seed beams into the crystal and distributing the energy to each wavelength. For the multiwavelength seed beams, we used multiple external cavity laser diodes (ECLDs) with semiconductor optical amplifier.

Figure 1 shows the experimental setup for the high-speed and stabilized THz spectroscopic imaging system. We used a microchip Nd:YAG laser (HA-MAMATSU LE0600DPS, duration 650 ps, wavelength 1064.4 nm, repetition rate 11 Hz, output 0.7 mJ/pulse) as the pump source and multiple ECLDs as multiwavelength seed beam sources. The emitted multiwavelength THz waves were split into two beams to obtain not only a sample measurement beam but also a reference beam simultaneously. After passing through a sample, the sample measurement beam was focused onto the crystal for detection. The reference beam was directly input to another detection crystal. Finally, the THz waves were detected based on nonlinear optical wavelength conversion [1,2], whereas the infrared (IR) detection beam intensities were measured using an IR beam profiler. The detection beams were angle-dispersive, allowing each wavelength to be detected separately. The simultaneous acquisition of the reference and detection beams improved measurement stability.

First, we confirmed the improvement in stability. For this measurement, we used three wavelength generation at 1.47, 1.64 and 1.81 THz. The correlation coefficient between the sample measurement beam and the reference beam was 0.94 at 1.47 THz, 0.86 at
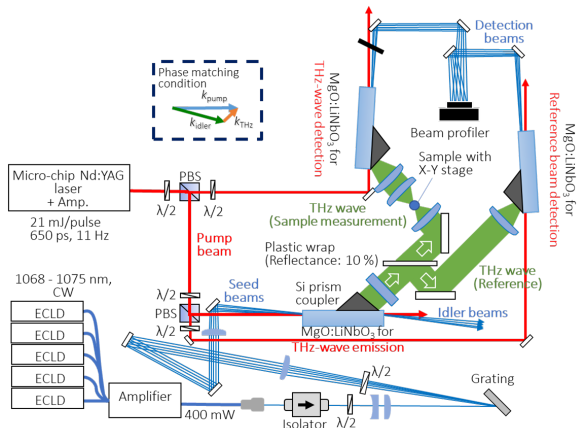


Fig. 1. Experimental setup of high-speed terahertz (THz) spectroscopic imaging system using multiwavelength injection-seeded THz parametric generator (is-TPG).
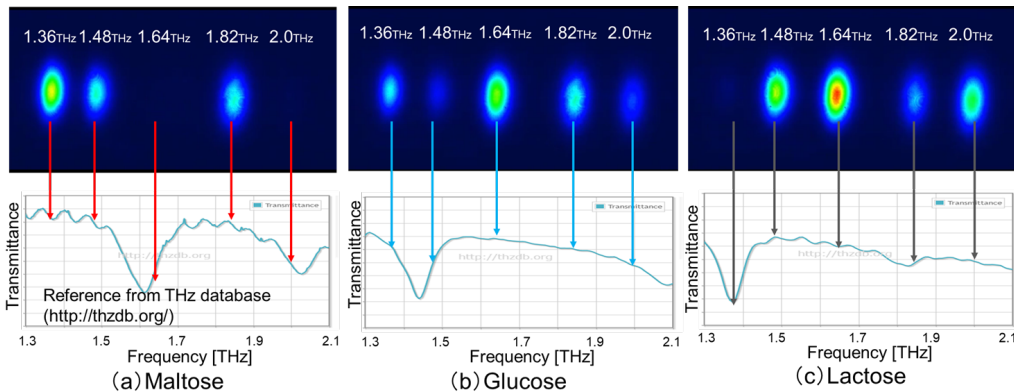


Fig. 2. Results of real-time one-shot spectroscopy and reference spectrum from THz database (Graph of the blue line under each image). Three saccharides were identified in real-time using five wavelength generation from the is-TPG.

1.64 THz, and 0.88 at 1.81 THz. Stability improvement was realized by dividing the sample measurement beam by the reference beam, with good correlation. The stability was improved from 1.42 % to 0.50 % at 1.47 THz, from 1.12 % to 0.59 % at 1.64 THz, and from 1.97 % to 0.93 % at 1.81 THz. Thus, the fluctuation was suppressed to less than 1 % in all frequencies.

Next, we report the one-shot spectroscopic measurement of three saccharides using this system. We placed pellets with 40% maltose, glucose, and lactose (60% polyethylene) in the THz-wave optical path and recorded the spectroscopic measurements. The central frequency of the absorption spectrum of each reagent is approximately 1.62 and 2.02 THz for maltose, 1.44 and 2.09 THz for glucose, and 1.36 and 1.82 THz for lactose, according to the reference spectrum from the THz database (blue line under each image in Fig. 2) [6]. We used five frequencies, 1.36, 1.48, 1.64, 1.82 and 2.00 THz, in the multi-wavelength is-TPG to match these reference frequencies. The measurement results are shown in Fig. 2. We confirmed that the attenuation of the THz waves matched the absorption spectra of the reagent, and qualitatively identified the saccharides using one-shot multi-wavelength is-TPG with good output stability. The measurement can be performed at a frame rate equal to the laser's repetition rate (11 Hz), enabling real-time reagent identification.

Finally, high-speed and stable THz spectroscopic imaging was realized. As a sample, three saccharides in the same proportions as the real-time spectroscopic measurements were hidden in an Express Mail Service (EMS) envelope, as shown in Fig. 3(a). We obtained multi-spectral images at five wavelengths (1.36, 1.48, 1.64, 1.83, and 2.00 THz) to observe the absorption peaks of the three saccharides. Figure 3(b) shows the results for each saccharide component extracted from multi-spectral images using component spatial pattern analysis [3,4]. Although only one pixel was acquired in a single pulse without averaging, spatial identification of the saccharide was similar to that achieved with conventional is-TPG [3,4]. However, the measurement time was shortened more than fivefold using this system.

A real-time spectroscopic system and a high-speed, stable THz spectroscopic imaging system were realized by multiwavelength THz generation/detection using is-TPG. This system could be used not only for real-time reagent identification, but also for the rapid spectroscopic imaging of saccharides hidden in enve-
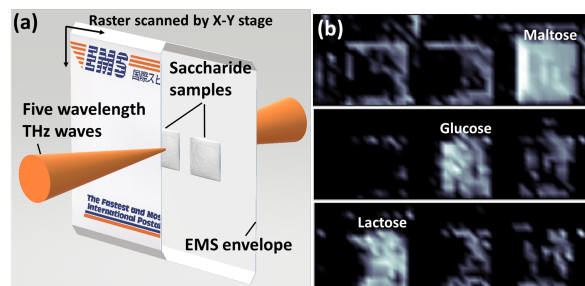


Fig. 3. (a) Measured sample; Three saccharide powders of maltose, glucose, and lactose hidden in an Express Mail Service (EMS) envelope. (b) The result of spectroscopic imaging of the sample measured by multiwavelength is-TPG (image size: 48 × 16 pixels, step size: 1 mm).

lopes. This work represents a significant contribution to future advancements of THz non-destructive imaging.

## References

1. *Hayashi, S., Nawata, K., Taira, T., Shikata, J., Kawase, K., Minamide, H.* Ultrabright continuously tunable terahertz-wave generation at room temperature // Sci. Rep. 2014. V. 4, P. 5045.

2. *Murate, K., Taira, Y., Tripathi, S. R., Hayashi, S., Nawata, K., Minamide, H., Kawase, K.* A High Dynamic Range and Spectrally Flat Terahertz Spectrometer Based on Optical Parametric Processes in LiNbO$_3$ // IEEE Trans. Terahertz Sci. Technol. 2014. V. 4, P. 523.

3. *Kawase, K., Ogawa, Y., Watanabe, Y., Inoue, H.* Non-destructive terahertz imaging of illicit drugs using spectral fingerprints // Opt. Express, 2003. V. 11, P. 2549-2554.

4. *Kato, M., Tripathi, S. R., Murate, K., Imayama, K., Kawase, K.* Non-destructive drug inspection in covering materials using a terahertz spectral imaging system with injection-seeded terahertz parametric generation and detection // Opt. Express, 2016. V. 24, P. 6425-6432.

5. *Murate, K., Hayashi, S., Kawase, K.* Multi-wavelength terahertz-wave parametric generator for one-pulse spectroscopy // Appl. Phys. Express, 2017. V. 10, P. 032401.

6. THz-database. Available at: http://thzdb.org/.

# Plasma mechanisms of terahertz electromagnetic wave generation due to intense laser-plasma interaction

A.S. Kuratov[1], A.V. Brantov[1,2], Yu.M. Aliev[2], V.Yu. Bychenkov[1,2],

[1] Center of Fundamental and Applied Research, VNIIA, Moscow, Russia, kuratov.andrew@gmail.com
[2] Lebedev Physical Institute RAS, Moscow, Russia,

## 1. Introduction

Terahertz radiation is important for applications in different fields of science and technology, i.e. in diagnostics, medicine and security to define and visualize object's structure, in chemistry and biology to manipulate and excite molecules, and even in astrophysics and communication. Continuous and broadband THz radiation source and detectors has already been successfully developed worldwide. The development of new sources of ultra-intense THz source is of most interesting issue at the time being [1]. THz emission via interaction of intense laser pulses with a plasma is one of the most promising approach. There is number of experiments which demonstrate generation of high energetic THz pulses such during laser-plasma interaction. High power THz pulses has special application capabilities. For example, such pulses are very desirable for nonlinear THz spectroscopy of condense matter, resonant/non-resonant control of materials, the nonlinear response of metamaterials, and nonlinear THz interactions.

Laser-plasma sources have certain advantages as compared to other high power THz radiation sources, e.g. the absence of power threshold. Optical rectification schemes generate high power THz pulses with high efficiency but they have limitation of THz energy output. Laser-plasma source system has relatively small size in comparison with free electron lasers, gyrotrons and other high power sources. Also THz generation via laser plasma source has energy conversion efficiency from laser to THz pulse at the level of $\sim 10^{-3-4}$ [2]. It seems to be a perspective to generate high power ultra-wideband THz radiation.

The process of THz generation in the interaction of high power laser with solid targets is still not clearly understood in spite of numerous studies [1, 3]. In this work we study theoretically several mechanisms of the THz radiation generation by relativistically strong laser pulses, e.g. radiation generation during sheath acceleration process at the planar target rear surface, THz emission by electrical current of fast electrons escaping a foil target and THz generation by thermoelectric currents. Here we report theoretical and numerical comparative study of these three different mechanisms of THz radiation generation from the laser plasma sources [4,5].

## 2. THz generation mechanisms

A typical mechanism for generating THz radiation is the coherent transition radiation produced by an electron bunch passing through a metal foil-vacuum interface. Such bunch of relativistic electrons can be produced during target irradiation by high-power short laser pulse. Heated by laser pulse electrons propagate through foil and cross the back surface to generate coherent transition radiation lying in the THz range. Perhaps this is one of possible generation mechanisms of the observed THz radiation in experiments on irradiation of solid targets by high-intensity laser radiation. The electron bunch escaping from the target includes a small part of all laser-accelerated (heated) electrons: only those whose energy is sufficient to overcome the confining electrostatic potential. In a typical case, this is a bunch of moving relativistic particles. These particles generate THz radiation very efficiently.

Second mechanism is related with that part of hot electrons which remains in the target, producing a strong electrostatic sheath field at the rear surface, which leads to target ionization and subsequent plasma expansion in to vacuum. During expansion, the moving uncompensated electric dipole formed at the plasma front is basically equivalent to a charge flying away from the target and, hence, can also generate transition radiation. This radiation mechanism, unlike the first one, is associated with the slow movement of the charge. However, the magnitude of a recoil charge is large compared with a charge of a relativistic escaping electron bunch, and its role in radiation should be considered.

Another mechanism is connected to the thermoelectric current. One of the main sources of strong quasi-stationary magnetic fields under conditions of noncollinearity of temperature and electron density gradients is thermoelectric currents. After solid target irradiation by intense ultrashort laser pulse a layer of hot electrons of submicron thickness (Debay length) is formed at its surface. Under normal incidence of high-intensity laser radiation on the target, the Lorentz force of the laser field causes near-surface heating of the target. This force causes oscillations of electrons along the normal to the surface at a doubled laser-light frequency. As a result, a highly inhomogeneous heated layer of electrons is produced which can be considered as a rarefied electron plasma with a density gradient along the normal to the surface and an effective temperature gradient in the transverse direction. The resulting temperature gradient is related both to the inhomogeneity of the laser radiation intensity itself and to the transverse expansion of the hot spot.

## 3. Results

THz radiation produced by the considered mechanisms has been estimated theoretically. An efficiency of THz generation as a result of plasma expansion into vacuum is always much less than the efficiency of THz

generation due to the emission of fast escaping electron beams. It is worth noting different angular directions of the generated transition radiation. If the fast electron beam causes the appearance of radiation directed along the beam axis, the radiation associated with the plasma expansion into vacuum is directed generally along the target surface [4].

We have compared spectral characteristics of a surface electromagnetic wave (SEW) exited by laser-induced thermoelectric currents with those for surface wave produced by a beam of electrons leaving the target. The frequencies of these SEWs lie in the terahertz range. It is shown that if the latter dominates in the long-wavelength region, then the thermoelectric mechanism prevails in the region of shorter wavelengths of the SEWs. With respect to the total radiation energy for typical parameters of relativistically intense short laser pulses, the proposed mechanism turns out to be comparable in efficiency with the mechanism of excitation of waves by the current of electrons leaving the target. Although discussion of the THz pulse generation is carried out for the front surface of the target, a similar effect occurs for its rear side in the case of laser irradiation of a thin foil [5].

Theoretical results obtained are confirmed in the performed 3D PIC simulations, that will be discussed somewhere else.

**Acknowledgments**

**References**

1. *Hafez, H. A., Chai, X., Ibrahim A., Mondal S., Ferachou D., Ropagnot X., Ozaki X.* Intense terahertz radiation and their applications // J. Opt. 2016. V. 18, 093004, P. 1-48.

2. *Gopal A., Herzer S., Schmidt A., Singh P., Reinhard A., Ziegler W., Brommel D., Karmakar A., Gibbon P., Dillner U., May T., Meyer H-G., and Paulus G.* Observation of giga-watt-Class THz pulses from a compact laser-driven particle acceleration // PRL. 2013. V. 111, 074802.

3. *Herzer S., Woldegeorgis A., Polz J., Reinhard A., Al-massaani M., Beleites B., Ronneberger F., Grosse R., Paulus G., Hubner U., May T., and Gopal A* An investigation on THz yield from laser-produced solid density plasmas at relativistic laser intensities // New J. Phys. 2018, V. 20, 063019 P. 1-15

3. *Kuratov A., Brantov V., Aliev Yu., Bychenkov V.* Terahertz radiation in laser-induced charge separation in the irradiated plasma target // Quantum Electronics. 2016, V. 46, N. 11, P. 1023-1030.

4. *Kuratov A., Brantov V., Aliev Yu., Bychenkov V.* Laser-induced thermoelectric current as a source of generation of THz surface electromagnetic waves // Quantum Electronics. 2016, V. 48, N. 7, P. 653-657.

# THz Nonlinear Photonics: Generation and Applications

Fabian Rotermund

Department of Physics, Advanced Institute of Science and Technology (KAIST), Daejeon 34141, South Korea
rotermund@kaist.ac.kr

Since high-power broadband terahertz (THz) generators are nowadays essential tools for a wide range of THz applications, diverse approaches have been proposed for developing such systems. Tilted-pulse-front method in combination with nonlinear frequency conversion process in a nonlinear crystal is one of the most efficient ways to generate high pulse energies and electric fields [1,2]. Furthermore, non-linear organic crystals are also considered as promising efficient THz emitters because they possess higher $2^{nd}$-order nonlinearity than inorganic crystals and provide excellent optical-to-THz conversion efficiency at room temperature with better controllability of phase matching properties covering broad spectral ranges in the THz region [3,4]. We recently demonstrated efficient THz wave generation based on pulse-front-tilted optical rectification in a prism-cut $LiNbO_3$ and newly developed organic crystals, and subsequently, such systems were used for diverse studies on THz nonlinear photonics. For instance, graphene and graphene-integrated structures have been widely investigated for a number of photonic applications in a wide spectral range. In recent years, we reported enhanced unique nonlinear optical characteristics of those materials in the THz range. The THz nonlinearity of mono- to multi-layer graphene can be remarkably accelerated by random stacking of monolayer graphene or in combination with meta-structures and in sub-nano-gap structures [5-8].

In this talk, diverse nonlinear methods for efficient generation of intense broadband THz waves and interesting results regarding graphene-based THz nonlinear photonics will be presented.

## References

1. *Stepanov, A. G., Hebling, J., Kuhl, J.* Efficient generation of subpicosecond terahertz radiation by phase-matched optical rectification using ultrashort laser pulses with tilted pulse fronts // Appl. Phys. Lett. 2003. V. 83, No. 15. P. 3000.

2. *G. Stepanov, A. G., Kuhl, J., Kozma, I. Z., Riedle, E., Almasi, G., Hebling, J.* Scaling up the energy of THz pulses created by optical rectification // Opt. Express 2005. V. 13, No. 15. P. 5762-5768.

3. *Schneider, A., Neis, M., Stillhart, M., Ruiz, B., Khan, R. U. A., Günter, P.* Generation of terahertz pulses through optical rectification in organic DAST crystals: theory and experiment // J. Opt. Soc. Am. B 2006. V. 28, No. 9. P. 1822-1834.

4. *Jeong, J.-H., Kang, B.-J., Kim, J.-S., Jazbinsek, M., Lee, S.-H., Lee, S.-C., Baek, I.-H., Yun, H., Kim, J., Lee, Y. S., Lee, J.-H., Kim, J. H., Rotermund, F., Kwon, O-P.* High-power broadband organic THz generator // Sci. Rep. 2013. V. 3. P. 3200.

5. *Bahk, Y.-M., Kang, B. J., Kim, Y. S., Kim, J.-Y., Kim, W. T., Kim, T. Y., Kang, T., Rhie, J., Han, S., Park, C.-H., Rotermund, F., Kim, D.-S.* Electromagnetic Saturation of Angstrom-Sized Quantum Barriers at terahertz frequencies // Phys. Rev. Lett. 2015. V. 115. P. 125501.

6. *Choi, H. J., Baek, I.-H., Kang, B. J., Kim, H.-D., Oh, S. S., Hamm, J., Pusch, A., Park, J., Lee, K., Son, J., Jeong, Y. U., Hess, O., Rotermund, F., Min, B.* Control of terahertz nonlinear transmission with electrically gated graphene metadevices // Sci. Rep. 2017. V. 7. P. 42833.

7. *Baek, I. H., Hamm, J. M., Ahn, K. J., Kang, B. J., Oh, S. S., Bae, S., Choi, S. Y., Hong, B. H., Yeom, D.-I., Min, B., Hess, O., Jeong, Y. U., Rotermund, F.* Boosting the terahertz nonlinearity of graphene by orientation disorder // 2D Mater. 2017. V. 4. P. 025035.

8. *Kang, B. J., Lee, S.-H., Kim, W. T., Lee, S.-C., Lee, K., Benacchio, G., Montemezzani, G., Jazbinsek, M., Kwon, O-P., Rotermund, F.* New Class of Efficient Terahertz Generators: Effective Terahertz Spectral Filling by Complementary Tandem Configuration of Nonlinear Organic Crystals // Adv. Funct. Mater. 2018. V. 28. P. 1707195.

# Terahertz Wave Generation from Liquied Gas

A.V.Balakin[1,2], A.F.Bunkin[3], V.A. Makarov[1,4], I.A. Kotelnikov[5,6], N.A. Kuzechkin[1,2], A.B.Savelev[1], P.M.Solyankin[1,2], A.P.Shkurinov[1,2,4]

[1]Faculty of Physics & International Laser Center, Lomonosov Moscow State University, Moscow 119991, Russia
[2]Institute on Laser and Information Technologies of RAS, Branch of the FSRC "Crystallography and Photonics", RAS, Shatura, Moscow Region 140700, Russia
[3]A.M. Prokhorov General Physics Institute of the RAS, 38 Vavilov Str., 119991 Moscow, Russia
[4]The National University of Science and Technology MISiS, Moscow 119049, Russia
[5]Budker Institute of Nuclear Physics, Novosibirsk, 630090, Russia
[6]Novosibirsk State University, Novosibirsk, 630090, Russia.
ashkurinov@physics.msu.ru

We present results of our research on generation of THz radiation in liquid nitrogen. We used a dual-frequency scheme when emissions of the main laser frequency and its second harmonic are mixed in the same medium. The research showed a possibility of effective conversion of optical radiation into THz radiation.

The source of electromagnetic radiation in the THz band on the basis of laser spark was firstly presented in [1]. An experiment in which a liquid, namely, water was used for the conversion of femtosecond radiation into the THz one is described in [2]. Water is a polar liquid which has high absorption in the THz frequency range and the authors of previously published works have to use for the experiments the very thin water films. Unlike water, considerable absorption both in THz and NIR ranges is absent in liquid nitrogen.

In our experiments the laser beam ω is directed vertically from top to bottom with the help of a set of mirrors and is focused by a lens inside the LN in Dewar vessel. The Dewar vessel is mounted on a microscopic translation stage and can be moved vertically, which enables the regulation of the position of the lens focus regarding the surface level of the LN. THz radiation generated in the beam-waist is reflected from a flat aluminum mirror and is collimated by the parabolic mirror.

First of all, we obtained the THz radiation with the use of a dual frequency scheme in an experimental set-up without liquid nitrogen, from a routine optical air breakout. After that, the laser beams on the fundamental and the second harmonic was focused into LN and the THz radiation was also observed. Figure 1 shows the dependences of the THz pulse energy on the lens focus position regarding the surface of liquid nitrogen (the laser beam waist is located inside the liquid if z < 0 and in the air if z > 0). The intensity of the generation changes exponentially as the beam-waist position varies and a and a leap in the level is observed when the level of the surface is passed.
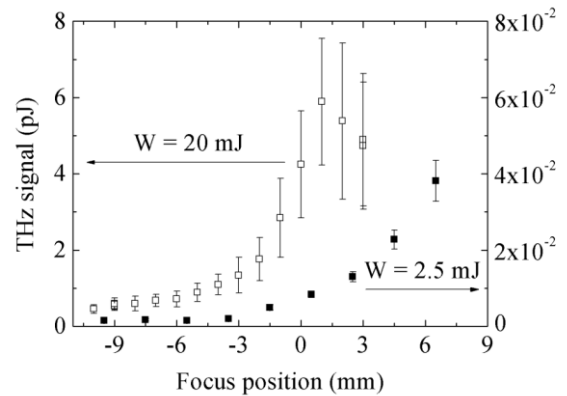


Fig. 1. Dependence of THz pulse energy on the lens focus position regarding the surface level of the liquid nitrogen. "black squares" indicate THz signal with 2.5 mJ pumping energy; "open squares" indicate THz signal with 20 mJ pumping energy.

Also we have studied how THz yield scales with laser pulse duration and its energy, angle of rotation of the BBO crystal and measured spectra of the THz radiation.

The present work describes broadband generation of THz radiation first obtained in liquid gas. Unlike previous attempts to generate THz radiation in water, in our experiments we used liquid nitrogen, and the results enabled us to suggest a physical mechanism of this process.

## REFERENCES

[1] H. Hamster, A. Sullivan, S. Gordon, W. White, and R. W.Falcone, "Subpicosecond, electromagnetic pulses from intense laser-plasma interaction," Phys. Rev. Lett., Vol 71, 2725–2728, 1993

[2] Q. Jin, Y. E, K. Williams, J. Dai, and X.-C. Zhang, "Observation of broadband terahertz wave generation from liquid water," App. Phys. Lett Vol 111, 071103, 2017

# Generation of DC fields ahead of ultrashort laser pulses in electro-optic crystals

E.S. Efimenko[1], S.A. Sychugin[2], M.V. Tsarev[3], M.I. Bakunov[2]

[1]Institute of Applied Physics RAS, Nizhny Novgorod, Russia
[2]University of Nizhny Novgorod, Nizhny Novgorod, Russia, bakunov@rf.unn.ru
[3]Ludwig-Maximilians-Universität München, Garching, Germany

Optical rectification of ultrashort laser pulses in electro-optic crystals is a commonly used technique for generating pulsed terahertz radiation. Nowadays, numerous applications require increasing optical pump intensity to obtain stronger terahertz fields. At high pump intensities, multi-photon absorption starts to play an important role in the process putting a limit on the generation efficiency. This is explained mainly by the generation of free carriers that absorb terahertz waves. Thus, free-carrier generation is commonly recognized as a negative effect for terahertz generation.

Recently, however, it was found that concurrent processes of optical rectification and free carrier generation can give rise to a new effect, namely, the generation of DC electromagnetic fields propagating ahead of the pump laser pulse as a precursor [1]. The fields in the DC precursor can exceed the fields of the ordinary terahertz pulse generated behind the laser pulse. The generation of the precursor is explained by following mechanism. The electric field of the rectified laser pulse accelerates the newly born carriers thus producing a burst of an electric current. The current burst generates the precursor.

In Ref. [1], the approximations of an infinitely wide laser beam and negligible depletion were used to demonstrate the effect. Here, we extend the consideration of Ref. [1] by exploring how the factors of finite beam width and pump depletion affect the precursor generation. Furthermore, we propose a way to overcome the negative effect of the pump depletion on the precursor generation by using chirped laser pulses as a pump. We also demonstrate that using the tilted-pulse-front pulses [2] as a pump allows to increase the precursor fields by orders of magnitude.

## Chirped-pulse pumping

In the standard scheme of terahertz generation with collinear propagation of optical and terahertz pulses, DC precursor can be generated in electro-optic crystals with $n_g > n_0$ ($n_g$ is the optical group refractive index and $n_0$ is the low-frequency phase refractive index), such as semiconductors GaP or ZnTe, pumped by Ti:sapphire laser [1]. It is assumed, that an ultrashort laser pulse propagates in an electro-optic crystal in the $+z$ direction with a group velocity $c/n_g$, $c$ is the speed of light. The optical intensity $I(z,t)$ is high enough to produce two-photon ionization with the density of free carriers

$$N(z,t) = \alpha \int_{-\infty}^{t} I^2(z,t)dt, \qquad (1)$$

where $\alpha = \beta_2/(2\hbar\omega)$, $\beta_2$ is the two-photon absorption coefficient, and $\hbar\omega$ is the quantum energy of the laser radiation.
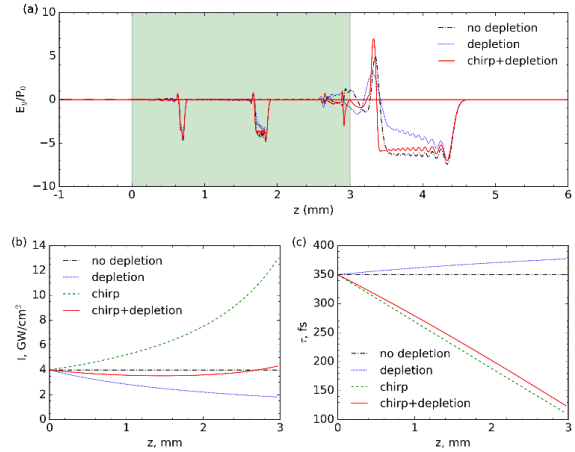


**Fig. 1.** (a) Snapshots of $E_y/P_0$ at three moments of time for the cases when pump depletion is neglected, included, and compensated by chirping the laser pulse. The crystal (shaded region) is 3 mm thick. The arrows depict the position of the pump pulse. (b) Intensity and (c) 1/e-duration of the pump pulse as a function of the distance in the crystal.

Figure 1(a) shows the snapshots of the electric field $E_y$ generated by a Ti:sapphire laser pulse (780 nm wavelength) in a 3-mm thick GaP crystal with $n_g = 3.66$, $n_0 = 3.31$, and $\beta_2 = 1$ cm/GW. The field is normalized to the amplitude of the nonlinear polarization $P_0$ induced by the laser pulse in the crystal.

If the pump pulse propagates without depletion, the precursor has a form of a plateau, whose size increases with distance in the crystal and due to transmission through the crystal boundary. With the non-linear coefficient $d = 25$ pm/V for GaP and peak optical intensity $I_0 = 4$ GW/cm², a unity of $E_y/P_0$ in Fig. 1(a) corresponds to $E_y = 0.2$ kV/cm and the precursor magnitude exceeds 1 kV/cm.

Pump depletion results in an attenuation of the rear part of the precursor [Fig. 1(a)]. Thus it is a significant detrimental factor for the precursor generation.

To counterbalance the effect of pump depletion, we propose to use pumping by a chirped laser pulse. Due to dispersive compression of a negatively chirped laser pulse [Fig. 1(c)], the optical intensity can be sustained practically constant in the crystal [Fig. 1(b)]. This provides efficient precursor generation with almost the same shape as in non-depletion approximation [Fig. 1(a)].

To verify this idea, we use nonlinear Schrodinger equation for the optical field envelope $A(z,\xi)$ in the local pulse frame ($z$, $\xi = t - zn_g/c$):

$$\frac{\partial A}{\partial z} = -\frac{i}{2} GVD \frac{\partial^2 A}{\partial \xi^2} - \frac{\beta_2}{2} IA, \qquad (2)$$

where GVD = 2393 fs$^2$/mm is the optical group velocity dispersion for GaP at 780 nm [3]. We solve this equation with the boundary condition (at $z = 0$)

$$A(0,t) = A_0 \exp\left(\frac{i\gamma t^2}{2\tau_0^2} - \frac{t^2}{2\tau_0^2}\right), \qquad (3)$$

where $\tau_0$ is the duration of the incident pulse and $\gamma$ is the chirp parameter, by using the split-step method. The duration of the initial Fourier limited laser pulse is $\tau_F = \tau_0(1 + \gamma^2)^{-1/2}$.

Results of the calculations for the pump pulse with a peak intensity $I_0 = 4$ GW/cm$^2$, $\tau_F = 30$ fs, and $\gamma = -12$ are shown in Fig. 1. It is seen that the peak optical intensity remains almost constant in the crystal [Fig. 1(b)], i.e., pump compression indeed counterbalances pump depletion. The pulse duration $\tau$ decreases from $\tau_0 = 350$ fs at $z = 0$ to about 130 fs at the exit boundary of the crystal [Fig. 1(c)]. The precursor's shape is almost completely restored due to chirped-pulse pumping [Fig. 1(a)].

## Tilted-pulse-front pumping

To extend the DC precursor generation to materials, such as LiNbO$_3$, with $n_g < n_0$, we propose to use the tilted-pulse-front pumping technique [2]. In fact, the tilted-pulse-front pumping is equivalent to pumping by ordinary non-tilted pulses but in a virtual medium with an effective optical group refractive index $n_{eff} = n_g/\cos\theta$ that depends on the tilt angle $\theta$ [4]. By a proper choice of $\theta$, i.e., $\theta > \cos^{-1}(n_g/n_0)$, the necessary condition for the precursor generation, $n_{eff} > n_0$, can be fulfilled.
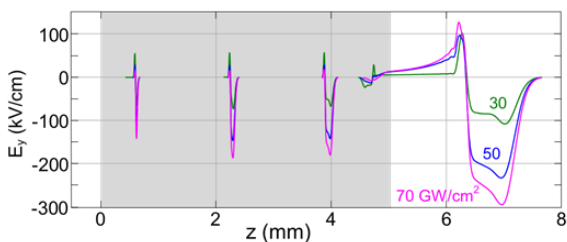


**Fig. 2.** Snapshots of the electric field $E_y$ generated in a LiNbO$_3$ crystal by the tilted-pulse-front ($\theta = 64.5°$) laser pulse with $I_0 = 30$, 50, and 70 GW/cm$^2$. The crystal (shaded region) is 5 mm thick.
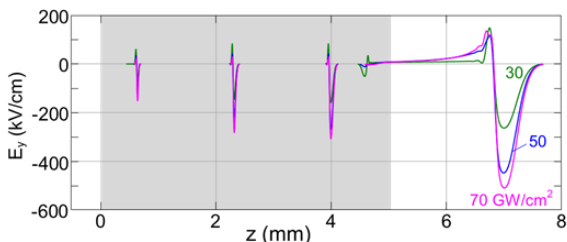


**Fig. 3.** The same as in Fig. 2 but for $\theta = 64°$.

Figure 2 shows the precursor generation in a 5-mm thick LiNbO$_3$ crystal ($n_0 = 4.94$, $n_g = 2.20$) by a non-chirped tilted-pulse-front laser pulse with a 1.05-µm central wavelength, $\theta = 64.5°$ ($n_{eff} = 5.12$), $\tau_0 = 300$ fs, and three different values of $I_0$. For $I_0 = 70$ GW/cm$^2$, the precursor magnitude (in free space) exceeds 250 kV/cm and its length is about 1 mm. By slightly decreasing the tilt angle $\theta$ to 64°, the field in the precursor can be enhanced up to 500 kV/cm but at the expense of its shorter duration (Fig. 3).
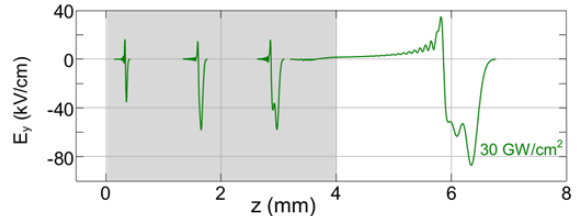


**Fig. 4.** Snapshots of the electric field $E_y$ generated in a ZnTe crystal by the tilted-pulse-front ($\theta = 33°$) laser pulse with $I_0 = 30$ GW/cm$^2$ and $\tau_0 = 200$ fs. The crystal (shaded region) is 4 mm thick.

Recently, a highly efficient monolithic semiconductor THz source was proposed and experimentally demonstrated [5]. In this source, ZnTe is pumped at 1.7 µm to avoid two-, and three-photon absorption. Pulse-front tilt of ~28° is provided by a grating formed on the entrance surface of the crystal. This structure can be used for generating dc precursors. For example, Fig. 4 shows the precursor with the electric field stronger than 50 kV/cm generated in a 4-mm ZnTe by the laser pulse with the pulse-front tilt angle of 33°.

## References

1. *Bakunov, M.I., Maslov, A.V., Tsarev, M.V.* Optically generated terahertz pulses with strong quasistatic precursors // Phys. Rev. A. 2017. V. 95, No. 6. P. 063817.

2. *J. Hebling, J., Almasi, G., Kozma, I.Z., Kuhl, J.* Velocity matching by pulse front tilting for large-area THz-pulse generation // Opt. Express. 2002. V. 10. P. 1161-1166.

3. *Dietze, D., Unterrainer, K., Darmo, J.* Dynamically phase-matched terahertz generation // Opt. Lett. 2012. V. 37. P. 1047-1049.

4. *Bakunov, M.I., Bodrov, S.B., Tsarev, M.V.* Terahertz emission from a laser pulse with tilted front: Phase-matching versus Cherenkov effect // J. Appl. Phys. 2008. V. 104. P. 073105.

5. *Fulop, J.A., Polony, G., Monoszai, B., Andriukatis, G., Balciunas, T., Pugzlys, A., Arthur, G., Baltuska, A., Hebling, J.* Highly efficient scalable monolithic semiconductor terahertz pulse source // Optica. 2016. V. 3. P. 1075-1078.

# Generation of sub GV/m longitudinal terahertz electric fields from intense laser-solid density plasma interactions

A. Woldegeorgis[1, 2], T. Kurihara[3], M. Almassarani[1, 2], R. Große[2], B. Beleites[2], F. Ronneberger[2], and A. Gopal[1, 2]

[1]Helmholtz-Institut Jena, Jena, 07743, Germany, abel.woldegeorgis@uni-jena.de
[2]Friedrich-Schiller-Universität Jena, Institute of Optics and Quantum Electronics, Jena, 07743, Germany
[3]University of Konstanz, Department of Physics, Konstanz, Germany

**We report on the generation and detection of longitudinal terahertz transient, with field strength in excess of 0.15 GV/m, by focusing a radially polarized terahertz beam emitted from the rear surface of a thin metal foil irradiated with a terawatt laser pulse. A noncollinear electro-optic detection technique was employed to determine the temporal waveform, spectral content and peak electric field strength of the transverse and longitudinal polarization components at the focus.**

High-power broadband terahertz (THz) radiation can be generated when an intense laser pulse interacts with matter. When the intensity of the laser pulse is higher than the ionization potential, plasma is generated. The charged particle dynamics and the resultant quasi-static fields and currents generated inside the plasma give rise to broadband electromagnetic radiation ranging from x-rays to THz radiation. In our work, we focus on the generation of a radially-polarized THz radiation from such interaction, in particular from the rear surface of a metal foil when its front surface is shined with a terawatt laser pulse. Focusing a radially THz polarized beam, compared to a linearly polarized beam, creates a strong and tightly focused longitudinal field. Owing to their fundamental characteristics, on-axis longitudinal THz fields have a promising potential in particle acceleration[1]. To date, few groups have reported on longitudinally polarized THz wave generation with field strengths higher than hundreds of kV/m up to 1.1 MV/m[2].

In this paper, we present a scheme to generate a single-cycle and longitudinally polarized THz transient with a record-breaking field amplitude of 0.15 GV/m. We performed the experiment at JeTi 40TW laser system of the University of Jena. Here, a radially polarized THz radiation is generated by the transient dynamics of charged particles exiting the rear surface. The THz beam, after collection and collimation, is focused on an electro-optic crystal by using an *f/1.5* off-axis parabola (Numerical aperture (NA) =0.33).

Noncollinear electro-optic technique was deployed to estimate the peak electric field and study the temporal and spectral properties. 100 μm and 500 μm thick gallium phosphide (GaP) electro-optic crystals cut in (110) – and (100) – orientations were placed at the focus of the THz beam to measure the transversal ($\varepsilon_r$) and the longitudinal ($\varepsilon_z$) field components respectively. The temporal waveforms of the transverse and the longitudinal fields are plotted in Fig. 1 and the corresponding spectral amplitudes are depicted in the

inset. Furthermore, a phase difference of $\pi/2$ between the two components, which is universal[3], can be observed from the temporal profile.
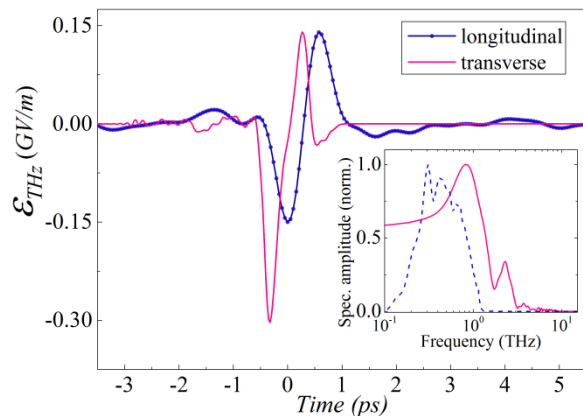


**Fig. 1.** Temporal waveform of the transverse ($\varepsilon_r$) and longitudinal ($\varepsilon_z$) field components measured at the focus of the THz beam measured using gallium phosphide (GaP) 110- and 100-cut crystal respectively. Inset shows the corresponding spectral amplitudes.

At the focus of the THz beam, a longitudinal field with 0.15 GV/m and a transverse field with 0.3 GV/m field amplitudes were measured. This is equivalent to a longitudinal-to-transverse field ratio of 0.5, comparable to the theoretical calculation of 0.43. In principle, it is possible to achieve even higher longitudinal field strength by employing a high NA focusing optics.
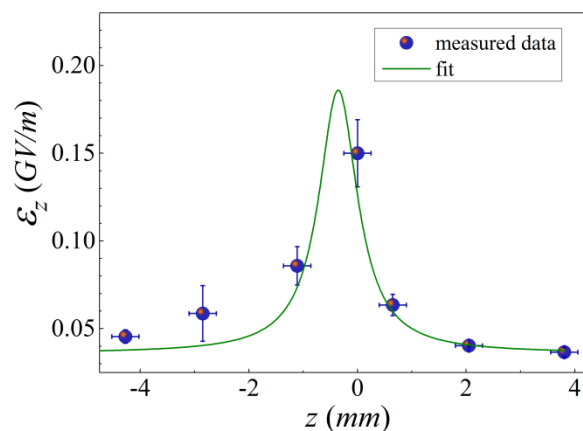


**Fig. 2.** Longitudinal field amplitude for different $z$-positions; the blue spheres are the measured mean $\varepsilon_z$ with shot-to-shot fluctuations indicated by the error bars (SEM).

Further analysis also determines that the THz pulse exhibits a single-cycle waveform with pulse duration of 600 fs and 220 fs for longitudinal and transverse polarizations respectively. This difference in pulse duration and spectrum between the two polarizations is attributed to the difference in the electro-optic response function, which depends on thickness, of the two crystals used here.

A $z$-scan was performed by translating the GaP crystal along the THz propagation direction in order to determine the nominal focal position and also to study the evolution of the amplitude and phase of the longitudinal field component. The peak amplitude as a function of $z$-position is shown in Fig. 2.
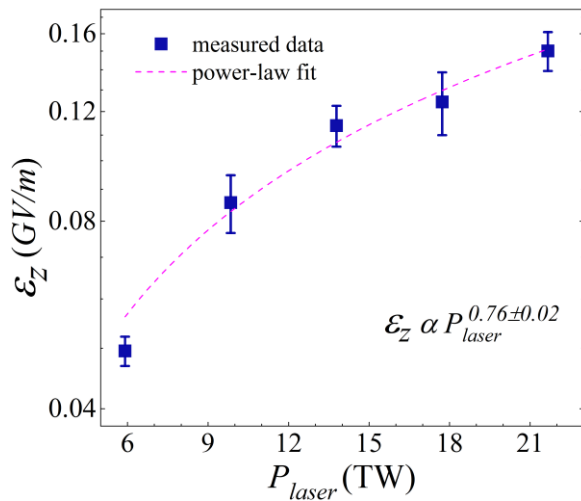


**Fig. 3.** Scaling of the longitudinal THz field amplitude as a function of incident laser power.

The influence of the driving laser power ($P_{laser}$) on the longitudinal field strength was also studied. The laser power was varied by changing the pulse energy while keeping the pulse duration and focusing condition unaltered. The fit to the measured data, plotted in Fig. 3, shows that $\varepsilon_z$ scaling with $P_{laser}$ follows a power-law of coefficient of $P_{laser}^{0.76\pm0.02}$.

To summarize, a longitudinally polarized THz pulse with field strength of 0.15 GV/m was generated and detected. To the best of our knowledge, this is the strongest longitudinally polarized THz radiation reported so far. In addition, a transverse field, albeit off-axis, with field strength of 0.3 GV/m was also measured at the focal plane. The availability of such a powerful source of longitudinal THz fields would enable efficient acceleration of charged particles in free space and novel experiments in nonlinear spectroscopy of 2D materials, etc.

### References

1. *Nanni, E., Huang, W. R., Hong, K.-H., Ravi, K., Fallahi, A., Moriena, G., Miller, R. J. D., and Kärtner, F.* Terahertz-driven linear electron acceleration // Nat. Commun. 2015, V. 6, No. 8486. P. 1–8.

2. *Minami, Y., Kurihara, Y., Yamaguchi, Y., Nakajima, M., Suemoto, T.* Longitudinal terahertz wave generation from an air plasma filament induced by a femtosecond laser // *Appl. Phys. Lett.* 2013. V. 102. No. 151106. P. 1-3 : Cliffe, M. J., Graham, D. M., and Jamison, S. P. Longitudinally polarized single-cycle terahertz pulses generated with high electric field strengths // *Appl. Phys. Lett.* 2016. V. 108. No. 221102. P. 1-4.

3. Winnerl, S., Zimmermann, B., Peter, F., Schneider, H., and Helm, M. Universal phase relation between longitudinal and transverse fields observed in focused terahertz beams // *New J. Phys.* 2012. V. 14. No.103049,P.1-12.

# Generation of terahertz radiation on the difference frequency in ZnGeP₂

N. N.Yudin [1], A.I. Gribenyukov[2], V.V. Dyomin[3] , I.G.Polovtsev[3]

[1] Laboratory of optical crystals, Tomsk, Russia, rach3@yandex.ru
[2] Institute of monitoring of climatic and ecological system SB RAS, Tomsk, Russia
[3] National Research Tomsk State University, Tomsk. Russia

In recent years terahertz (THz) range of the electromagnetic spectrum ~ of 0.2-2 THz is intensively investigated. Advances in laser physics, nonlinear optics, semiconductor physics and microwave electronics, stimulated a surge of interest of researchers to this region of the spectrum. Creation of powerful pulse sources of coherent terahertz radiation is an urgent task. For Efficient parametric generation requires the use which have high penetrating ability and radiation in THz range is a highly efficient diffrent frequency generation conversion of radiation of well-established lasers middle IR range 2. For Efficient diffrent frequency generation requires the use of crystals with high optical transparency in the frequency range (at all wavelengths of pump, signal and idler waves), with large value of quadratic nonlinear susceptibility, with high optical breakdown threshold and spatial uniformity. the ZnGeP2 single crystal is the most promising for the generation of radiation in THz range by its characteristics (from a wide variety of nonlinear optical crystals)[1-4].

Today in countries such as Russia, USA and China were developed and implemented to production tunable high-power sources operating in the spectral range of ~ 3-4 μm, which are a key element of the counteraction systems from infrared sensors, also have found application in medicine and spectroscopy. These sources represent an optical parametric oscillator which is pumped by a laser with a wavelength of ~ 2 μm. As a source of modulated radiation with a wavelength of 2,097 μm is used Ho:YAG laser with optically pumped by radiation of a Tm:YLF laser. The conversion efficiency in this scheme reaches ~ 50 %, while implementing a level of average output power of ~ 15 W 8-9. This laser source has small overall dimensions and service life ~ 10,000 hrs.

is considered possibility of creating a source of terahertz radiation by pumping a parametric oscillator based on single crystal ZnGeP2 by parametric radiation of mid-IR range tunable sources. Generation of the difference frequency THz range radiation is expected to implement from single crystal ZnGeP2 with pumped by two parametric sources based on the ZnGeP2 single crystals with optically pumped Ho:YAG laser, according to the scheme shown in Fig.1.
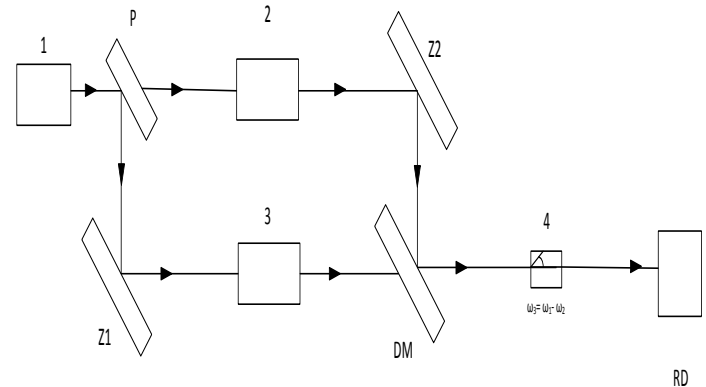


**Fig. 1.** Diagram of the tunable terahertz source, where: 1 – Ho:YAG laser; 2 – optical Parametric oscillator based of ZnGeP2; 3 – tunable optical Parametric oscillator based of ZnGeP2; L - lens; P - dividing plate; Z1, Z2 - blind mirror; DM - dichroic mirror; 4-single crystal ZnGeP2; RD - registered device.

The analysis showed the possibility of creating terahertz radiation sources with the possibility of wavelength tuning in a wide range based on the generation of radiation of the difference frequency in the nonlinear optical crystal ZnGeP2 with pumping radiation tunable laser sources of the mid-IR range based on the parametric oscillator based on nonlinear ZnGeP2 crystal

## References

1.Shi W., Ding Y.J. // Appl. Phys. Let. 2003.V.83. P.848

2. Tanabe T., Suto K., Nishizawa J., Sasaki T. // J. Phys. D: Appl. Phys. 2004. V.37. P. 155-158.

3. Luo C., Reimann K.,Woerner M., Elsaesser T. // Appl. Phys. 2004. V.A78. P. 435- 440

4. Shi W., Ding Y.J. // Appl. Phys. Lett. – 2004. – V.84. – P. 1635-1637

# Coherent Multichannel Dynamics of Aligned Molecules Resolved by Two Dimensional High-Harmonic and Terahertz Spectroscopy（2D-HATS）

Dongwen Zhang[1], Yindong Huang[1], Zengxiu Zhao[1], and Jianmin Yuan[1,2]

[1]Department of Physics, National University of Defense Technology, Changsha, China, dwzhang@nudt.edu.cn
[2]Graduate school of China Academy of Engineering Physics, Beijing, China

There are infinity ways of breaking atoms or molecules into parts, each of which is associated with a "channel". As one of the fascinating natures of the quantum world, all the channels are indeed coherent which could manifest as entanglement of the individual parts. By controlling the coherence among different channels, quantum dynamics, e.g, chemical reactions, can be steered through quantum interference. With the rapid developing of atto-technology, such coherent manipulation has advanced from controlling nuclear motion into electron dynamics pushing the field of femtochemisty into attochemistry.

With pump-probe schemes, the dynamics can be monitored in the time domain. However it often takes a great deal of efforts to identify the dominant quantum channels and to retrieve the related quantum phases in mulitelecrtron dynamics. It is therefore intriguing to "zoom in and out" by measuring the electron dynamics in distinct spectral range covering frequency of more than 5 orders of magnitudes with our recently developed high-harmonic and terahertz spectroscopy (HATS) technique [1, 2].

In this work we combine the simultaneous measurement of terahertz (THz) wave and high harmonic emission to resolve the coherent multichannel electron dynamics of aligned $CO_2$ molecules driven by femtosecond laser pulses. Based on the single electron picture, high harmonic generation (HHG) can be understood by the rescattering model. Within each half optical cycle, the electron is accelerated away from the ion following tunneling ionization, and then driven back to recombine into the original state generating attosecond burst. For multielectron systems, however, the ionization could leave the ions in different cofigurations. In terms of the concept of molecular orbital (MO), HHG process can start from and end in the same orbitals, either the highest occupied MO (HOMO) or the lower lying MOs (HOMO-1or HOMO-2) (for example) of $CO_2$ molecules. As shown in Fig. 1, each participating orbital is associated to a particular channel and the total harmonic emission is their coherent summation. The amplitude and the phase of each channel that are to be scrutinized are related to the ionization, propagation and recombination of electron wave packets. Different from HHG, THz emission can be attributed to the coherent current generated by the continuum electron from all the channels. Combing measurement of both radiations for alignment controlled molecules, it is possible to resolve the coherence between these channels by observing in full details of the related dynamics.

As illustrated in Fig. 1(a), a two-color pulse consisting of the 800nm fundamental pulse and its second harmonics is acting on the $CO_2$ molecular gases which are prealigned by the aligning pulse. Due to the weak second harmonic, the symmetry between the consecutive half cycle is broken generating the even harmonics and the terahertz (THz) wave. All these emissions from one physical process are inherently phase-locked, making the synchronous modulation over a large spectral range possible. The measured harmonic spectra and the time profile of THz wave are shown for examples in Fig. 1(c) and (e). The transient molecular alignment can be monitored, e.g., the yields of 25th harmonic (H25) as a function of the time-delay between the aligning pulse and the two-color pulse (see Fig. 1(b)). At the revival moment that the molecules are aligning maximumly, the modulation of harmonics yield and THz yields are simultaneously measured against the dual-color relative phase (DRP) between the fundamental and the second harmonic. The measurements repeat for different polarization of the two-color pulse. We thus obtain the two-dimensional (alignment and DRP) dependent HATS (2D-HTAS).
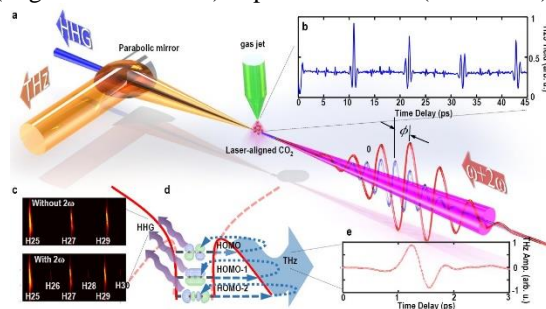


**Fig. 1.** Schematic diagram of 2D-HATS

Unlike the perpendicular dual-color method, we employ the parallel polarized dual-color fields to form the Michelson interferometry in time domain of HHG. Through controlling the DRP and the molecular alignment, the quantum phases and the contributions of multiple MOs are manipulated, enabling us to tune the complex amplitude of the contributions from different generating channels. While the harmonic yields reflect the coherence of the HHG channels each of which is involved of the three steps, the generation of THz wave is sensitive to the ionization process which measures the coherence of ionization from different orbitals. The temporal profile of THz radiation shown in Fig. 1(e) implies that THz generation can be considered as a rectification of the driving laser pulse via current injection which is the tunneling ionization in the present situation. Previously, we have shown that the THz yields from dual-color laser pulses can serve as a robust measure to calibrate the DRP and the

alignment-dependent ionization probability. With the 2D-HATS, we are able to resolve the tunneling phase and the coherence of multichannel electron dynamics.

The *in site* manipulation on the generation process can be treated as an optical modulator for the corresponding emissions, as well as the combined attosecond pulse. In the present work, all three steps of the rescattering process are controllable. We achieve 2 degrees angular tuning of the harmonic minima by controlling the electron dynamics. Our method is not only an alternative to for the further investigations on multi-channel dynamics, but also an approach for in site shaping attosecond emissions, which helps the direct application of attosecond extrume ultraviolet (XUV).

Using this THz phase benchmark, the optimal phase (OP) of the even harmonics jumps between different aligned angles for harmonics from 28 to 32. It should be noted that the intensity modulations of harmonic 26 vanishes for alignment angle less than 40 degrees, while the regular modulations clearly reappear around the perpendicular alignment. This can be understood by considering the participation of the lower-lying orbitals other than the highest occupied molecular orbital (HOMO). We compare the experimental deduced OPs for different even harmonics to the calculated for HOMO, HOMO-1 and HOMO-2 respectively. The OPs for harmonic 22 and 24 maintain nearly unchanged at all aligned angles, which agrees with the calculation results from HOMO. However, the discrepancies become so great for harmonic from 28 to 32 that only by considering the interference between the multi-channels can the experiment results be explained.

In conclusion, we demonstrate the 2D-HATS measurements on $CO_2$ molecules to resolve the phase and amplitude of multi-channel dynamics within harmonic generation process. Our measurements take advantage of the synchronous measurements on THz yields to give a benchmark on the alignment dependent ionization and the phase between the dual-color fields. Former researches only modify the phase of the action accumulated within the propagation, which is between the moment of ionization and the moment of re-collision. As we advance this to polyatomic systems, in which multi-channel dynamics are expected to be observed, our approach can alter the ratio between different participated channels. We also show the control on the harmonic minima angles via tuning the DRPs and the aligned angle, i.e. the propagation and the recombination of the electronic wavepacket. Our demonstrated approach to measuring the electronic process via a large spectral range provides a new tool for detecting and resolving these multi-electron phenomena.

Furthermore, this dual-color method also hold the potential of observing and controlling the unobserved electronic dynamics. For instance, the attochirp of the generalized attosecond pulse trains can be varied by tuning the DRP, which can be served as a chirp-modulatable light source to conduct the pump-probe experiment.

### References

1. *Zhang, D. W., Lv Z. H., Meng C., Du X. Y., Zhou Z. Y., Zhao Z. X., Yuan J. M.* Synchronizing terahertz wave generation with attosecond bursts // Phys. Rev. Lett. 2012. V. 109, 243002.

2. *Huang, Y. D., Meng, C., Wang X. W., Lv Z. H., Zhang D. W., Chen W. B., Zhao J., Yuan J. M., Zhao Z. X.* Joint measurements of terahertz wave generation and high-harmonic generation from aligned nitrogen molecules reveal angle-resolved molecular structures // Phys. Rev. Lett. 2015. V. 115, 123002.

# A modified tilted-pulse-front excitation scheme for efficient terahertz generation in LiNbO₃

S.B. Bodrov,[1,2] A.N. Stepanov[2], E.A. Burova[1], and M.I. Bakunov[1]

[1]University of Nizhny Novgorod, Nizhny Novgorod 603950 Russia
[2]Institute of Applied Physics of the Russian Academy of Sciences, Nizhny Novgorod 603950 Russia

Pumping of LiNbO₃ by femtosecond optical pulses with tilted intensity front (pulse front) allows one to obtain high efficiency of optical-to-terahertz conversion (up to 1% at room temperature [1]), large energy of generated terahertz pulses (up to sub-mJ level [2]), and high strength of terahertz fields (exceeding 1 MV/cm [3]). Strong terahertz pulses are in demand for various applications, including terahertz-driven particle acceleration [4], terahertz nonlinear spectroscopy [5], and terahertz streaking techniques [6].

Tilted-pulse-front optical pulses are conventionally obtained by diffraction of a laser pulse off an optical grating. A lens (or two-lens telescope) is used to relay-image such pulses into the LiNbO₃ crystal [7,8]. In order to maximize the optical-to-terahertz conversion efficiency, the tilt angle $\alpha$ in the crystal should be close to a value defined by the equation $\cos\alpha = n_g / n_{\text{THz}}$, where $n_g$ is the optical group refractive index and $n_{\text{THz}}$ is the terahertz phase refractive index. Additionally, it is postulated that a good quality of the terahertz beam can be achieved if the image of the grating is parallel both to the pulse front and to the exit surface of the crystal [7,8].

Here, we extend the analysis of the tilted-pulse-front excitation scheme [7,8] to a more general geometry, namely, with the pulse front not parallel to the exit surface of the crystal (the grating image is still assumed to be parallel to the surface).

In our theory, the generated terahertz radiation is found analytically from the Maxwell equations with a nonlinear polarization included as a source [9,10]. The nonlinear polarization is found as a result of optical rectification of the tilted-pulse-front optical pulse, which experiences effects of both material and angular dispersion.

At first, we consider the conventional geometry of the tilted-pulse-front excitation scheme, i.e., with the pulse front parallel to the exit surface of the crystal, but for an arbitrary orientation of the grating image plane, defined by the angle $\theta$ [Fig. 1(a)]. Figures 1(b)-(e) show the effects of the grating image orientation on the efficiency and spatial distribution of the generated spectrum along the exit surface of the crystal (y-axis). In the optimal case, when $\theta = \alpha$, the spectrum distribution is rather uniform [Fig. 1(d)]. For $\theta \neq \alpha$, the bandwidth and shape of the spectrum varies considerably with $y$ [Figs. 1(c) and 1(e)]. The spectral non-uniformity across the terahertz beam can give strong divergence of the beam and prevent its further focusing. Interestingly, for $\theta < \alpha$, the spectral amplitude in the interval $-5 < y < -1$ mm is larger than for the optimal configuration $\theta \neq \alpha$ [Figs. 1(c)

and 1(d)]. As a result, the energy of generated terahertz radiation does not decrease and even somewhat increases at a deviation of $\theta$ from the optimal value $\theta = \alpha$ to $\theta < \alpha$ [Fig. 1(b)]. In the case $\theta > \alpha$, the terahertz energy [Fig. 1(b)] and maximal spectral amplitude [Fig. 1(e)] decrease rapidly with deviation of $\theta$ from $\alpha$.
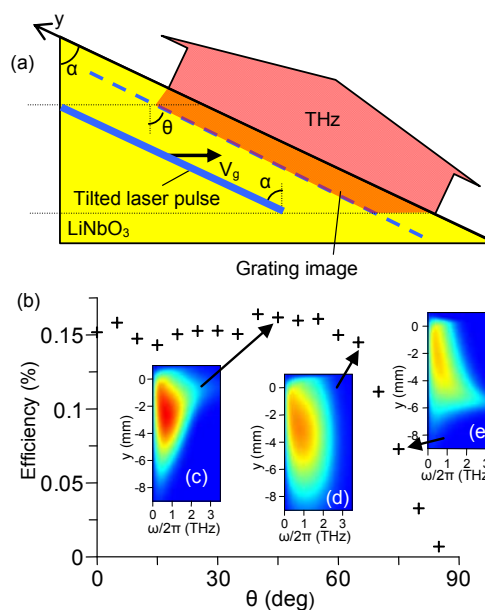


**Fig. 1.** (a) The conventional geometry of the tilted-pulse-front excitation technique with the pulse front parallel to the exit surface of the crystal. (b) Efficiency as a function of $\theta$. (c-e) Distribution of the amplitude spectrum near the exit surface for (c) $\theta = 45°$, (d) $\theta = \alpha = 63.3°$, and (e) $\theta = 75°$. The optical pulse has a 3 mm transverse size and 100 fs duration.

Now let us consider a more general geometry, depicted in Fig. 2, with the pulse front not parallel to the exit surface of the crystal (the grating image plane is assumed to be parallel to the exit surface). In this geometry, the generated terahertz radiation propagates normally to the pump pulse front and, therefore, impinges obliquely on the exit surface of the crystal. To prevent total internal reflection of the radiation and minimize Fresnel losses, a Si prism should be attached to the exit surface of the LiNbO₃ crystal (Fig. 2).
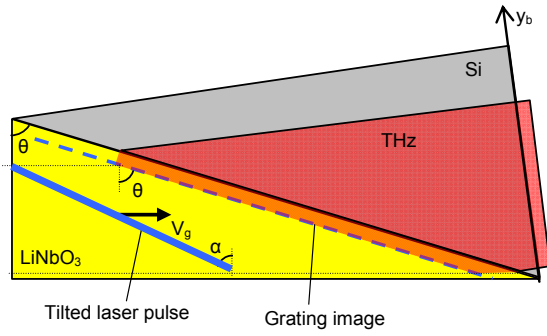
20

**Fig. 2.** The generalized tilted-pulse-front excitation geometry with the pulse front not parallel to the exit surface of the crystal.

Figures 3(a) and 3(b) show the distributions of the amplitude frequency spectrum along the exit boundary of the Si prism ($y_b$-axis) for two different angles $\theta = 45°$ and $\theta = 75°$, respectively. The distributions are rather uniform, similar to the optimal case in Fig. 1(d), and have practically the same spectral bandwidth for both angles. However, the maximal value of the spectral amplitude and size of its spatial localization differ substantially. The maximal value of the spectral density is two times higher for $\theta = 45°$ than for $\theta = 75°$, but the size of the terahertz beam is 2-3 times lager for $\theta = 75°$. The last fact is explained by a larger projection of the pump beam on the exit boundary of the LiNbO$_3$ crystal.
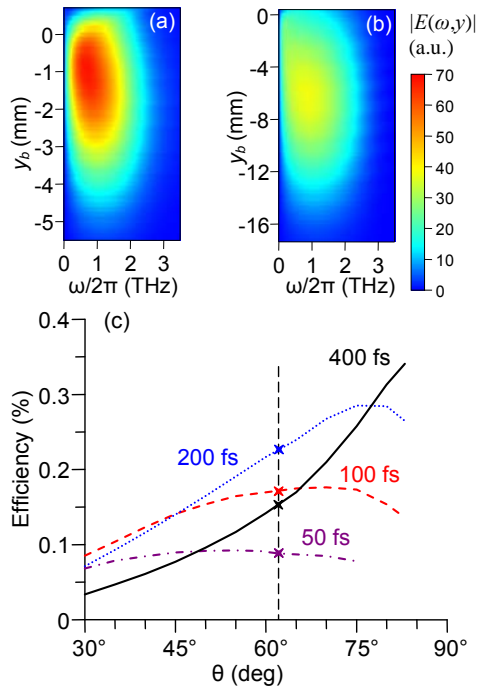


**Fig. 3.** Distribution of the amplitude spectrum along the exit boundary of the crystal for (a) $\theta = 45°$ and (b) $\theta = 75°$. (c) The conversion efficiency as a function of $\theta$ for different pulse durations. The optical pulse energy is fixed and corresponds to 10 GW/cm$^2$ at a pulse duration of 100 fs. The pump beam transverse size is 3 mm. Vertical line marks the optimal case $\theta = \alpha$.

Figure 3(c) shows the optical-to-terahertz conversion efficiency as a function of $\theta$ for different pump pulse durations. For a short pump pulse (50 fs), the efficiency is almost independent of $\theta$ in the interval from 30° to 75° and decreases rapidly for $\theta > 75°$. With increase of the pump pulse duration, the maximum becomes more pronounced and shifts to larger $\theta$. The maximal efficiency also increases (for a fixed energy of the pump pulse) and for pulse duration >100 fs exceeds the efficiency in the optimal case. For the pump pulse of a 400 fs duration, the maximum efficiency at $\theta \approx 85°$ is about two times higher than in the optimal geometry, i.e., at $\theta = \alpha = 63.3°$.

To conclude, we have shown that a deviation of the grating image plane from the optimal orientation in the tilted-pulse-front excitation technique leads to a deterioration of the terahertz beam quality but does not affect significantly the terahertz energy (in the case $\theta < \alpha$). We have proposed a modified variant of the tilted-pulse-front excitation scheme with the pulse front not parallel to the exit surface of the crystal. We have shown that this geometry allows one to double the terahertz generation efficiency for long (>200 fs) laser pulses still preserving a high quality of the generated terahertz beam.

**References**

1. *S.-W. Huang, E. Granados, W. R. Huang, K.-H. Hong, L. E. Zapata, and F. X. Kärtner.* High conversion efficiency, high energy terahertz pulses by optical rectification in cryogenically cooled lithium niobate // Opt. Lett. 2013. V. 38. P. 796.

2. *J. A. Fülöp, Z. Ollmann, C. Lombosi, C. Skrobol, S. Klingebiel, L. Pálfalvi, F. Krausz, S. Karsch, and J. Hebling.* Efficient generation of THz pulses with 0.4 mJ energy // Opt. Express. 2014. V. 22. P. 20155.

3. *H. Hirori, A. Doi, F. Blanchard, and K. Tanaka.* Single-cycle terahertz pulses with amplitudes exceeding 1 MV/cm generated by optical rectification in LiNbO$_3$ // Appl. Phys. Lett. 2011. V. 98. 091106.

4. *E. A. Nanni, W. R. Huang, K.-H. Hong, K. Ravi, A. Fallahi, G. Moriena, R. J. Miller, and F. X. Kärtner.* Terahertz-driven linear electron acceleration // Nat. Commun. 2015. V. 6. P. 8486.

5. *S. Bodrov, Yu. Sergeev, A. Murzanev, and A. Stepanov* Terahertz induced optical birefringence in polar and nonpolar liquids // J. Chem. Phys. 2017. V. 147. P. 084507.

6. *U. Fruhling*, Light-field streaking for FELs, // J. Phys. B. 2011. V. 44. P. 243001.

7. *J. A. Fülöp, L. Pálfalvi, G. Almási, and J. Hebling.* Design of high-energy terahertz sources based on optical rectification // Opt. Express. 2010. V. 18. P. 12311.

8. *L. Tokodi, J. Hebling, and L. Pálfalvi.* Optimization of the tilted-pulse-front terahertz excitation setup containing telescope // J. Infrared Milli. Terahz. Waves. 2017. V. 38. P. 22.

9. *M. I. Bakunov, S. B. Bodrov, and E. A. Mashkovich.* Terahertz generation with tilted-front laser pulses: dynamic theory for low-absorbing crystals // J. Opt. Soc. Am. B 2011. V. 28. P. 1724.

10. *M. I. Bakunov and S. B. Bodrov.* Terahertz generation with tilted-front laser pulses in a contact-grating scheme // J. Opt. Soc. Am. 2014. V. 31. P. 2549.

# Laser induced THz Sommerfeld waves along metal wire

A.V.Brantov[1,2], A.S.Kuratov[1], A. Maksimchuk[3], Yu. M. Aliev[2] and V.Yu.Bychenkov[1,2]

[1] Dukhov Research Institute of Automatics (VNIIA), Moscow, Russia, brantov@lebedev.ru
[2] P.N. Lebedev Physics Institute, Russian Academy of Sciences, Moscow, Russia
[3] Center for Ultrafast Optical Science, University of Michigan, Ann Arbor, USA

The thin metal wires can be utilized for guiding electron bunches [1, 2] as well as surface waves [3] during generation from irradiation of a wire target by short relativistically intense laser pulse. In such interaction a strong impulse type Thz surface wave can be excited at the metal surface due to a current of the high energy escaping electrons and electric sheath formation. These waves may propagate along wire without strong damping in the form of Sommerfeld wave. In this paper the electron bunch guiding along wire and supported by strong Sommerfeld surface wave is modeled and compared with experimental results.

To describe the initial stage of electron bunch formation and electromagnetic surface wave formation we have performed PIC simulation of laser-wire interaction considering a target as a plasma cylinder with given plasma density. The 3D simulations have been performed by using 3D PIC code Mandor and commercial code VSim (Vorpal). As example, we illustrate our findings with the following parameters. A linearly polarized laser pulse with maximum intensity of $(1-3)\times10^{19}$ W cm$^{-2}$ has a Gaussian shape in both the temporal (FWHM duration $\tau_0 = 50$ fs) and transverse dimensions (FWHM focal spot size $d = 4$ μm). The maximum intensity corresponds to dimensionless laser field amplitude $a_0 = (2.7-4.7)$ for laser wavelength $\lambda = 1$μm. The laser is focused at the front surface of a cylindrical plasma target (with the axis along Y) with diameter of 8 μm consisting of electrons and heavy ions ($Z m_i/m_e = 4 \times 1836$). The plasma density is $5n_c$ ($n_c$ is the electron critical density) inside interaction aria (cylinder piece of 10μm length from the focal spot center in both directions) and $2n_c$ outside. The simulation box has the size $x\times y\times z = 20$μm$\times200$μm$\times20$μm and the spatial resolution is $\Delta$, $x\times\Delta y\times\Delta z = 0.02$μm $\times0.1$μm $\times0.05$μm.

The electron density after irradiation of a wire by laser pulse focused in the wire center is presented in Fig.1. Two symmetrical electron bunches propagated along wire from interaction area with velocity of the order of speed of light are clearly seen. Under the action of laser pulse, significant number of electrons inside a hot spot is heated to the high, multi-MeV, energies. The most of them form a sheath field electrostatic structure around wire as uncompensated positive target charge prevented them from escaping. At the same time, these electrons propagates along wire increasing a heated target surface, the length, $L_0$, of which is defined by the initial focal spot size, laser pulse duration and characteristic electron cooling time, i.e. $L_0 \sim d + c(\tau_0 + \tau_c)$ [4]. This heated area size roughly coincides with electron bunch longitudinal size, which is formed after a laser pulse termination.

Because of the symmetry of electron bunch generation, several simulation runs have been performed with laser pulse, which was focused near the wire edge. It has been confirmed that the electron bunch length increases with laser pulse duration reaching the value $L_0 \sim c\tau_0$ for $\tau_0> 300$ fs. The simulations show that all electrons forming a bunch originate from the laser-target interaction area and electrons moving along a wire are accompanied by the propagating surface electromagnetic wave (see Fig. 2). The amplitude of this electromagnetic wave is much high as compared to the intrinsic electron bunch filed.
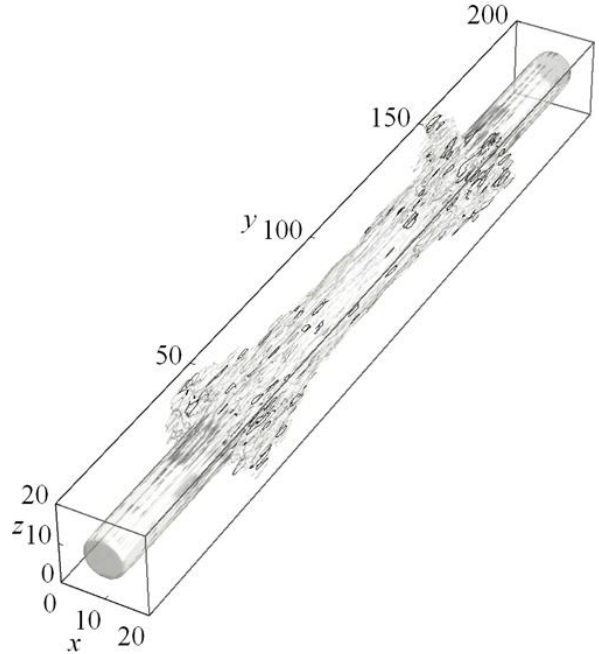


**Fig. 1.** Electron density contour plot at instant of 350 fs after wire irradiation by laser pulse with $a_0 = 2.7$.
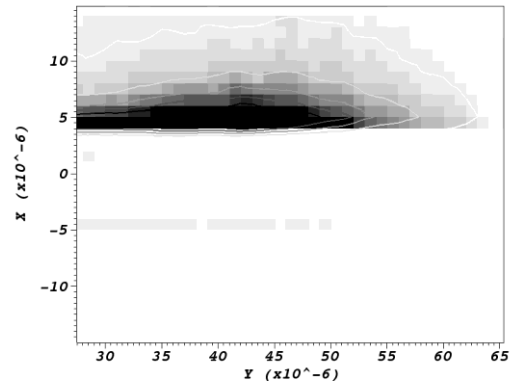


**Fig. 2.** Transversal (x>0) and longitudinal (x<0) electric field distributions in x-y plane at the instant of 350 fs after wire irradiation by laser pulse with $a_0 = 4.7$. Wire lies be-

tween x = -4 and x = 4 and a laser pulse is focused to y = 10µm.

The theory of Sommerfeld surface wave generation due to current of heated electrons has been developed. Based on solution of Maxwell equations the surface wave profile in a wave zone (far field) has been calculated. Expression for the magnetic field outside a wire with the radius $R$ generated due to the radial electron current density, $j_r$, has the following form

$$B^s = \frac{2}{cR} \int \frac{d\omega\, k^s K_1\left(k_+^s r\right)}{k_+^{s2} d'\left(k^s, \omega\right)} e^{i\left(\omega t \pm k^s z\right)} \int_R^\infty dx \frac{x K_1\left(k_+^s x\right)}{K_0^2\left(k_+^s R\right)} j_r(x)$$

Here $k_+^2 = k^2 - \omega^2/c^2$, $k_-^2 = k^2 - \varepsilon\omega^2/c^2$, $\varepsilon$ is wire dielectric permittivity, $I_{(0,1)}$, $K_{(0,1)}$ are the modified Bessel functions and $k^s$ is a solution of the standard dispersion relation for Sommerfeld wave $d=0$, where

$$d(k, \omega) = \frac{K_1\left(k_+ R\right)}{k_+ K_0\left(k_+ R\right)} + \frac{\varepsilon I_1\left(k_- R\right)}{k_- I_0\left(k_- R\right)}$$

As a radial current we have used both the current of the electrons forever leaving a target and the current of hot electrons forming a sheath structure. We assumed the Gaussian current profile along the wire with characteristic length of $L_0$, as well as the temporal Gaussian profile (with characteristic time scale of $\tau_0$). We also assumed that heated electrons move in $r$-direction with speed of light and have exponential distribution with characteristic scales of their Debay length, $r_{De}$. Density of the hot electrons can be estimated from energy balance, assuming 30% laser energy deposition to the electrons, an average hot electron energy from simple ponderomotive scaling $\sim a_0\, m_e c^2$ and the current volume $\sim L_0 2\pi R r_{De}$. Some of the electrons may overcome potential barrier and escape from the target. Escaping electron density depends on magnitude of the electrostatic potential and can be estimated as $\sim a_0 m_e c^2 / 2\pi e^2 R^2$. Based on the above estimates, one can calculate a polar magnetic field of the surface wave (see. Fig. 3). We conclude, that electron current due to the escaping electrons and due to those, which form a sheath give comparable contribution to Sommerfeld wave generation.
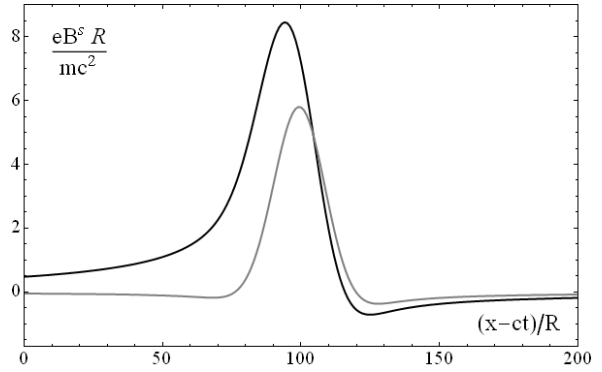


**Fig. 3.** Surface magnetic field at the tungsten wire boundary ($r=R=25$µm) for the laser pulse with $a_0 = 4.7$, d=4 µm and $\tau_0 = 400$ fs, generated due to the escaping electrons (black curve) and the sheath forming electrons (gray curve).

To conclude, the numerical simulations performed have shown a formation of relativistic electron bunches propagating along the wire together with electromagnetic surface waves in the process of wire target irradiation by short relativistically intense laser pulse.

### References

1. *Nakajima H., Tokita S., Inoue S., Hashida M., Sakabe S.* Divergence-free transport of laser-produced fast electrons along a meter-long wire target// Phys. Rev. Lett. 2013. V. 110. P. 155001

2. *A. Maksimchuk, P. Belancourt, M. J.-E. Manuel et al* Study of surface current confinement in high-intensity laser interactions with wire targets // Bull. Am. Phys. Soc. 2013. V. 58. P. 242; *A. Maksimchuk, P. Belancourt, P. Kordell et al.,* Guiding of high-energy electrons in high-intensity-laser interactions with wire targets through surface wave excitation // Bull. Am. Phys. Soc. 2014. V. 59, No. 15, NP8.00101

3. *Tokita S., Sakabe S., Nagashima T., Hashida M., Inou S.* Strong sub-terahertz surface waves generated on a metal wire by high-intensity laser pulses // Sci. Rep. 2015 V. 5. P. 8268.

4. *Kuratov A.S., Brantov A.V., Aliev Yu.M., Bychenkov V.Yu.* Laser-induced thermoelectric current as a source of generation of THz surface electromagnetic waves // Quantum Electronics 2018 V.48. No. 7. P. 653.

# Modulation of two-color laser-induced filament terahertz emission by effective length variation

P. A. Chizhov[1], A. A. Ushakov[1,2], V. V. Bukin[1], S. V. Garnov[1]

[1]A. M. Prokhorov General Physics Institute RAS, Moscow, Russia, pvch@inbox.ru
[2]Lomonosov Moscow State University, Moscow, Russia

Terahertz (THz) radiation is of great scientific interest for its applications in spectroscopy and imaging [1]. Terahertz generation in femtosecond filament in gases has the specific features as compared with other THz sources [2, 3]. As the gaseous media are self-healing, one can use high-energy laser pulse focusing into small volumes without concern about material damage. Here one of the most effective ways to produce THz radiation is to use two-color (usually fundamental and second harmonics of fs-laser) laser pulse focusing for plasma creation [3]. However, in this case the efficiency of optical-to-terahertz conversion is highly dependent on mutual phase difference between harmonics. Moreover, for long filaments this difference varies along plasma channel. It has been demonstrated previously that this effect leads to off-axis peak in spatial THz distribution [4] and to possibility of waveform control by initial phase shift adjustment between harmonics [5]. In atmospheric air the distance for $\pi$ phase walk-off between fundamental and second harmonic of Ti:Sapphire laser is about 25 mm.

In this paper, we show strong influence of phase matching between harmonics on overall THz power output and demonstrate that screening of a part of THz emission allows increasing the output power up to 20% of that for undisturbed emission. We also demonstrate the possibility of spectral modulation by means of $\pi$-retarder screens for a distinct THz frequency.
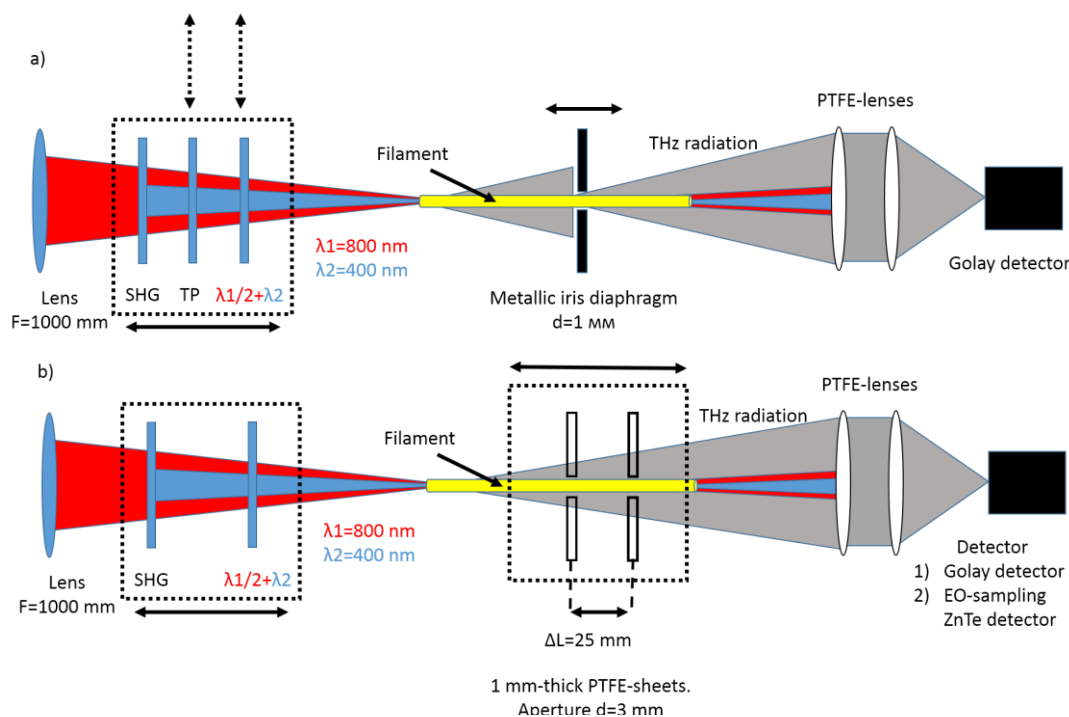
We use Ti:Sapphire laser system with following characteristics: 800 nm central wavelength, 40 fs pulse duration, 2.8 mJ pulse energy, $\varnothing$12 mm ($1/e^2$ level), 1 kHz repetition rate. A Glan-Taylor polarizer with a half-wave plate to control laser pulse energy is used.

A lens ($\varnothing$25.4 mm, 1000 mm focal length) focuses laser radiation to create a filament in ambient air. A BBO crystal (SHG, 10x10x0.2 $mm^3$, I-type) converting part of radiation into second harmonic is placed on the optical pump path before the plasma. After the SHG a group delay compensator plate (TP) and a dual-wave plate ($\lambda/2$@800 nm+$\lambda$@400 nm) may be placed to provide more powerful THz generation due to use of collinear polarizations of harmonics in two-color pulse. The SHG and plates are mounted on a moving table to change air path of two-color pulse before the filament and so the initial phase difference between harmonics.

To collect THz radiation a system of two PTFE-lenses (first: $\varnothing$50 mm, 150 mm focal length; second: $\varnothing$50 mm, 100 mm focal length) is used. Laser pulse duration is lengthened up to ~120 fs by adding positive chirp to maximize THz output [6]. The length of visible plasma string is approximately 80 mm for maximal laser pulse energy of 2.3 mJ.

A metallic iris diaphragm with a ~1 mm diameter aperture centered at filament is mounted to screen THz radiation emitted before its position. Another moving table is utilized to control the position of the iris along the filament. Corresponding scheme is de-



a)
λ1=800 nm
λ2=400 nm
Filament
PTFE-lenses
THz radiation
Golay detector
Lens F=1000 mm
SHG    TP    λ1/2+λ2
Metallic iris diaphragm d=1 мм

b)
Filament
λ1=800 nm
λ2=400 nm
PTFE-lenses
THz radiation
Detector
1) Golay detector
2) EO-sampling ZnTe detector
Lens F=1000 mm
SHG    λ1/2+λ2
ΔL=25 mm
1 mm-thick PTFE-sheets.
Aperture d=3 mm

modulation by $\pi$-retarder PTFE-screens.

picted on Fig.1 (a).

The second thing we want to realize is spectral and spatial modulation of the emitted THz radiation. The idea is to make the THz emission collected by PTFE-lenses from all the points along filament interfere constructively for a distinct THz frequency. So one need to insert additional $\pi$-retardation for the part of the THz radiation that has previously interfered destructively. Ideally, there should be also a non-zero on-axis value in THz power distribution in this case. Thus, instead of the metallic iris diaphragm we place a 1 mm-thick ($\pi$-retardation for ~0.7 THz) PTFE-sheet with ~3 mm diameter aperture or a set of 2 such screens with a 25 mm distance between them (the distance corresponding to $\pi$ walk-off in the air). Scheme is depicted on Fig.1 (b).
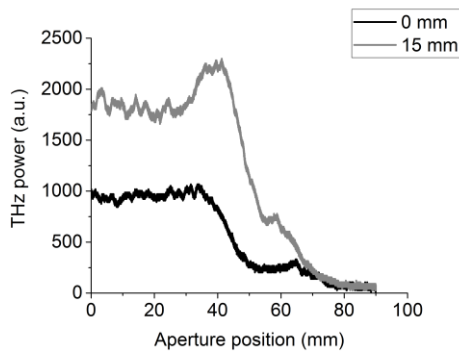


**Fig. 2.** Terahertz power dependence on iris diaphragm position along the filament created by 2.3 mJ laser-pulse for two positions of second harmonic crystal (SHG).
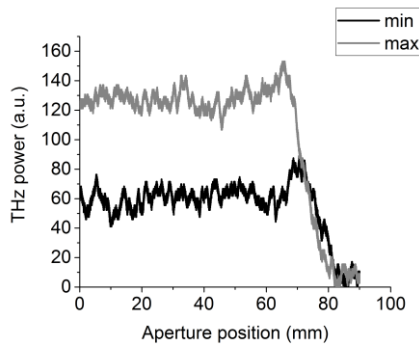


**Fig. 3.** Terahertz power dependence on iris diaphragm position along the filament created by 1.0 mJ laser pulse for two positions of second harmonic crystal (SHG).

For THz power measurements, a Golay cell (Tydex GC-1P) is used. For THz field measurements a standard electro-optical sampling scheme with ZnTe crystal (3x3x1 mm$^3$, <110> cut) is applied.

We measure THz power dependence on the iris diaphragm position along the two-color filament for different laser pulse energies from 1.0 to 2.3 mJ and for different initial phase difference between fundamental and second harmonics (SHG positions). We see strong influence on overall THz power due to constructive and destructive interference of THz emission from different parts of filament. For optimal initial phase and screening diaphragm position one can achieve significant increase in THz power. Exam-

ples of such dependencies for 2.3 mJ laser pulse with co-polarized harmonics are given on Fig. 2.

However, for short filament (low laser pulse energy) the effect of phase walk-off along plasma channel is sufficiently decreasing. See dependencies for 1.0 mJ laser pulse with co-polarized harmonics on Fig. 3.

For the experiment on spectral modulation, we collected waveforms of THz pulses and THz power value for different positions of $\pi$-retarder screen/set of screens. Thereafter waveforms are processed with fast Fourier transform to get spectra of THz pulses. Here one can see significant narrowing of spectrum for some position of the screens with peak amplitude on 0.7 THz frequency, that corresponds to the thickness of the PTFE-sheets used. There is also a bright peak on the doubled frequency — 1.4 THz. However, spectral change is accompanied with a dramatic drop in emitted THz power, so that even the amplitude on peak frequency is lower than that in spectrum with no screens placed. On Fig. 4 are given spectra of THz pulses for different positions of the set of two PTFE-screens: 0 mm position corresponds to undisturbed emission (screens placed before the whole filament), 40 mm position corresponds to significant influence of the $\pi$-retarders on emitted THz radiation.
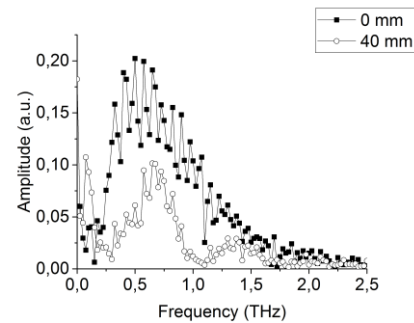


**Fig. 4.** Terahertz pulse spectra for two PTFE-screens positions.

### References

1. *Zhang, X.-C., Shkurinov, A., Zhang, Y.* Extreme terahertz science // Nature Photonics. 2017. V. 11, No. 1. P. 16–18.

2. *Hamster, H., Sullivan, A., Gordon, S., White, W., Falcone, R. W.* Subpicosecond, Electromagnetic Pulses from Intence Laser-Plasma Interaction // Phys. Rev. Lett. 1993. V. 71, No. 17. P. 2725–2728.

3. *Cook, D. J., Hochstrasser R. M.* Intense terahertz pulses by four-wave rectification in air // Opt. Lett. 2000. V. 25, No. 18. P. 1210–1212

4. *You, Y. S., Oh, T. I., Kim, K. Y.* Off-Axis Phase-Matched Terahertz Emission from Two-Color Laser-Induced Plasma Filaments // Phys. Rev. Lett. 2012. V. 109, No. 18. P. 183902.

5. *Zhang, Z., Chen, Y., Chen, M., Zhang, Z., Yu, J., Sheng, Z., Zhang, J.* Controllable Terahertz Radiation from a Linear-Dipole Array Formed by a Two-Color Laser Filament in Air // Phys. Rev. Lett. 2016. V. 117, No. 24. P. 243901.

6. *Wang, T.-J., Chen, Y., Marceau, C., Théberge, F., Châteauneuf, M., Dubois, J., Chin, S. L.* High energy terahertz emission from two-color laser-induced filamentation in air with pump pulse duration control // Appl. Phys. Lett. 2009. V. 95, No. 18. P. 131108.

# CO laser down-conversion into the THz range with ZnGeP$_2$ crystal

A. A. Ionin[1], I.O. Kinyaevskiy[1], Yu. M. Klimachev[1], Yu. M. Andreev[2, 3], A. M. Sagitova[1]

[1]P.N. Lebedev Physical Institute of the Russian Academy of Sciences, Moscow, Russia, aionr@sci.lebedev.ru
[2]Institute of Monitoring of Climatic and Ecological Systems of the Siberian Branch of Russian Academy of Sciences, Tomsk, Russia
[3]Siberian Physical Technical Institute of Tomsk State University, Tomsk, Russia

At the moment, intensive researches have been carried out all over the world to develop high-power frequency-tunable terahertz (THz) laser sources. One of promising THz laser applications is atmosphere sensing due to a number of favorable factors. The first is atmosphere transparency windows in THz shortwave part and an absence of the water vapor absorption, as a main perturbation factor in the long-wave part. The long wavelength of THz radiation minimizes the scattering on dust particles and active weather. Also the THz radiation is safe for living organisms that allows wide using of such laser systems in practice.

A lot of THz generators of femtosecond and picosecond pulses based on nonlinear crystals pumped by powerful Ti: Sapphire laser systems (for example [1, 2]) were developed, but they did not allow us to enter kilometer measurement distance. A demonstration of small atmospheric components measuring and a creation of a constructively simple, convenient device for atmosphere sensing were not achieved [1, 3]. Therefore in this work we considered another way to create powerful reliable and constructively simple THz source based on down-conversion of powerful molecular gas lasers in nonlinear crystals.

A choice of a down-conversion process (a type of three ways mixing) and a nonlinear crystal is the key factor determining an efficiency of the THz laser source. Limit of down-conversion efficiency is determined by the Manley-Row relation, i.e. the ratio of the energies of frequency-converted (THz) radiation quantum to pump light quantum [4]. This means that an application of high-power mid-IR molecular gas lasers (CO$_2$ and CO lasers) for ZnGeP$_2$ (ZGP) crystal pumping (the most effective, so-called "standard of mid-IR nonlinear crystals" [5]) should be more effective for obtaining THz radiation than with near-IR lasers. Before a possibility of difference frequency generation (DFG) (down-conversion) between CO-laser rotational-vibrational transitions to the THz range was noted [6], but the potential and capabilities of the CO laser to produce THz radiation have not been considered in details. In this paper, a numerical study of DFG between rotational-vibrational transitions of CO laser in a ZGP crystal to the THz range was carried out.

Mostly, multi-line Q-switched CO laser emits about one hundred rotational-vibrational lines in the wavelength range from 5 to 6 μm [7, 8]. Such spectrum of CO laser makes it possible to obtain about 10$^3$ narrow lines in the wavelength range from 50 μm to 5000 μm.

In the first we calculated phase-matching angles θ for DFG in ZGP crystal. The calculation method is described elsewhere, for example [9]. In the calculation one CO laser wavelength was locked at 5.5 μm, second one was variable form 5 to 6 μm, DFG wavelength was in interval from 50 μm (6 THz) to 3000 μm (0.2 THz). The calculation show that two types of collinear phase matching are possible in the ZGP crystal: type I (*ooe*) and type II (*eoe*), where o and e correspond to an ordinary and an extraordinary waves, respectively. The interacting waves are listed in order of decreasing their wavelength. The dependence of calculated phase-matching angles on DFG radiation frequency for both interaction types are presented in Fig. 1. Also the transmittance of ZGP crystal taken in the Ref. [10] is presented in Fig. 1.
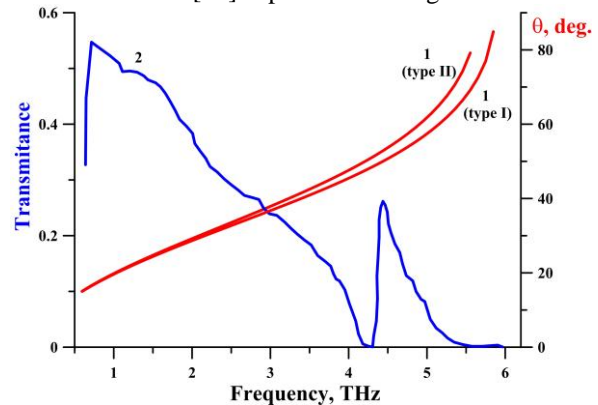


**Fig. 1.** The dependence of calculated phase-matching angles (1) on DFG radiation frequency for I and II interaction types and Transmittance (2) [ol] of ZGP crystal.

The calculation indicates that DFG of CO laser radiation in ZGP crystal is possible in wide range from 0.2 THz to ~6 THz. However down-conversion to frequency interval 0.6 -3 THz will be most attractive due to high crystal transmittance. Phase-matching angles in this case are in the range 15 – 40 deg for both types of three-wave mixing.

The next step of the study was a calculation and an analysis of effective nonlinear coefficient $d_{eff}$, which high value is necessary to obtain high frequency conversion efficiency. Since the ZGP crystal has the $\bar{4}m2$ point symmetry group, $d_{eff}$ to THz range (when the Kleiman conditions are not satisfied) were calculated by the following formulas [9]:

$$\text{type I: } d_{eff}(ooe)=d_{36}\sin(\theta)\sin(2\varphi) \qquad (1)$$

$$\text{type II: } d_{eff}(eoe)=(d_{14} + d_{36})\sin(\theta)\cos(\theta)\cos(2\varphi), \quad (2)$$

where θ is the phase-matching angle, φ is the azimuth angle of the interaction direction (optimized by a cut angle of the crystal), $d_{ij}$ are the second-order nonlinear coefficients. The values of the second-order nonlinear coefficients were taken $d_{36} = d_{14} = 75$ pm/V [9]. The calculated $d_{eff}$ for I and II types of interactions are presented in Fig. 2.
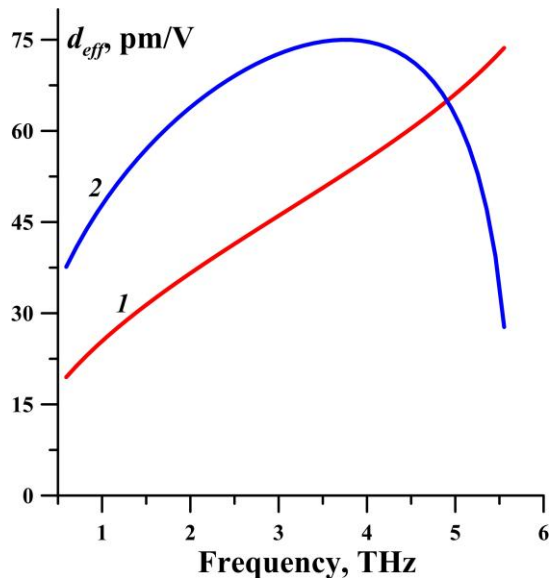
**Fig. 2.** The calculated $d_{eff}$ for I (1) and II (2) types DFG of CO laser lines to THz range

Fig. 2 shows that the type II of DFG is more effective than type I in wide frequency range including most transparent interval 0.6 - 3 THz. It should be noted that in [11] the DFG of $CO_2$ laser radiation to the THz range was carried out only at type I phase-matching.

Thus, the numerical study of difference frequency generation (down-conversion) between rotational-vibrational transitions of CO-laser in $ZnGeP_2$ crystal confirmed promising of this technique for multiple narrow line generation in THz range. It is shown that collinear phase-matching is possible for two types of frequency conversion: I: *ooe* and II: *eoe*. However, a main interest has the type II of frequency conversion because higher effective nonlinear coefficient. Our estimations indicate that for high-power nanosecond CO lasers (such as reported in [12]) the conversion efficiency may rich $10^{-3}$ at kW-range THz radiation power.

## References

1. *Stepanov A.G., Henin S., Petit Y. et al.* Mobile source of high-energy single-cycle terahertz pulses // Appl Phys B. 2010. V. 101. P. 11–14

2. *Hoffmann M.C., Fülöp J.A.* Intense ultrashort terahertz pulses: generation and applications // J. Phys. D: Appl. Phys. 2010. V. 44. P. 083001 (17pp)

3. *Kim G.-R., Jeon T.-I., Grishkowsky D.* 910-m propagation of THz ps pulses through the Atmosphere // Optics Express. 2017. V. 25. P. 25422

4. *Zernike F., Midwinter J.E.* Applied nonlinear optics // John Willey & Sons. N.Y. 1973. P. 213

5. *Schunemann P.* Nonlinear crystals provide high power for the mid-IR // Laser Focus World. 1999. V. 35. P. 85

6. *Lai-ming Zh., Ji-Jiang X., Jin G. et al.* CO laser frequency mixing in nonlinear crystal $ZnGeP_2$ and GaSe // Optics and Precision Engineering. 2012. V. 20. P. 277

7. *Ionin A. A., Kinyaevskiy I. O., Klimachev Yu. M. et al.* Spectral characteristics of multi-line Q-switched CO laser radiation frequency converted in $ZnGeP_2$ // Appl. Phys. B. 2017. V. 123. P. 234

8. *Ionin A. A., Kinyaevskiy I. O., Klimachev Yu. M. et al.* Three-stage frequency conversion of sub-microsecond multiline CO laser pulse in a single $ZnGeP_2$ crystal // Opt. Lett. 2018. V. 43. P. 3184-3187

9. *Dmitriev V.G., Gurzadyan G.G., Nikogosyan D.N.* Handbook for nonlinear optical crystals, 3d ed // Springer, Berlin. 1999. V. 64. P. 413

10. *Kai Zhong, Chu Liu, Maorong Wang et. al.* Linear optical properties of ZnGeP2 in the terahertz range. Opt. Mater. Express. 2017. V. 7. P. 3571-3579

11. *Kumbhakar P., Kobayashi T., and Bhar G.C.* Sellmeier dispersion for phase-matched terahertz generation in $ZnGeP_2$ // Applied Optics. 2004. V. 43. P. 3324

12. *Ionin A. A., Kinyaevskiy I. O., Klimachev Yu. M. et al.* Selection of CO laser single nanosecond pulse by electro-optic CdTe shutter // Infrared Physics & Technology. 2017. V. 85. P. 347-351

# THz sources based on frequency conversion of multi-line molecular lasers in nonlinear crystals and on optically pumped molecular lasers

A. A. Ionin, I. O. Kinyaevskiy, Yu. M. Klimachev, A. A. Kotkov, A. M. Sagitova

P.N. Lebedev Physical Institute of the Russian Academy of Sciences, Moscow, Russia, umk@sci.lebedev.ru

At present, the main method for generating terahertz radiation is down-conversion of laser radiation in nonlinear crystals. However, at converting the radiation frequency from the visible or near infrared to the terahertz range, the efficiency of the process is limited by the Manley-Row ratio, i.e. the ratio of the photon energies of the converted and incident light on the crystal. Therefore, for applications that require high power of terahertz radiation, the use of a $CO_2$ laser operating at wavelength of 10 μm is more preferable than using solid-state near-IR lasers. At the present time in the scientific literature one can find several papers on the conversion of the frequency of the $CO_2$ laser radiation in nonlinear crystals to the terahertz range (see, for example, [1-5]). Note that the conversion efficiency of the super high-power $CO_2$ laser system (UCLA, Neptune Laboratory) under collinear interaction in the GaSe crystal turned out to be lower than for the non-collinear interaction in the GaAs crystal [2], that can be explained by a number of factors: the use of GaSe crystals with low optical quality and realized non-optimal type of interaction. In practice, $CO_2$ lasers with much lower energy are usually used, and the use of non-collinear phase matching becomes less effective in this case (see, for example, [3]). In turn, the implementation of collinear phase matching allows one the use of a longer length of nonlinear crystal and an increase conversion efficiency. Thus, in [4], at crystal length of 47 mm, the average power of pulsed-periodic terahertz radiation reached 0.26 mW with efficiency of $10^{-4}$, which is three orders of magnitude greater than in [1]. The use of a doped GaSe crystal instead of a pure one, made it possible to increase the conversion efficiency by additional factor of 2 [5]. It should be noted that in papers [1-5] two $CO_2$ lasers or a two-channel $CO_2$ laser with independent resonators on the same active medium were used. Usually, the generation of the $CO_2$ laser radiation occurs only on one spectral line, although a fundamental possibility of generating a $CO_2$ laser on two or more spectral lines has already been demonstrated (see, for example, the review [6]). The use of pulsed laser emission acting synchronously on two or more spectral lines will allow us to realize a collinear three-frequency interaction in our RFBR project, simplify the optical scheme of the terahertz radiation generator, thanks to the automatic spatial-temporal matching of laser pulses, and reduce optical losses due to a decrease in the number of used elements, that increase the reliability of the entire system. Such a variant of the optical scheme was realized, for example, in [1] mentioned above. However, it should be emphasized that it will be necessary to solve a set of problems in order to ensure real synchronism of the generation of radiation pulses on laser spectral lines both in the Q-switched mode and in the of active mode locking. In addition, it will be necessary to investigate the influence of the parameters of the electric-discharge pump, the quality factor of the laser cavity, and the composition of the active medium of the laser on its spectral characteristics.

Other promising sources of terahertz radiation are optically pumped lasers operating on those molecular gases in which the radiating transition is either purely rotational (for diatomic molecules, molecules of the asymmetric and symmetrical top type except $NH_3$), or by inversion or inversion-rotational lasers (for $NH_3$) [7]. It was on inversion-rotational transitions of $NH_3$ molecule that laser radiation was generated by French colleagues on our project during optical pumping of ammonia by a quantum-cascade laser [8]. Typically, a $CO_2$ laser is used as the pumping source of terahertz gas lasers [7, 9-10] as the most convenient and well-studied source of radiation. In contrast to a $CO_2$ laser, a molecular CO laser is capable of operating in the mid-IR range almost simultaneously on hundreds of spectral lines in the wavelength range from 2.5 to 8.7 μm, which makes it possible to significantly increase the number of excited molecules and, accordingly, to enrich spectrum of radiation in the terahertz range.

Gas Lasers Laboratory of P.N. Lebedev Physical Institute of the Russian Academy of Sciences is one of the leading teams in Russia in the field of research of molecular lasers with electric discharge pumping. Unique wide-aperture pulsed electron beam sustained discharge laser devices with the possibility of cryogenic cooling of the laser medium working on vibrational-rotational transitions of CO, $CO_2$, and $N_2O$ molecules and also on isotopically substituted modifications of these molecules have been created and investigated in the laboratory. An investigation was made of $NH_3$ laser with optical pumping by $CO_2$ laser radiation. Compact slab CO laser system with pumping by a transverse capacitive radio-frequency (RF) discharge with the possibility of cryogenic cooling of electrodes was developed. At such facilities, the mode of generation of a slab CO laser was realized for the first time, both on the fundamental vibrational transitions and on the first-overtone vibrational transitions of the CO molecule.

Within the framework of this project, it is planned to use laser systems that will be developed on the basis of existing laser devices pumped with an active medium by a pulsed electron beam sustained discharge [11], a pulsed-periodic RF discharge [12] and a DC discharge [13]. In addition, the members of

the scientific team have experience in the implementation Q-switching modes and of the active mode-locking of molecular CO [14] and $CO_2$ lasers [15]. Our studies have been carried out on the frequency conversion of molecular gas lasers in various nonlinear crystals, some of which are expected to be used in carrying out work under this project.

The most close to the tasks of the project are the results of generation of the sum and difference frequencies of CO and $CO_2$ laser emission in nonlinear GaSe and $AgGaSe_2$ crystals [13, 16], as well as $PbIn_6Te_{10}$ [17] into wavelength interval from 2.5 to 16.6 μm. A large number (more than 1000) of the spectral lines of a CO laser makes it possible to realize single-stage frequency converters by generating the difference frequencies of both bands (fundamental and first-overtone) and covering the long-wave part of the mid-IR band up to 30 μm. The generation of difference frequencies between closely spaced spectral lines of a CO laser from one or another radiation band allows one to cover the entire terahertz spectral range [18]. In the paper [19], based on an analysis of the nonlinear optical properties of the new $PbIn_6Te_{10}$ crystal, the possibility of conversion of radiation on the lines of CO and $CO_2$ lasers into the spectral interval of wavelengths from 130 to 1000 μm (from 0.3 to 2.3 THz) is shown.

## References

1. *V.V. Bezotosnyi, E.A. Cheshev, M.V. Gorbunkov et al.,* Coherent THz repetitive pulse generation in a GaSe crystal by dual-wavelength Nd:YLF laser // Physics Procedia 72, 405 (2015).

2. *S.Ya. Tochitsky, J.E. Ralph, C. Sung, C. Joshi,* Generation of megawatt-power terahertz pulses by noncollinear difference-frequency mixing in GaAs // J. of Appl. Phys. 98, 026101 (2005).

3. *Y. Lu, X. Wang, L. Miao, et. al.,* Efficient and widely step-tunable terahertz generation with a dual-wavelenght $CO_2$ laser // Appl. Phys. B 103, 387 (2011).

4. *Y. Jiang, Yu.J. Ding,* Efficient terahertz generation from two collinearly propagating $CO_2$ laser pulses // Appl. Phys. Lett. 91, 091108 (2007).

5. *D.-D. Sie, D. Guo, L.-M. Zhang et al.,* Frequency conversion of a nanosecond $CO_2$ laser to the THz range in doped GaSe crystals // Fundamental problems of modern materials science, 9 (4) 486 (2012) (in Rissian).

6. *D.J. Biswas, A.K. Nath, U. Nundy, U.K. Chatterjee,* Multiline CO2 lasers and their uses // Prog. Quant. Electr. 11, 1 (1990).

7. *A.A. Vedenov, G.D. Myl'nikov, D.N. Sobolenko,* Generation of coherent far-infrared radiation using lasers // Physics-Uspekhi (Advances in Physical Sciences). 25, 833 (1982).

8. *A. Pagies, G. Ducournau, J.-F. Lampin,* Low-threshold terahertz molecular laser optically pumped by a quantum cascade laser // APL Photonics. 1, 031302 (2016).

9. *L.F.L. Costa, J.C.S. Moraes, F.C. Cruz, et al.,* Infrared and far-infrared spectroscopy of $^{13}CH_3OH$: TeraHertz laser lines and assignments // Applied Physics B. 86(4) 703 (2007).

10. *F.C. Cruz, T. Nogueira, L.F.L. Costa, et al.,* Continuous and Pulsed THz generation with molecular gas lasers and photoconductive antennas gated by femtosecond pulses // AIP Conference Proceedings 992, 383 (2008).

11. *A. Ionin, Yu Klimachev, A. Kotkov, et al.,* Multiline Laser Probing for Active Media CO:He, $CO:N_2$, and $CO:O_2$ in Wide-Aperture Pulsed Amplifier // Journal of Russian Laser Research. 27(1) 33 (2006).

12. *A.A. Ionin, Yu.V. Kochetkov, A.Yu. Kozlov, et al.,* Q-switched slab RF discharge CO laser // Laser Phys. Lett. 14, 055001 (2017).

13. *A. A. Ionin, I. O. Kinyaevskiy, Yu. M. Klimachev, and A. A. Kotkov,* Frequency Conversion of Radiation of IR Molecular Gas Lasers in Nonlinear Crystals (A Review) // Optics and Spectroscopy. 119, 356 (2015).

14. *O.V. Budilova, A.A. Ionin, I.O. Kinyaevskiy, et al.,* Mode-locked and Q-switched carbon monoxide laser system // Optics Communications 345, 163 (2015).

15. *A.A. Ionin, I.O. Kinyaevskiy, Yu.M. Klimachev et al.,* $CO_2$ laser with active mode-locking or Q-switching // VI International Scientific Youth School-Conference "Modern Problems of Physics and Technology", Theses of reports, Part 1, M: NRNU MEPhI, 322 (2017). (in Rissian).

16. *O.V. Budilova, A.A.Ionin, I.O.Kinyaevskiy, et al.,* Ultra-broadband hybrid infrared laser system // Optics Communications 363, 26 (2016).

17. *A.A. Ionin, I.O. Kinyaevskiy, Yu.M. Klimachev, et al.,* Frequency conversion of molecular gas lasers in $PbIn_6Te_{10}$ crystal within mid-IR range // Optics Letters. 41, 2390 (2016).

18. *Yu.M. Andreev, A.A. Ionin, I.O. Kinyaevskiy, et al.,* Frequency doubling and mixing of the radiation of carbon monoxide lasers in nonlinear $ZnGeP_2$ and GaSe crystals // Journal of Optical Technology. 78, 102 (2011).

19. *Yu.M. Andreev, V.V. Badikov, A.A. Ionin, et al.,* Optical properties of $PbIn_6Te_{10}$ in the long-wave IR // Laser Physics Letters. 13, 125405 (2016).

# Temperature variation in the process

# of terahertz wave generation by intense laser pulses

G. Kh. Kitaeva[1], E.V. Moiseenko[2], and A.V. Shepelev[3]

[1]*Lomonosov Moscow State University, Moscow, Russia*
[2] *Nuclear Safety Institute of the Russian Academy of Sciences, Moscow, Russia,moi@ibrae.ac.ru*
[3] *I.M.Gubkin Russian State University of Oil and Gas, Moscow, Russia*

To reach satisfactory energy efficiency of the optical-to-terahertz frequency conversion, femtosecond and nanosecond pulsed periodic lasers are used. This considerably affects the lattice temperature and can lead to the dramatic decrease in conversion efficiency.

Nevertheless, the calculations done during the development of a conversion method are often based on the parameters of the non-linear medium taken without an account for its heating up by focused laser radiation. This can result in unpredicted effects.

We have developed a method for the account for non-linear medium heating based on first-principle analytical study of thermo-optical processes that take place in nonlinear-optical crystal structures under periodic femtosecond or nanosecond pumping. The developed approach will allow the experimentalists evaluate the temperature and thermo-optical anomalies just inside a pumped volume in every particular case.

It is generally considered that the refractive index of a crystal is uniquely defined by the crystal temperature and its stress-strain state. In case of short laser pulses, the situation is more complicated: 1) for times less than the highest relaxation time of photo-excited carriers and phonon subsystem, the concept of crystal temperature cannot be defined. In this time interval, even if the dielectric constant can be correctly defined at each moment, the computation of the refraction coefficient is a kinetics-type problem; 2) if the time interval exceeds the relaxation time, but is shorter than the sound propagation time, it is necessary to take into account the temperature waves; 3) if the time interval exceeds the sound propagation time, the standard parabolic equation for temperature is quite correct. We demonstrate that with a short pump pulse and a high pulse repetition frequency, the parabolic equation gives the correct results.

We have developed analytical and numerical methods for calculating the temperature for pulsed-periodic pumping. Numerical methods are not considered here. For the established periodic regime, an analytical solution for a specific experimental scheme can be obtained using known solutions from existing reference materials, replacing the time dependence.

In experiments for measuring $dn/dT$ in some cases it is not this value that is directly determined, but the temperature coefficient of the optical path length change $ds/dT$, which describes the thermally induced distortion of a beam during its passing through a sample. Transversal inhomogeneity of crystal heating will lead to variation in change of optical path length for radiation propagating at different distances from the pumping beam optical axis. In turn, this will result in inclination, spherical deformation ("thermooptical lens" effect) or more complicated distortion of optical pumping wave front. Spatially inhomogeneous depolarization of radiation is also possible
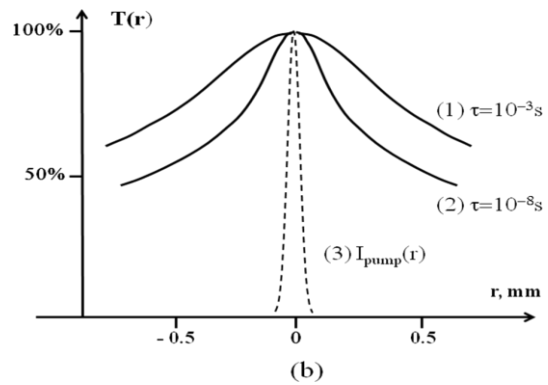
**Some concrete results (LiNbO$_3$ crystals)** [1].
Case A. A cylinder-shaped crystal with radius 0.5 cm,
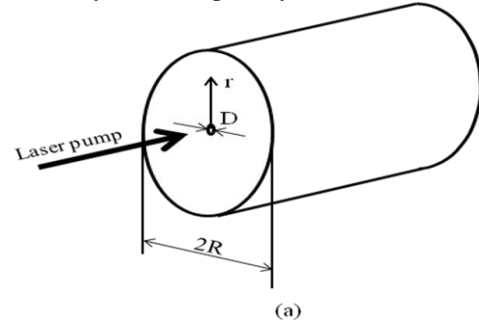


**Fig.1a**

much smaller than its doubled length (**Fig.1(a)**). Pumping radiation with Gaussian profile of diameter 100 μm propagates along the cylinder axis. On the crystal surface the heat exchange with air at 300 K



**Fig.1(b)**

temperature takes place according to Newton's law. The heat exchange coefficient is taken 8 W/m$^2$K. The graph of the corresponding dependence on the transversal coordinate $r$ is shown in **Fig.1(b)**. With an increase in the repetition period of the pump pulses from $10^{-8}$ seconds to $10^{-3}$ seconds, the width of the profile of the temperature distribution increases approximately twice.

<u>Case B</u>. Cherenkov geometry, **Fig.2a**. A specially line-focused laser beam generally propagates as near as possible to one of the side facets of the 8 mm slab-shaped crystal equipped with a special prismatic massive Si-coupler. Here a pump laser beam (average power 8 W) propagates at the distance of 0.5 mm from the working side surface.

<u>Case B1</u>. The non-working surface of crystal is thermally insulated, the temperature of the Si-prism is 100 $K$, the repetition time frequency of the laser pulses is 3 kHz. In **Fig.2b (a) and (b),** the result of the numerical calculations of the temperature and $dT/dr$ dependence on the distance $r$ is shown; the scaled pump intensity profile is shown also there. The value of $d^2T/dr^2$ on the axis is 7 K/mm².

<u>Case B2</u>. The same as Case B1, but the temperature of the Si-prism is 300 $K$, the repetition time frequency of the laser pulses is 80 MHz, non-working surface experiences heat with air. **Fig.2c (a) and (b)** presents the spatial dependences of the temperature and $dT/dr$. The value of $d^2T/dr^2$ is 33 K/mm². $d^2T/dr^2$ on the axis of the laser beam is 7 K/mm².

<u>Case B3</u>. The same as in Case B2, but the non-working lateral surface contacts with a metallic cold loop. In **Fig.2d** the result of the numerical calculation of the temperature dependence on the distance $r$ is shown. The value of $d^2T/dr^2$ is 18 K/mm².

**References**

1. *Kitaeva, G.Kh.., Moiseenko, E.V., Shepelev, A.V.* Temperature variation induced by the pulsed-periodic laser pumping under terahertz wave generation // Las. Phys. Lett. 2017, V.4, No.9, P.095401.
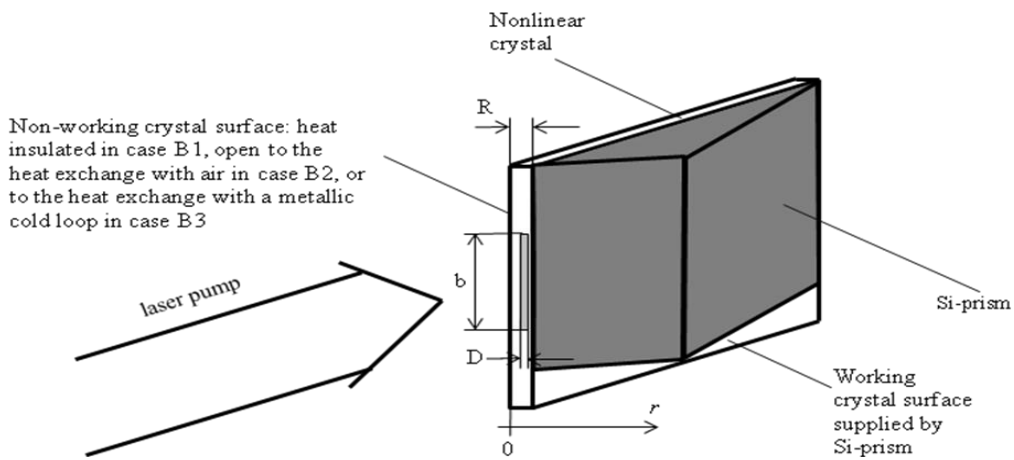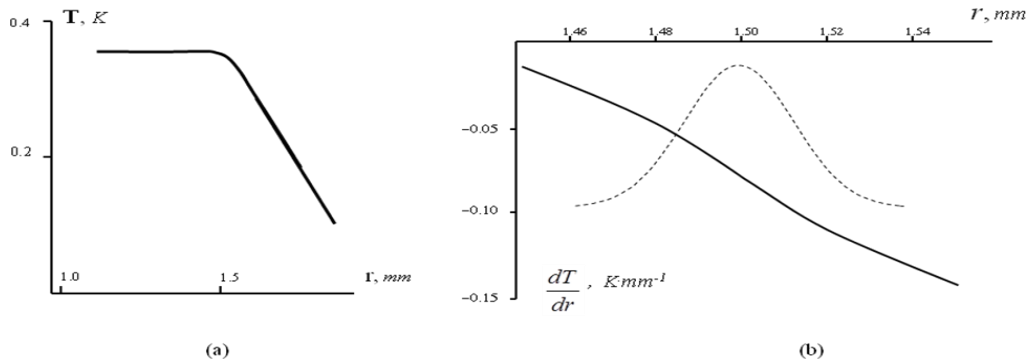


**Fig.2a**
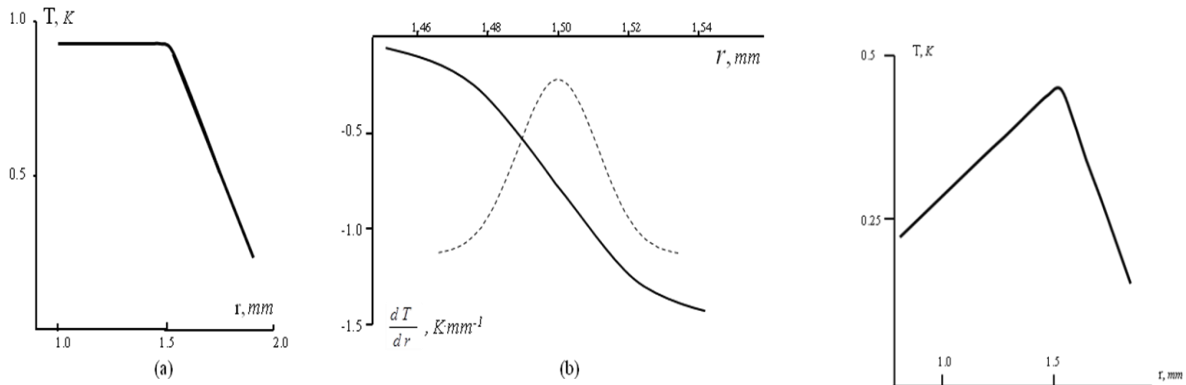


**Fig.2b**



**Fig.2c**



**Fig.2d**

# Role of surface plasmons in laser-induced THz generation from metals

I. V. Oladyshkin, D. A. Fadeev, V. A. Mironov

Institute of Applied Physics of the Russian Academy of Sciences, Nizhny Novgorod, Russia
oladyshkin@gmail.com

## Introduction

The paper is devoted to the analysis and preliminary theoretical interpretation of the last experimental results in laser-induced THz generation from metal structures. The main attention will be paid to metal gratings where resonant excitation of surface plasmons by the incident laser pulse is possible. Despite not a record efficiency level, study of optical-to-THz conversion on metal surfaces is relevant because of future applications in structural diagnostics and due to the fundamental interest in transformation mechanisms. Now there is no clear microscopic theory which is able to interpret the process of THz generation by metal gratings; in particular, the role of surface plasmons is not understood.

The first experimental measurements of THz signal from metal grating were performed more than 10 years ago [1]. In general, the strong influence of surface plasmon excitation on the THz generation was experimentally proved for different experimental conditions [1-3]. In the typical case a smooth resonant dependence of THz signal energy on the incidence angle is observed, where the resonant angle corresponds to the synchronism between the surface plasmon (on the optical frequency) and one of the diffraction waves [1, 2]. In the same time, one of the most complicated experimental features is non-quadratic dependence of the THz radiation energy on the optical fluence.

## Mechanisms of plasmon-assisted THz generation

There are several possible microscopic mechanisms of plasmon-enhanced THz generation which were proposed before. The first one is based on the emission and acceleration of electrons above the surface, the second one – on the ponderomotive action of the plasmon field inside the metal, the third one takes into account thermal effects in the electronic gas.
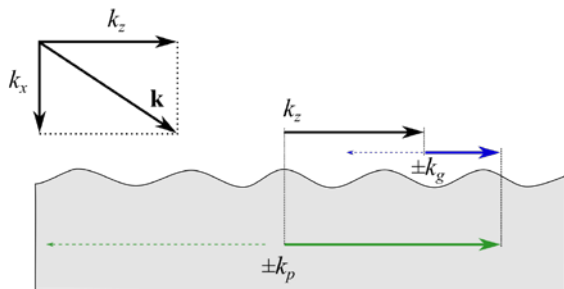


**Fig. 1.** Synchronism between the surface plasmon $k_p$ and incident optical wave **k** in the case of periodical grating with wavenumber $k_g$: $k_z + k_g = k_p$

The first mechanism was previously experimentally refuted in [3], where the authors irradiated structured gold foil and observed THz emission from both incidence and rare side of the sample. Since electron emission and their acceleration into the substrate are impossible, the theory considering emitted electrons cannot be applicable in this case. The second mechanism can be also neglected since thermal nonlinear effects estimated to be stronger than ponderomotive-like ones in the case of metals [4]. So, here we will focus on the third (thermal) mechanism.

Thermal mechanism of THz generation for the case of flat metal surfaces was first proposed in [4], where analytical and numerical analysis was performed. Here we consider the same generation mechanism taking into account the possibility of surface plasmon excitation as an additional mechanism of the laser radiation absorption. Numerical model is based on Maxwell equations and hydrodynamical equations which describe electron gas motion and include heating by the laser field and heat diffusion.

## Resonance THz generation

Well-known condition of synchronism between the surface plasmon wave and the optical wave above the metal grating is shown in the Fig. 1. In the first series of numerical calculations we study behavior of the THz response of the metal surface varying the grating period while the incidence angle was fixed (30°).
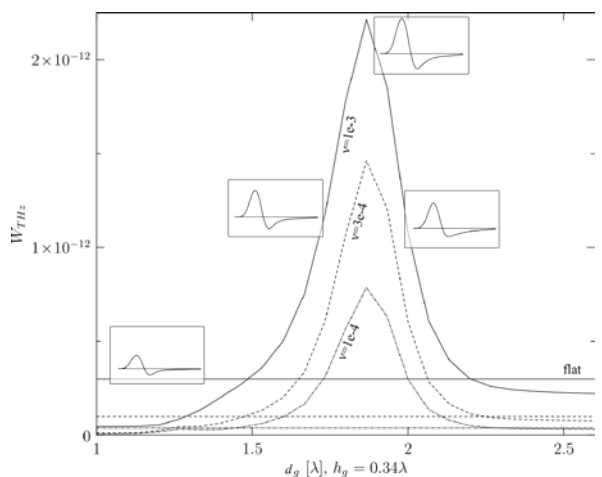


**Fig. 2.** Calculated dependence of the THz pulse energy on the grating period (angle of incidence = 30°, three different values of collision frequency are chosen). Insets: THz waveforms for different values of grating period.

Results presented in the Fig. 2 clearly indicate resonant character of the dependence (three curves correspond to three values of the scattering rate in metal, the grating period is measured in wavelengths

of the incident optical pulse). Characteristic width of resonant curves equals to 10-15% of the resonant period which is in good agreement with experimental data from [2]. With the rise of collision frequency characteristic width also slightly increases.

### Optimal grating depth

In the second series of numerical calculation we studied dependence of the conversion efficiency on the grating depth in the resonant point (see Fig. 3).
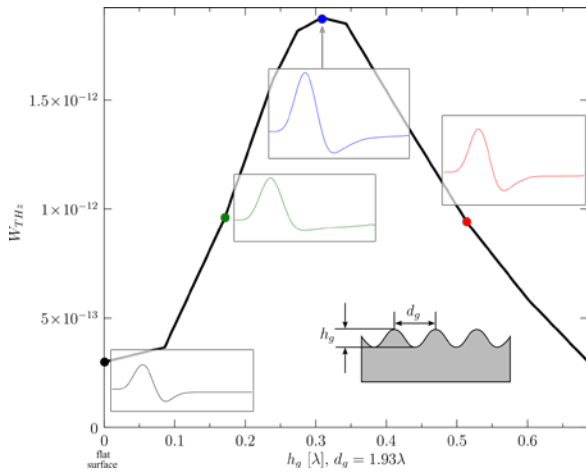


**Fig. 3.** Calculated dependence of the THz pulse energy on the grating depth (measured in the incident wavelengths). Angle of incidence equals to 30°. Insets: THz waveforms for different values of grating depth.

Obtained results are in good qualitative agreement with the experimental data from [3] where it was found that there is some optimal depth for THz generation (of about 150 nm for the optical wavelength 785 nm and incidence angle ≈45°). The further growth of the grating depth decreases THz signal. Quantitative comparison with the experiment requires modeling of the concrete grating profile (rectangular in most of cases). Calculated optimal value is about 0.3 wavelengths. The physical reason of this fact is a finite radiative lifetime of the surface plasmon which becomes shorter than the absorption time for too deep surface modulations.

To summarize, we perform numerical modeling of the THz signal generation process during the laser pulse reflection from the metal with periodically modified boundary. The key mechanism of low-frequency radiation generation is the medium polarization under the action of electronic temperature gradients. Here surface plasmon resonance can be treated an additional channel for the laser pulse absorption, so the resonance in absorption leads to rise of THz signal energy. Obtained numerical results (see Fig. 2 and Fig. 3) give a preliminary interpretation of the recent experimental data [2, 3]

### Acknowledgements

### References

1. *Welsh, G. H., Hunt, N. T., Wynne, K.* Terahertz-pulse emission through laser excitation of surface plasmons in a metal grating // Phys. Rev. Lett. 2007. V. 98, No. 2. P. 026803.

2. *Ramanandan, G. K. P., Ramakrishnan, G., Kumar, N., Adam, A. J. L., Planken, P. C. M.*, Emission of terahertz pulses from nanostructured metal surfaces // J. of Phys. D: Appl. Phys. 2014. V. 47, No. 37. P. 374003.

3. *Garwe, F., Schmidt, A., Zieger, G., May, T., Wynne, K., Hübner, U., Zeisberger, M., Paa, W., Stafast, H., Meyer, H.-G.,* Bi-directional terahertz emission from gold-coated nanogratings by excitation via femtosecond laser pulses // Appl. Phys. B. 2011. V.102, No. 3. P. 551—554.

4. *Oladyshkin, I. V., Fadeev, D. A., Mironov, V. A.*, Thermal mechanism of laser induced THz generation from a metal surface // J. of Optics 2015. V. 17, No. 7. P. 075502

# Interplay effects of carrier-envelope phase and plasmon resonances in terahertz generation by ionizing ultrashort optical pulses

I. V. Osovitskaya[1,2], V. A. Kostin[1,2], N. V. Vvedenskii[1,2]

[1]Institute of Applied Physics, Russian Academy of Sciences, Nizhny Novgorod, Russia, oivnn121@mail.ru
[2]University of Nizhny Novgorod, Nizhny Novgorod, Russia

The direct conversion of femtosecond ionizing laser pulses into low-frequency radiation attracts considerable attention due to associated possibilities for creating sources of powerful broadband terahertz (THz) pulses. Previous studies of this phenomenon were mainly related to two limiting cases: (i) few-cycle (extremely short) ionizing pulses with several optical field cycles and (ii) multicycle (quasimonochromatic) pulses with a large number of field cycles. In the first case, the amplitude and energy of THz oscillations strongly depend on the carrier-envelope phase (CEP) in the ionizing pulse [1–3], whereas for multicycle pulses the CEP dependence is unnoticeable [4–6]. The spectral and mode structures of generated radiation also differ in these two cases. For the few-cycle pulses, the plasmonic oscillations corresponding to the dipole geometric resonance are excited and emitted from the laser-produced plasma filament to the surrounding space. For multicycle pulses, the radiation is produced by a relaxing current directed along the plasma filament, and the spectrum width and central frequency are determined by the collision frequency of electrons with heavy particles. Thus, the shape of low-frequency spectrum strongly depends on the pump pulse duration, and there is a range of durations where transition between different spectral shapes occurs. In this range of durations, the spectrum shape also significantly depends on the CEP, as was apparently observed in experiment [7]. Here, we study this intermediate case based on the universal model that considers the motion of the plasma electrons under forces both linear and quadratic with respect to the optical field strength.

The calculation of the THz radiation employs the two-stage approach [3, 5] which assumes that the characteristic frequency $f_{THz}$ of the generated THz radiation is small compared with the inverse pump duration $1/\tau$: $f_{THz}\tau << 1$. During the short (femtosecond) first stage, a gas medium is ionized and the free-electron currents are excited in the produced plasma by the optical pump pulse. In the longer (picosecond) second stage, there is a self-consistent evolution of these free-electron currents and the electromagnetic fields generated by them. Such separation into stages is convenient since one can neglect low-frequency plasma fields and assume the electric and magnetic fields given in the first stage, and one can consider fields and currents weak enough and neglect the nonlinear terms in the second stage.

Equations solved in the first stage are obtained directly from the kinetic equation

$$\frac{\partial f}{\partial t}+\mathbf{v}\cdot\frac{\partial f}{\partial \mathbf{r}}-\frac{e}{m}\left(\mathbf{E}+\frac{\mathbf{v}}{c}\times\mathbf{B}\right)\cdot\frac{\partial f}{\partial \mathbf{v}}=I$$

for the single-electron distribution function $f(\mathbf{r}, \mathbf{v}, t)$ (over positions $\mathbf{r}$ and velocities $\mathbf{v}$) with the ionization source term $I = (N_m - N)w_{\mathbf{v}}(\mathbf{E}, \mathbf{v})$. Here $e$ is the elementary charge, $m$ is the electron mass, $c$ is the speed of light, $\mathbf{E}(\mathbf{r}, t)$ and $\mathbf{B}(\mathbf{r}, t)$ are the electric and magnetic fields, $w_{\mathbf{v}}(\mathbf{E}, \mathbf{v})$ is the differential (with respect to the initial photoelectron velocities) ionization probability per unit time in the static field $\mathbf{E}$, $N_m$ is the initial density of neutral particles, and $N(\mathbf{r}, t)$ is the plasma density. Assuming the plasma being cold and the average velocity of newly-born electrons being zero, $\int w_{\mathbf{v}}(\mathbf{E}, \mathbf{v})\mathbf{v}\, d^3\mathbf{v} = 0$, one obtains equations for the plasma density, the electron density perturbation $n(\mathbf{r}, t) = \int f(\mathbf{r}, \mathbf{v}, t)\, d^3\mathbf{v} - N(\mathbf{r}, t)$, and the electron current density $\mathbf{j}(\mathbf{r}, t) = -e\int f(\mathbf{r}, \mathbf{v}, t)\mathbf{v}\, d^3\mathbf{v}$ as follows:

$$\frac{\partial N}{\partial t}=(N_m-N)\,w(\mathbf{E}),\quad \frac{\partial n}{\partial t}=\frac{\nabla\cdot\mathbf{j}}{e},\quad \frac{\partial \mathbf{j}}{\partial t}=\frac{Ne^2}{m}\mathbf{E}+\mathbf{S}, \quad (1)$$

$$\mathbf{S}=\frac{1}{e}\left[(\mathbf{j}\cdot\nabla)\frac{\mathbf{j}}{N+n}+\frac{\mathbf{j}}{N+n}(\nabla\cdot\mathbf{j})\right]+\frac{ne^2}{m}\mathbf{E}-\frac{e}{mc}\mathbf{j}\times\mathbf{B}, \quad (2)$$

where $w(\mathbf{E}) = \int w_{\mathbf{v}}(\mathbf{E}, \mathbf{v})\, d^3\mathbf{v}$ is the ionization probability per unit time. For numerical calculations below, we use the atmospheric density value $N_m = 3\cdot 10^{19}$ cm$^{-3}$ and the empirical formula for the hydrogen atom [8]:

$$w(\mathbf{E}) = 4\omega_a(E_a/|\mathbf{E}|)\exp(-2E_a/3|\mathbf{E}| - 12|\mathbf{E}|/E_a),$$

where $\omega_a = 4.13\cdot 10^{16}$ s$^{-1}$ and $E_a = 5.14\cdot 10^{9}$ V/cm are the atomic units of frequency and electric field. To find fields and currents, we develop the perturbation approach for Eqs. (1) and (2) assuming that $n << N$ and all characteristic spatial scales (optical wavelength, size of plasma inhomogeneity) are large compared to the amplitude of electron oscillations.

In the first stage, we solve Eqs. (1) and (2) for the given fields $\mathbf{E}$ and $\mathbf{B}$ of the optical Bessel beam defined by the magnetic Hertz vector $\mathbf{\Pi}^m=\hat{\mathbf{y}}\int_{-\infty}^{\infty}A_\omega J_0(k_\perp r)e^{-i\omega\xi}d\omega/2\pi$, where $\theta$ is the focusing angle of the Bessel beam, $k_\perp = \sin\theta\, \omega/c$ is the transverse wavenumber, $\xi = t - z/V$ is the shifted time, $V = c/\cos\theta$ is the phase velocity, $r$ is the distance to the beam axis (the $z$ axis of the Cartesian and cylindrical coordinate systems), $J_0$ is the zero-order Bessel function of the first kind, $A_\omega$ is the Fourier spectrum of the $y$ component of the Hertz vector at the beam axis (since $E_x=c^{-2}\cos\theta\, d^2\Pi_y^m/d\xi^2$, the spectrum of $E_x$ at the axis is $-\cos\theta\,(\omega/c)^2 A_\omega$). In numerical calculations, the temporal profile of the pulse at the axis is chosen as

$$\Pi_y^m=-\left[(8\pi c^3 I_0)^{1/2}/(\omega_0\cos\theta)^2\right]\sin^4(\pi\xi/2\tau)\cos(\omega_0\xi+\psi)$$

for $|\xi + \tau| < \tau$, $\Pi_y^m = 0$ for $|\xi + \tau| \geq \tau$, where $\omega_0$ is the

central frequency of the ionizing field (which corresponds to the wavelength $2\pi c/\omega_0 = 800$ nm in calculations), $I_0$ is the maximum field intensity at the axis, $\psi$ is the CEP. Thus, the fields depend on the shifted time $\xi$ and transverse coordinates (radial coordinate $r$ and azimuth angle $\varphi$ in the cylindrical coordinate system. Another simplification is related to the cylindrical symmetry of the beam: The calculations show that the plasma density depends weakly on $\varphi$ for small enough angles $\theta$, and this dependence can be neglected. The current density in the first order of perturbation theory has a dipole structure, i.e., its components in cylindrical coordinates have one azimuthal variation and are proportional to $\cos\varphi$ or $\sin\varphi$. The current density in the second order is a superposition of the symmetric term (the components do not depend on $\varphi$) and the term with two variations (components are proportional to $\cos 2\varphi$ or $\sin 2\varphi$).

We integrate the equations for the first and second orders inside the cylindrical area $r < a = \mu_0 c/\omega_0 \sin\theta$, and determine the plasma density transverse profile remaining after the pump pulse has passed, $N_R(r) = N(r, \xi = 0)$, and the residual current density (RCD) distribution $\mathbf{j}_R(r, \varphi) = \mathbf{j}(r, \varphi, \xi = 0)$, which is a superposition of components with 0, 1, and 2 azimuthal variations; here $\mu_0 \approx 2.405$ is the first zero of $J_0$. We assume the field is so weak outside this cylindrical domain that the plasma and currents produced there do not significant affect the generated radiation. Then, the calculated distributions are used as parameters and initial conditions for the second stage, where the Maxwell equations and the linear equation for the electron current density in a cold collision plasma are solved,

$$\nabla\times\mathbf{E}=-\frac{1}{c}\frac{\partial\mathbf{B}}{\partial\xi}, \quad \nabla\times\mathbf{B}=\frac{1}{c}\frac{\partial\mathbf{E}}{\partial\xi}+\frac{4\pi}{c}\mathbf{j}, \quad \frac{\partial\mathbf{j}}{\partial\xi}+\nu\mathbf{j}=\frac{\omega_p^2}{4\pi}\mathbf{E},$$

where $\omega_p(r) = [4\pi N_R(r)e^2/m]^{1/2}$ is the plasma frequency and $\nu$ is the collision frequency of electrons with heavy particles ($5\cdot 10^{12}$ s$^{-1}$ in calculations). The initial conditions for fields are $\mathbf{E}|_{\xi=0}=0$, $\mathbf{B}|_{\xi=0}=0$; the RCD found in the first stage serves as the initial condition for the electron current density, $\mathbf{j}|_{\xi=0}=\mathbf{j}_R$. At the boundary $r = a$, the radiation conditions are set under assumption that there is no plasma in the external area, $N(r > a) \equiv 0$. We solve this initial problem separately for each of three azimuthal components of the RCD by applying the Laplace transform with respect to the variable $\xi$. After that, we calculate the spectral density $w_{\text{rad}}(f)$ and the radiated energy $W_{\text{rad}} = \int_0^{f_{\max}} w_{\text{rad}}(f)df$ per unit length along the $z$ axis in THz range, where $f_{\max}$ is the upper bound of the THz range under consideration. The spectral density can be expressed in terms of the Laplace images of the longitudinal field components at the boundary of the computational area $w_{\text{rad}} = w_{\text{rad}}^{[0]} + w_{\text{rad}}^{[1]} + w_{\text{rad}}^{[2]}$, where

$$w_{\text{rad}}^{[M]}(f)=\frac{c^2}{2\pi^2 f\sin^2\theta}\frac{\left|\widetilde{E}_z^{[M]}(a,0)\right|^2+\left|\widetilde{B}_z^{[M]}(a,\pi/2M)\right|^2}{\left|H_M^{(1)}(2\pi\sin\theta\, fa/c)\right|^2}$$

is the spectral density of the radiated energy of the component with $M$ azimuthal variations, $\widetilde{E}_z^{[M]}(r,\varphi)$ and $\widetilde{B}_z^{[M]}(r,\varphi)$ are the Laplace images of the longitudinal components of the electric and magnetic fields, respectively, for the Laplace variable $p \to 2\pi if + 0$, and $H_M^{(1)}$ is the Hankel function of the first kind and order $M$.

We solve numerically the above equations for a wide range of focusing angles $1° \le \theta \le 30°$, durations $4$ fs $\le \tau_p = [2\arcsin(2^{-1/8})/\pi]\tau \le 50$ fs, and intensities $10^{14}$ W/cm$^2 \le I_0 \le 10^{15}$ W/cm$^2$ of ionizing pulses for different CEPs $0 \le \psi \le \pi$. The dipole RCD strongly depends on $\psi$ for any pumps considered, whereas the distribution of the plasma density and the RCD terms with 0 and 2 azimuthal variations practically do not depend on $\psi$ even for extremely short durations $\tau_p$. Although the dipole RCD proves to be the weakest, for few-cycle pulses its contribution to THz radiation can be determinant. However, the dipole component decrease rapidly with increasing duration, and the contributions from different azimuthal components to THz radiation are already comparable at not too long durations. Under these conditions, the THz spectrum shape can vary greatly as $\psi$ changes. With a further increase in the duration, the dipole component becomes negligibly small, and the dependence on the CEP disappears.

### References

1. *Löffler, T., Jacob, F., Roskos, H. G.* Generation of terahertz pulses by photo-ionization of air // Appl. Phys. Lett. 2000. V. 77, No. 3. P. 453–455.

2. *D'Amico, C., Houard, A., Franco, M.* Conical forward THz emission from femtosecond-laser-beam filamentation in air // Phys. Rev. Lett. 2007. V. 98, No. 23. P. 235002.

3. *Kostin, V. A., Vvedenskii, N. V.* Ionization-induced conversion of ultrashort Bessel beam to terahertz pulse // Opt. Lett. 2010. V. 35. No. 2. P. 247–249.

4. *Kreß, M., Löffler, T., Thomson, M. D.* Determination of the carrier-envelope phase of few-cycle laser pulses with terahertz-emission spectroscopy // Nat. Phys. 2006. V. 2, No. 5. P. 327–331.

5. *Gildenburg, V. B., Vvedenskii, N. V.* Optical-to-THz wave conversion via excitation of plasma oscillations in the tunneling-ionization process // Phys. Rev. Lett. 2007. V. 98, No. 24. P. 245002.

6. *Silaev, A.A., Vvedenskii, N. V.* Residual-current excitation in plasmas produced by few-cycle laser pulses // Phys. Rev. Lett. 2009. V. 102, No. 11. P. 115005.

7. *Bai, Ya, Song, L., Xu, R., Li, C., Liu, P., Zeng, Z., Zhang, Z., Lu, H.* Waveform-controlled terahertz radiation from the air filament produced by few-cycle laser pulses // Phys. Rev. Lett. 2012. V. 108, No. 25. P. 255004.

8. *Tong, X. M., Lin, C. D.* Empirical formula for static field ionization rates of atoms and molecules by lasers in the barrier-suppression regime // J. Phys. B. 2005. V. 38. No. 15. P. 2593–2600.

# New Approach to Generation and Amplification of the THz Radiation in Plasma Created by Intense Two-Color Laser Fields

A. M. Popov[1,2,3], A. V. Bogatskaya[1,3]

[1]D. V. Skobeltsyn Institute of Nuclear Physics, Moscow State University, Moscow, Russia, alexander.m.popov@gmail.com
[2]Department of Physics, Moscow State University, 119991, Moscow, Russia
[3]P. N. Lebedev Physical Institute, RAS, Moscow Russia

Construction of new types of THz radiation sources is nowadays of sufficient fundamental and practical interest. This interest is motivated by the prospects of using THz radiation for THz imaging in a lot applications in science and technology [1]. However, till now THz frequency band is still insufficiently studied in comparison with infrared and microwave ones. Among others, THz generators based on the gas ionization by high-intensity femtosecond lasers are widely studied now. Such a way of THz generation allows to obtain radiation with a continuous spectrum throughout the terahertz bandwidth that is of importance for different spectroscopy applications. Typically, optical-to-THz conversion results from the four wave mixing process (FWM) in high-intensity femtosecond two color laser field ($\omega + 2\omega$). Unfortunately, the efficiency of such conversion remains rather small - about 0.001- 0.01%. In this respect, problems of amplification of THz pulses as well as the development of new more efficient methods of optical to terahertz energy conversion are of significant importance. In this paper we propose an alternative way to enhance significantly the process of optical-to-THz conversion by using the resonance in four-wave mixing process. Such resonant enhancement is possible in the aluminum vapor irradiated by Ti-Sa laser pulse and its second harmonic via the aluminum atom excited state $4s(^2S_{1/2})$ with the energy $E_{4s} \approx 3.14$ eV close to the frequency of the Ti-Sa second harmonic $\hbar(2\omega) \approx 3.1$ eV. Schematically this process is shown at fig.1 We demonstrate that the THz output can be increased up to two orders of magnitude in comparison with the non-resonant process.
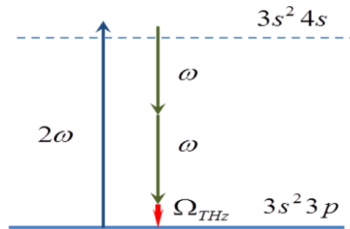


**Fig 1.** Nearly resonance four-wave-mixing process in aluminum atom

It is known that irradiation of gas by intense two color ($\omega + 2\omega$) laser pulse results in low-frequency polarization of the medium $P_\Omega \sim \chi^{(3)} E_\omega^2 E_{2\omega}$ and THz emission [2] which arises from the four-wave mixing (FWM) process ($\Omega = \omega' + \omega'' - 2\omega'''$) and in the limit of perturbation theory is governed by the cubic susceptibility $\chi^{(3)}(\omega' + \omega'' - 2\omega'')$ ($\omega', \omega''$ are the frequencies from the spectral width of the pulse with frequency $\omega$ while $\omega'''$ is the frequency from the spectral width of second harmonic $2\omega$.). For femtosecond laser pulses this low-frequency spontaneous emission appears in the THz and far IR frequency band. In this paper we plan to study low frequency spontaneous background from gas or plasma irradiated by two-color laser field which could be further amplified according to the mechanism proposed in [3].

Below we analyze the resonant FWM process and the formation of the spontaneous THz background for xenon and aluminum atoms using the approach developed in [4] that is based on the accurate consideration of quantum system interaction with vacuum quantized field modes in the first order of perturbation theory while the intense laser field is considered classically beyond the perturbation theory.

The electric field strength in the two-color pulse was chosen in a form

$$E(t) = f(t) \times (E_\omega \cos(\omega t) + E_{2\omega} \cos(2\omega t)),$$

where $\omega$ the frequency of the Ti-Sa laser and $f(t)$ is the envelope being the same for both pulses. It was chosen in the sine-squared form with the half-duration $\tau = 880$ atomic units (~20 fs), that corresponds to 8 optical cycles of the Ti-Sa laser or 16 optical cycles for its second harmonic.

The study of atomic emission was performed in the range of intensities for both fundamental and second harmonic $\sim 10^{-5} - 2 \times 10^{-3}$ at. un. and the intensity of second harmonic is assumed to be several time less than the intensity of the fundamental one. On the one hand, the increment of the intensity gives rise to more efficient FWM process, on the other hand the ionization and the depletion of the ground state will reduce the probability of the resonance FWM.

Typical spontaneous emission spectra obtained in our simulations for aluminum atom are presented at figure 2. Curves 1, 2 and 3 represent the spectra obtained for Ti-Sa laser irradiation, its second harmonic as well as combined two-color action respectively. First of all, the peaks of Rayleigh scattering at $\hbar\omega_{k\lambda} = 1.55$ eV for fundamental frequency and $\hbar\omega_{k\lambda} = 3.1$ eV for the second harmonic are observed. The last peak has the triple structure (triplet Mollow) due to the near-resonant transition to 4s state. There are also some additional peaks appearing for the Ti-Sa laser resulting from different processes. Most important to highlight that for two-color laser pulse one more low-frequency peak with a maximum at $\hbar\Omega_{k\lambda} \approx 0.2$ eV is well pronounced. This peak manifests the FWM process when the second harmonic

quantum absorption and two quanta of Ti-Sa laser stimulated emission is accomplished by spontaneous emission of THz - far IR quantum (see figure 1).
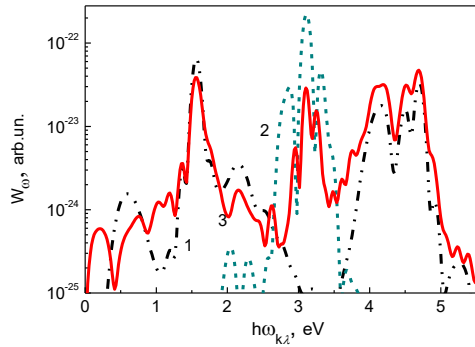


**Fig. 2**. Spectrum of spontaneous emission of aluminum atom irradiated by Ti-Sa laser pulse with $I_\omega = 1.4 \times 10^{-3}$ (in atomic units) (1), its second harmonic with $I_{2\omega} = 10^{-4}$ (2) and by two-colour pulse (3) with $I_\omega = 1.4 \times 10^{-3}$ and $I_{2\omega} = 10^{-4}$.

The detailed analysis of the low-frequency emission in the near resonant FWM process leads to the conclusion that optimal values for THz emission exist near the intensities $I_\omega = 1.4 \times 10^{-3}$ and $I_{2\omega} = 4 \times 10^{-4}$.

The resonant character of FWM can dramatically increase THz emission in comparison with the non-resonant case. To demonstrate it, the simulation of THz background from the xenon atom was also analyzed for nearly the same laser radiation parameters [5]. Comparative analysis of these data leads to the conclusion that resonant character of FWM provides the enhancement of the emission in THz bandwidth up to two orders of value.

Further amplification of a seed low-frequency pulse can be realized in the nonequilibrium plasma channel formed independently by the UV laser pulse. Earlier it was demonstrated in [6] that such a plasma produced in the process of multiphoton ionization of heavy rare gases by powerful UV laser pulse is characterized by population inversion that can be used for amplification of THz-band radiation. This amplification is possible if the energy of photoelectron peak is located in the interval of increasing with energy (faster than the linear dependence) electron transport cross section.
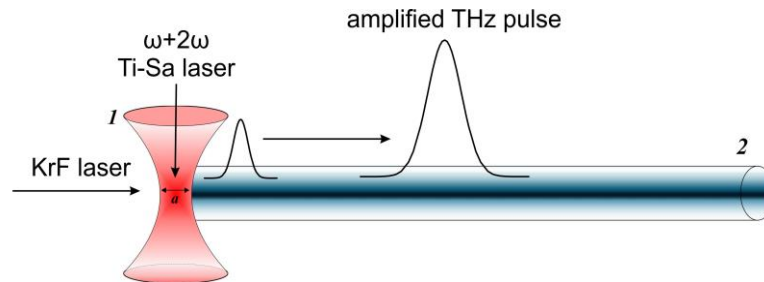
Possible realization of such a concept is performed at figure 3. Terahertz spontaneous signal emerges in the region of intense two-color laser action and then propagates through the amplifying zone which is formed by KrF laser pulse. In the frames of our concept the presence of two different lasers is mandatory because we require high-intensities for the two-color pulse to reach high level of nonlinearity for FWM process but at the same time we do not need high level of ionization in the amplifying plasma channel as domination of electron-electron collisions will cause the fast relaxation of the nonequelibrium electron energy distribution function (EEDF) and destroy the population inversion..

To conclude, in this paper we demonstrate that the resonance between quanta of the laser radiation and energy transition from the ground to one of the excited states of the atomic system can result in the dramatic enhancement of the four-wave mixing process in two-colour laser field ($\omega + 2\omega$) providing more efficient optical to THz conversion scheme. Possibility of further amplification of the THz background is discussed. Also, the new concept allowing to enhance the THz output from the two-color scheme in a nonequilibrium plasma channel formed by UV laser was proposed.

**References**

1. *Mittleman, D. M.* Twenty years of terahertz imaging // Opt. Express 2018.V. 26, P. 9417

2. *Cook, D. J. and Hochstrasser, R. M.* Intense terahertz pulses by four-wave rectification in air // Opt. Lett. 2000. V. 25, P. 1210

3. *Bogatskaya, A. V., Volkova, E. A., Popov, A. M.* Generation and amplification of sub-THz radiation in a plasma of rare gases formed by two-color femtosecond laser pulse // Las. Phys. Lett. 2018. V. 15, P. 065301

4. *Bogatskaya, A. V., Volkova, E. A., Popov, A. M.* Spontaneous transitions in atomic system in the presence of high intensity laser field // Europhysics Letters 2016. V. 116, P. 14003

5. *Bogatskaya, A. V., Popov, A. M.* New approach to the problem of THz generation by intense two-color laser fields // Laser Phys. 2018. V. 28 submitted

6. *Bogatskaya, A. V., Popov, A. M.* On the possibility of the amplification of subterahertz electromagnetic radiation in a plasma channel created by a high-intensity ultrashort laser pulse // JETP Lett. 2013. V. 37. P. 388-392

**Fig. 3.** Principal scheme of THz pulse generation and amplification in case of perpendicular geometry. THz signal is produced in the region of focal waist of two-color Ti-Sa laser action (channel 1) and then enhanced in the 2nd channel formed in xenon by KrF laser pulse.

# Terahertz radiation in two-color laser fields: from single atom to extended gas response

S. Yu. Stremoukhov[1,2], A.V. Andreev[1]

[1]Faculty of Physics, Lomonosov Moscow State University, Leninskie Gory, 1, build.2, 119991, Moscow, Russia,
sustrem@gmail.com
[2]National Research Centre "Kurchatov Institute", pl. Akademika Kurchatova, 1, 123182, Moscow, Russia

One of the promising methods of the THz radiation generation is the use of the two-color laser field focused into the gas media [1, 2]. The polarization of the low frequency THz field generated in gas is linear [2], although, in some conditions, it is elliptical due to the modulation of the laser phase and its polarization in the gas plasma [3]. At the same time, for some practical applications, it is critical to have the elliptically polarized THz radiation [4]. For its generation certain methods [2, 5] mostly based on the mixing of the elliptically polarized laser fundamental radiation ($\omega$) with linear (or elliptically polarized) second harmonic radiation ($2\omega$) exist, the generated elliptical THz radiation lies in low frequency region (<5THz).

Here, we demonstrate the method of generation of the highly elliptical high-frequency THz radiation (>25 THz) by the extended gas media interacting with the two-color laser field having linearly polarized components but with a nonzero angle between them [6]. The consistent quantum-mechanical description is given. The two spatial levels are introduced. Initially, the time-dependent Schrodinger equation for single atom "placed" in a finite number of positions in the extended gas (i.e. being under the action of the two-color laser field having various intensities and relative phases between the pulses [7]) is solved. Then, we calculate the response of extended system by changing the spatial parameters of the gas (mainly, the gas length, $l$) and the laser beam (mainly, beam width, $\sigma$)).

For the calculation of the properties of the THz radiation emitted by a single atom we have used the non-perturbative theory [8, 9] and the model of the Ar atom described in [7, 10]. In simulations we assume that the components of the two-color laser field have the fixed intensity ($I_\omega = 6.77 \times 10^{12}$ $W \cdot cm^{-2}$ and $I_{2\omega} = 5.85 \times 10^{11}$ $W \cdot cm^{-2}$), fixed temporal width of the laser field components ($\tau_{1,2} = 30$ $fs$), zero delay time between the pulses ($\Delta t_{1,2}=0$) and relative phase equal to $\varphi_0=\pi/2$. At these parameters of laser field the ionization-free regime of interaction occurs [10]. In this way we obtain a series of photoemission spectra for different angles between the polarizations of two-color laser field components ($\theta$) and different delay times between the pulses.

Single atom numerical calculations demonstrate that at frequences $>25$ $THz$ there are some regions of high ellipticity (up to circular), the maximum value of the ellipticity and the widths of these regions decrease along with an increase in the THz frequency [6].

Basing on the single-atom response we have calculated the response of the extended gas media. Previously we have used the formula (4) from [7] for describing the linearly polarized THz laser field spa-

tial distribution in an aria around the gas. In that calculations we have summarized two projections onto perpendicular axes of THz fields emitted from individual atoms and have extracted total intensity of the THz radiation at given points of the area. In current calculations of the elliptically polarized THz field response each atom emits elliptically polarized radiation which could be expanded on two projections on the perpendicular axes $E_{xj} = |E_{xj}| e^{i\sigma_{xj}}$ and $E_{yj} = |E_{yj}| e^{i\sigma_{yj}}$ (see Fig. 1).
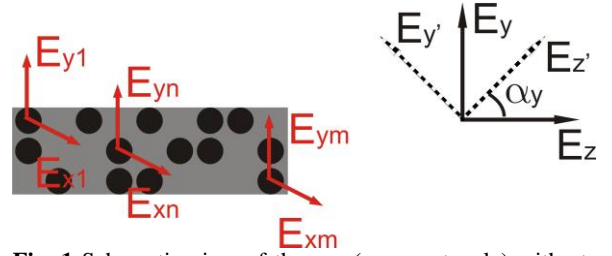


**Fig. 1** Schematic view of the gas (gray rectangle) with atoms (black circles) emitting the THz field (red arrows indicate two projections). By the black solid arrows and black dashed arrows indicated the two projections of the field formed by the sum of projections of the single color field on the one axes. $\alpha_y$ denotes the rotation angle.

By using formulae (4) from [7] two projections of the summarized field could be found at given point of the area for each projections ($x-$ and $y-$) of the THz field separately (see Fig.1 with shown projections only for $y-$ component of the THz field, the other two projections for $x-$ component of the THz field lies in the perpendicular plane). As a result, two projections of the single atom THz field response are transformed at four ones when the problem of extended gas media response is under consideration. But the turning of two perpendicular axes on the angle can decrease the number of projections. Indeed, if we turn $yz-$ axes on the angle $\alpha$, the projections of the THz field on the new $y'z'-$ axes become

$$E_{y'} = E_y \cos\alpha + E_z \sin\alpha,$$
$$E_{z'} = -E_y \sin\alpha + E_z \cos\alpha.$$

If the rotation angle will be chosen by the following way

$$\tan\alpha_y = \frac{E_z}{E_y},$$

then $E_{z'} = 0$ and $E_{y'}$ will have the form of

$$E_{y'} = E_y \cos\left(\arctan\left(\frac{E_z}{E_y}\right)\right) + E_z \sin\left(\arctan\left(\frac{E_z}{E_y}\right)\right).$$

As a result, only one complex projection have non-zero value. Providing the following procedure with other two projections (with are corresponding to the $x$–component of the atoms THz components) we will have only one projection of the THz field which has the form of

$$E_{x'} = E_x \cos\left(\arctan\left(\frac{E_z}{E_x}\right)\right) + E_z \sin\left(\arctan\left(\frac{E_z}{E_x}\right)\right).$$

So, there are only two complex projections of the THz field at each point of space. Using them and providing some standard procedures ones can extract properties of the THz field (intensity, ellipticity, polarization angle).
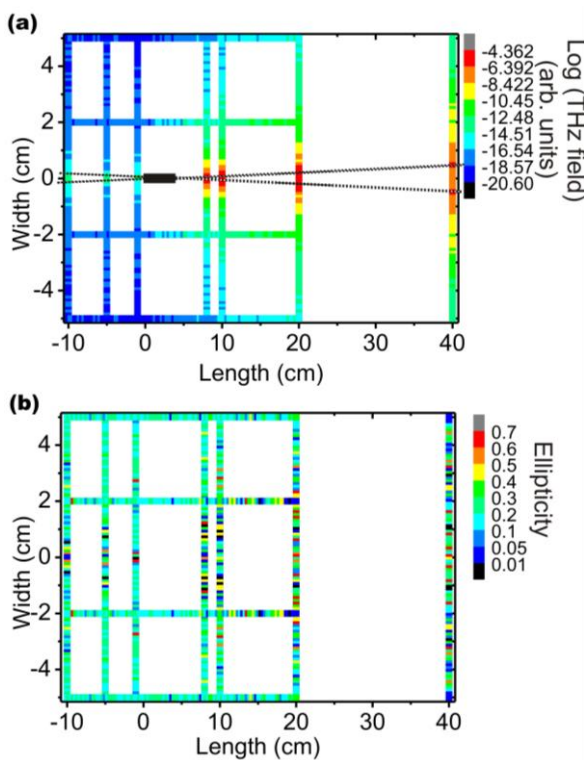


**Fig. 2** Spatial distribution of the THz field strengths (a) and ellipticities (b) calculated for $v$=29 THz for l=6 cm and σ=0.1 cm. The black rectangle is the emitted medium.

The typical THz field distributions calculated for *l=6 cm, σ=0.1 cm, θ=π/4* and *v=29 THz* are presented in Fig. 2. The THz field distributions demonstrate the cone structure mainly. These distributions also contain the conical structure in the backward direction [11], which is possible due to the complete orders in "emitted atoms" locations in the gas (with a fixed period). The backward emission is less intensive compared to the forward one. Fig. 2b demonstrated the ellipticity distribution of the generated radiation.

We have investigated three possibilities to control the value of ellipticity (and the THz field strength) of the generated radiation. The first one is to change the relative phase between the pulses of the two-color laser field at the left side of the gas (the same method was previously investigated in [2]).

The second way to an effective control of the value of the ellipticity of the generated THz radiation is to change the spatial geometry of the interaction (the length of the gas *l* and the width of the laser beam σ).

The third method of the effective control of the ellipticity value of the generated THz radiation is by changing the spatial profile of the laser beam, i.e. by using an iris and a mask which is completely opposite to the iris: the iris transmits, in this case, the central part of the laser pulses, and the mask transmits the periphery one [6].

**References**

1. *Cook, D. J., Hochstrasser, R. M.* Intense terahertz pulses by four-wave rectification in air // Opt. Lett. 2000. V. 25, p. 1210.

2. *Dai, J., Karpowicz, N., Zhang ,X. C.* Coherent Polarization Control of Terahertz Waves Generated from Two-Color Laser-Induced Gas Plasma // Phys. Rev. Lett. 2009. V. 103, p. 023001.

3. *Xu, J., Galan, J., Ramian, G., Savvidis, P., Scopatz, A., Birge, R. R., Allen, S. J., Plaxco, K.* Terahertz Circular Dichroism Spectroscopy of Biomolecules // Proc. SPIE. 2004. 5268, 19–26.

4. *Hughes, S., Citrin, D.S.* Interaction of terahertz transients and broadband optical pulses in quantum wells // J. Opt. Soc. Am. B. 2000. V. 17, p. 128.

5. *Sato, M., Higuchi, T., Kanda, N., Konishi, K., Yoshioka, K., Suzuki, T., Misawa, K., Kuwata-Gonokami, M.* Terahertz polarization pulse shaping with arbitrary field control // Nat. Photonics. 2013. V. 7, p. 724.

6. *Stremoukhov, S., Andreev, A.* Quantum-mechanical fingerprints in generation of elliptical terahertz radiation by extended media interacting with two-color laser field // J. Opt. Soc. Am. B. 2017. V. 34(2), p. 232-237.

7. *Stremoukhov, S. Yu., Andreev, A. V.* Spatial variations of the intensity of THz radiation emitted by extended media in two-color laser fields // Laser Phys. Lett. 2015. V. 12, p. 015402.

8. *Andreev, A.V., Stremoukhov, S. Yu., Shoutova, O. A.* Light-induced anisotropy of atomic response: prospects for emission spectrum control // Eur. Phys. J. D. 2012. V. 66, 16.

9. *Stremoukhov, S., Andreev, A., Vodungbo, B., Salières,P., Mahieu, B., Lambert, G.* Origin of ellipticity of high-order harmonics generated by a two-color laser field in the cross-polarized configuration // Phys. Rev. A. 2016. V. 94, p. 013855.

10. *Andreev, A. V., Stremoukhov, S. Yu.* Terahertz-radiation generation in the ionization-free regime of light-atom interaction // Phys. Rev. A. 2013. V. 87, p. 053416.

11. *Jahangiri, F., Hashida, M., Nagashima, T., Tokita, S., Hangyo, M., Sakabe, S.* Intense terahertz emission from atomic cluster plasma produced by intense femtosecond laser pulses // Appl. Phys. Lett. 2011. V. 99, p. 261503.

# Backward terahertz emission from two-color laser induced plasma spark

Aleksandr Ushakov[1,2], Pavel Chizhov[1], Vladimir Bukin[1], Nikolay Panov[2], Daniil Shipilo[2], Olga Kosareva[2], Andrei Savel'ev[2], Sergey Garnov[1]

[1]A.M. Prokhorov General Physics Institute RAS, Moscow, Russian, ushakov.aleksandr@physics.msu.ru
[2]M.V. Lomonosov Moscow State University, Moscow, Russia

## Introduction

Femtosecond gas plasma created by focusing of two-color laser pulses is one of the promising laser-driven THz sources [1]. Investigation of spatial distribution of THz radiation from plasma is of great interest [2-4]. Several theoretical works have predicted an essential backward emission of terahertz radiation from two-color femtosecond plasma under tight focusing conditions [5]. We proved experimentally the presence of such radiation previously in [6]. However, to get a clear insight into mechanisms leading to backward emission one has to investigate characteristic features of this radiation. Here we perform its spectral and energetic investigation.

## Experimental setup

A Ti:Sa femtosecond laser (800 nm, 40 fs, 2.8 mJ, 1 kHz rep. rate, 12 mm dia.) is used. Laser radiation is partially converted into second harmonic in BBO crystal ($10\times10\times0.2$ mm$^3$, I-type). To provide efficient THz generation polarizations of fundamental and second harmonic pulses are made collinear by a dual-wavelength phase plate and adjusted for optimal temporal shift by a delay compensator plate. Two-color femtosecond laser pulse is focused in ambient air by a parabolic mirror with 0.8 inch focal length to create plasma.

To perform forward THz radiation measurements we use two PTFE-lenses (5 cm diameter, 6 and 10 cm focal lengths). The first lens collimates radiation and the second focuses it on a THz detector. We use Golay cell for power measurements and electro-optical sampling in ZnTe crystal ($10\times10\times0.5$ mm$^3$, <110> cut) for spectral analysis.

The parabolic mirror that is used for laser beam focusing collimates backward THz radiation. Thereafter it is partially reflected on 90° by a metal plate with an aperture cut for passing of the laser beam. Then THz radiation is focused by a PTFE-lens on the THz detector. For power measurements it is 5 cm diameter 6 cm focal length lens. For electro-optical sampling it is 5 cm diameter 4 cm focal length lens with a 1 mm aperture for passing of a probe laser pulse.

## Results

We have obtained waveforms (see Fig.1(a)) and corresponding spectra of THz radiation spreading from two-color femtosecond laser plasma both in forward and backward directions. The backward pulse spectrum is somewhat narrower than the forward one.

A numerical simulation based on a simple interferometric model is performed to support experimental data [6, 7]. During the calculations we assume the length of plasma channel to be 250 μm; the length of plasma channel recorded in our experiment is $(256 \pm 6)$ μm (see inset in Fig. 1b). The backward $P_{bwd}$ and forward $P_{fwd}$ spectral powers of THz radiation are calculated with taking into account the collecting angles of the parabolic mirror and PTFE lenses; the transmission of the metal plate with $\varnothing15$-mm hole is accounted. The spectral powers $P_{bwd}$ and $P_{fwd}$ are found for the THz frequencies $\nu_{THz}$ from 0.05 to 3 THz with the step 0.05 THz. The ratio $E(\nu_{THz})=P_{bwd}(\nu_{THz})/P_{fwd}(\nu_{THz})$ is the estimation the transmission function from the forward THz spectrum $S_{fwd}(\nu_{THz})$ to the backward one $S_{bwd}(\nu_{THz})$:

$$E(\nu_{THz})=P_{bwd}(\nu_{THz})/P_{fwd}(\nu_{THz}) \qquad (1)$$

The ratio $E(\nu_{THz})$ has the order of unity only for $\nu_{THz}\leq0.5$ THz (see Fig. 1b), so one can expect the shift of backward THz spectrum to the lower frequencies within the agreement with the experiment. We reconstruct the backward THz spectrum from the experimentally measured forward one for calculated function $E(\nu_{THz})$. The adequate semi-quantitative agreement between measured and reconstructed spectra supports the conclusion about the low-frequency bias in the backward THz spectrum. The qualitative explanation of this effect is the following: for the spectral THz components with the wavelength much longer than the plasma channel length of about 250 μm (i.e. $\nu_{THz} \ll 1.2$ THz in good agreement with the previous estimation $\nu_{THz}\leq0.5$ THz) the plasma spark is closer to point-source as compared with shorter THz wavelength components. This point-source emits the low-frequency THz radiation both in forward and backward directions. We note, that the THz spectrum of two-color optical breakdown spreads up to ~50 THz, and the EO system can measure its only small part up to 3 THz. However, the transmission function, which determines the backward THz spectrum mostly, has the width of ~0.5 THz (see Fig. 1(b)) within the EO system detection range. Therefore, we measure the whole spectrum of the backward THz emission from two-color microplasma.

They also demonstrate narrowing of the spectrum of radiation emitted in backward direction. This feature arises from destructive interference from local emitters along plasma spark. The less the wavelength is, the more periods of radiation correspond to the plasma length. Thus, overall interference is more destructive. However, the experimentally observed narrowing is less dramatic as compared to the simulations.
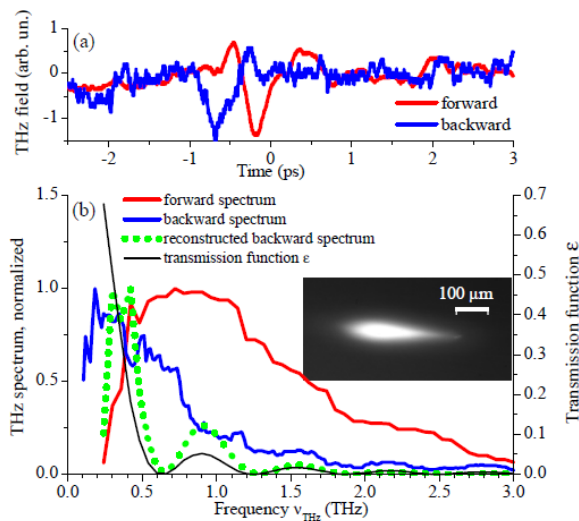
**Fig. 1**. (a) Waveforms of THz field measured in backward and forward directions. (b) Spectra of experimentally measured forward (red line) and backward (blue line) THz emission with plasma channel, transmission function received from formula 1 (black line), numerically calculated backward THz emission (green dotted line).

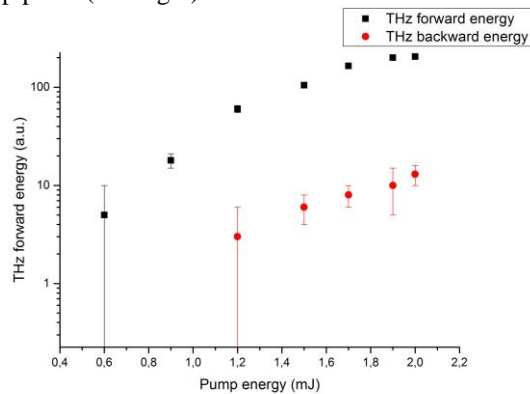We also get backward/forward emission energy dependencies on the energy of the two-color laser pump pulse (see Fig.2).



**Fig. 2**. Energy of forward and backward THz radiation dependence on laser pump pulse energy.

### Conclusions

We have performed investigation of spectral parameters of forward and backward terahertz radiation from optical breakdown plasma created by tightly focused two-color femtosecond laser pulses. It appears that backward THz emission spectrum is narrower as compared to that of THz radiation co-directed with the optical pump. This result is supported by numerical simulation with simple interferometric model.

Dependencies of forward/backward THz energy on laser pump energy are measured. This can be useful for indirect control of forward spreading radiation by monitoring of backward one.

### References

1. *Cook, D. J., Hochstrasser R. M.,* Intense terahertz pulses by four-wave rectification in air // Opt. Lett. 2000. V. 25, No. 16. P. 1210-1212.

2. *Zhong H., Karpowicz N., Zhang X.-C.* Terahertz emission profile from laser-induced air plasma // Appl. Phys. Lett. 2006. V. 88, No 26. P. 261103.

3. *Andreeva V. A., Kosareva O. G., Panov N. A., Shipilo D. E., Solyankin P. M., Esaulkov M. N., Gonzalez De Alaiza Martinez P., Shkurinov A. P., Makarov V. A., Berge L., Chin S. L.,* Ultrabroad terahertz spectrum generation from an air-based filament plasma // Phys. Rev. Lett. 2016. V. 116, No 6. P. 63902.

4. *Shkurinov A. P., Sinko A. S., Solyankin P. M., Borodin A. V., Esaulkov M. N., Annenkov V. V., Kotelnikov I. A., Timofeev I. V., Zhang X.-C.* Impact of the dipole contribution on the terahertz emission of air-based plasma induced by tightly focused femtosecond laser pulses // Phys. Rev. E. 2017. V. 95, No 4. P. 43209.

5. *Panov N., Andreeva V., Kosareva O., Shkurinov A., Makarov V. A., Bergé L., Chin S. L.* Directionality of terahertz radiation emitted from an array of femtosecond filaments in gases // Laser Phys. Lett. 2014. V. 11, No12. P. 125401.

6. *Ushakov A. A., Matoba M., Nemoto N., Kanda N., Konishi K., Chizhov P. A., Panov N. A., Shipilo D. E., Bukin V. V., Kuwata-Gonokami M., Yumoto J., Kosareva O. G., Garnov S. V., Savel'ev A. B.* Backward terahertz radiation from a two-color femtosecond laser filament // JETP Letters. 2017. V. 106, No 11. P. 706–708.

7. *Panov N. A., Kosareva O. G., Andreeva V. A., Savel'ev A. B., Uryupina D. S., Volkov R. V., Makarov V. A., Shkurinov A. P.* Angular distribution of the terahertz radiation intensity from the plasma channel of a femtosecond filament // JETP Letters. 2011. V. 93, No 11. P. 715-718.

# Resonant Effects in Terahertz Generation with Laser-Induced Gas Plasmas

I. Thiele [1,2], B. Zhou [3], A. Nguyen [4], E. Smetanina [1,5], R. Nuter [1], P. González de Alaiza Martínez [1], K. J. Kaltenecker [3], J. Déchard [4], L. Bergé [4], P. U. Jepsen [3], and S. Skupin [1,6]

[1]Univ. Bordeaux - CNRS - CEA, Centre Lasers Intenses et Applications, Talence, France
[2]Department of Physics, Chalmers University of Technology, Göteborg, Sweden
[3]DTU Fotonik, Technical University of Denmark, Kongens Lyngby, Denmark
[4]CEA/DAM Ile-de-France, Bruyères-le-Châtel, 91297 Arpajon, France
[5]Department of Physics, University of Gothenburg, Göteborg, Sweden
[6]Institut Lumière Matière, Université Lyon 1 - CNRS, Villeurbanne, France, stefan.skupin@univ-lyon1.fr

Research on intense terahertz (THz) electromagnetic sources has received an increasing attention owing to numerous applications, for example, in time-domain spectroscopy, biomedical imaging or security screening [1]. Among the various techniques employed to generate THz radiation, focusing intense two-color femtosecond pulses in air or noble gases provides interesting features like absence of material damage, large generated bandwidth (up to ~100 THz) and high amplitudes of the emitted THz pulses (> 100 MV/m) [2]. First reported by Cook et al. [3], THz emission from intense two-color pulses was initially attributed to optical rectification via third-order non-linearity. However, it was shown later that the plasma built-up by tunneling photoionization is necessary to explain the high amplitudes of the THz field [4], and a quasi-dc plasma current generated by the temporally asymmetric two-color field is responsible for THz emission [5].

Numerous experimental results show that the laser-induced free electron density has a strong impact on the THz emission [4,6,7]. While it is frequently observed that a larger free electron density leads to broader THz spectra, the origin of the effect remains controversial. In [6,7], homogeneous plasma oscillations were proposed as an explanation, even though those oscillations are in principle non-radiative [8,9]. Moreover, nonlinear propagation effects have been held responsible for THz spectral broadening as well [10]

On the other hand, the gas plasma produced by the fs laser pulse is a finite conducting structure with a lifetime largely exceeding the fs time scale. Thus, one can expect that the gas plasma features plasmonic resonances which may have a strong impact on the THz emission propertie [11]. However, no direct evidence of plasmonic effects in laser-induced gas-plasmas was observed so far: To make an evidence of plasmonic effects, those need to be distinguished from nonlinear propagation effects. Also from the theoretical point of view capturing plasmonic effects is not trivial: plasmonic effects require at least a full two-dimensional Maxwell-consistent description, and reduced models like the unidirectional pulse propagation equation [12], which are frequently used to describe plasma-based THz generation [5,7,10], are by construction not capable of capturing such resonant effects.

In this work, we consider the two-color-laser-induced plasma as a plasmonic structure, and investigate under which conditions such plasmonic perspective is important. In the context of plasmonic nanoantennas (or metamaterials), e.g, for second-harmonic generation, tailoring plasmonic resonances by tuning the shape of the plasmonic particle is a standard approach. Therefore, we follow a similar strategy and modify the usually prolate spheroidal plasma shape. Going to tri-axial ellipsiods which can be achieved by using elliptically shaped laser beams turns out to be already sufficient [13]. Depending on whether the laser polarization is oriented along the long beam axis (quasi transverse electric, qTE) or along the short beam axis (quasi transverse magnetic, qTM), plasmonic resonances are triggered or not (see Fig. 1).
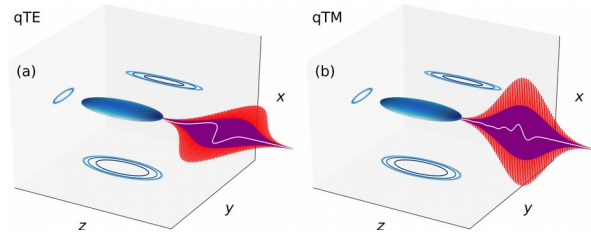


**Fig. 1.** Illustrated configurations of THz emission from an ellipsoidal plasma induced by a two-color Gaussian laser pulse~(funamental in red, second-harmonic in purple) with strongly elliptical beam shape propagating along z. The laser electric field is y-polarized (along the long axis of the beam, qTE) in (a) and x-polarized (along the short axis, qTM) in (b). The plasma is sketched as blue surface. Simulated forward emitted THz pulses are presented as white lines demonstrating a significantly shorter pulse duration for qTM polarization, which can be attributed to triggering a plasmonic resonance.

While nonlinear propagation effects are in both cases equally present, any difference between the THz emission spectra in this two cases is linked to plasmonic effects. We demonstrate experimental results which reveal a significant difference: THz pulses are shorter and have a broader emission spectrum when the plasma is excited by the laser field in the direction with the short focal beam width and plasma width (see Fig. 2). A simple analytical model allows us to link the broadening to a leaky mode. It turns out that the resonance has a strong impact on the spectrum whenever electrons are excited along a direction where the plasma size is smaller than the plasma wavelength. Finally, direct three-dimensional (3D) Maxwell consistent simulations in tightly focused geometry confirm that these plasmonic resonances indeed broaden the emitted THz spectrum significantly.
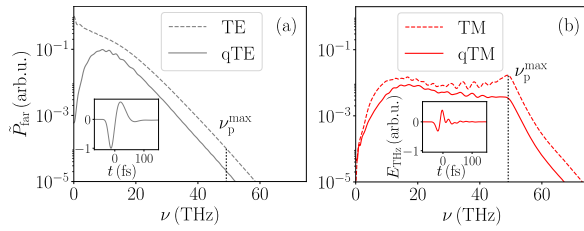
**Fig. 2.** Experimental THz spectra for qTE (a) and qTM (b) polarization (see text for details). Corresponding on-axis THz waveforms are shown as insets. The dashed lines specify the estimated maximum plasma frequency.

### References

[1] M. Tonouchi. Cutting-edge terahertz technology. Nature Photon., 1:97, 2007.

[2] K. Kim et al. High-Power Broad¬band Terahertz Generation via Two-Color Photo-ionization in Gases. IEEE J. Quant. Electron., 48:797, 2012.

[3] D. Cook et al. Intense terahertz pulses by four-wave rectification in air. Opt. Lett., 25:1210, 2000.

[4] K. Kim et al. Coherent control of terahertz supercontinuum generation in ultrafast laser-gas interactions. Nature Photon., 2:605, 2008.

[5] L. Bergé et al. 3D numerical simulations of THz generation by two-color laser filaments. Phys. Rev. Lett., 110:073901, 2013.

[6] H. Hamster et al. "Short-pulse terahertz radiation from high-intensity-laser-produced plasmas," Phys. Rev. E, 49:671, 1994.

[7] V. A. Andreeva et al. Ultrabroad terahertz spectrum generation from an air-based filament plasma," Phys. Rev. Lett., 116:063902, 2016.

[8] V. T. Tikhonchuk, Comment on "generation of electromag-netic pulses from plasma channels induced by femtosecond light strings", Phys. Rev. Lett., 89:209301, 2002.

[9] I. Thiele et al. Theory of terahertz emission from femtosecond-laser-induced microplasmas, Phys. Rev. E, 94:063202, 2016.

[10] E. Cabrera-Granado et al. "Spectral self-action of thz emission from ionizing two-color laser pulses in gases, New J. Phys., 17:023060, 2015.

[11] V. A. Kostin at al. Dc to ac field conversion due to leaky-wave excitation in a plasma slab behind an ionization front, New J. Phys., 17:033029, 2015.

[12] M. Kolesik at al., Nonlinear optical pulse propagation simulation: From Maxwell's to unidirectional equations, Phys. Rev. E, 70:036604, 2004.

[13] I. Thiele et al. Terahertz emission from laser-driven gas-plasmas: a plasmonic point of view. arXiv:1803.06889 [physics.optics], 2018.

# Study of the cluster formation dynamics and its affect on generation of THz and X-Ray radiation in the expanding gas jet.

A. V. Balakin,[1,2] M. S. Dzhidzhoev,[1] V. M. Gorgienko,[1] I. A. Zhvaniya,[1] I. E. Ivanov,[1]
N. A. Kuzechkin,[2,1] P. M. Solyankin,[2,1] A. P. Shkurinov[1,2,3]

[1]Faculty of Physics & International Laser Center, Lomonosov Moscow State University, Moscow 119991, Russia
[2]Institute on Laser and Information Technologies of RAS, Branch of the FSRC "Crystallography and Photonics", RAS,
Shatura, Moscow Region 140700, Russia
[3]The National University of Science and Technology MISiS, Moscow 119049, Russia

Presently the interaction of intense femtosecond laser pulses with cluster target is a subject of active researches. Laser-cluster interaction proceeds with high efficiency and is accompanied with a plenty of nonlinear effects [1-3]. That makes it very attractive and promising as the basis for elaboration of a source for generation of intense coherent electromagnetic pulses in a wide spectral range from X-ray up to THz.

For detailed understanding and interpretation of the processes occuring in the gas-cluster nanoplasma, as well as for further optimization of their effectivity, a detailed information about properties of the gas-cluster jet is required. This information include distributions of the clusters size, cluster concentration, condensation degree and average atomic density along the spatial coordinates. In general, the process of the clusters formation in the gas jet is quite complex and possesses the probabilistic nature. The efficient method to get detailed information regarding the properties and parameters of the gas-cluster jet is the straight numerical simulation of the clusterization process.

In this work, we have carried out the numerical simulation and computing of dynamic picture of clusterization of argon atoms passed through the supersonic conical nozzle and future propagation of the jet into vacuum at a distance of up to 60 mm below the nozzle throat. The result of numerical simulation has demonstrated that ratio between argon monomers, small and large clusters fractions dramatically changes both as along the jet propagation direction, and as across the jet when the distance from the nozzle throat increase.

Some results of the numerical simulation of cluster formation process are shown on Fig. 1,2. The following parameters of the conical nozzle which was applied in our experiments were used for simulation: throat diameter 0.7 mm, output diameter 4.7 mm, and the nozzle length 24.7 mm. Backing pressure of argon was 2 Mpa. Fig.1 depicts spatial distribution of the average argon atoms density inside and outside of the nozzle. The direction along the axis of symmetry of the nozzle is denoted as an axis of abscissa (X-axis), that coincides with the jet propagation direction as well. The nozzle throat position is noted as X=0 mm, and X=24.7 mm corresponds to position of the nozzle output edge. Radial direction, which is perpendicular to the axis of the symmetry, is denoted as Y-axis. There are five stream lines (SL) indicated by dashed lines on the Fig. 1. Distributions of mean cluster size and mean cluster concentration through the stream

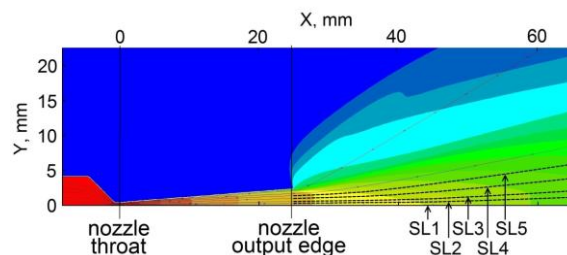lines as a function of distance from the nozzle are presented on Fig.2.



**Fig. 1.** Distribution of Ar atom density inside and outside of the conical nozzle (Y = 0 corresponds to the axis of symmetry of the nozzle, SL1-SL5 represent five stream lines). The magnitude of the density is represented by a color scale: ~5 kg/m$^3$ (red), ~0.3 kg/m$^3$ (yellow), ~$10^{-2}$ kg/m$^3$ (green), ~$3\times10^{-4}$ kg/m$^3$ (blue), and ~$10^{-5}$ kg/m$^3$ (dark blue).
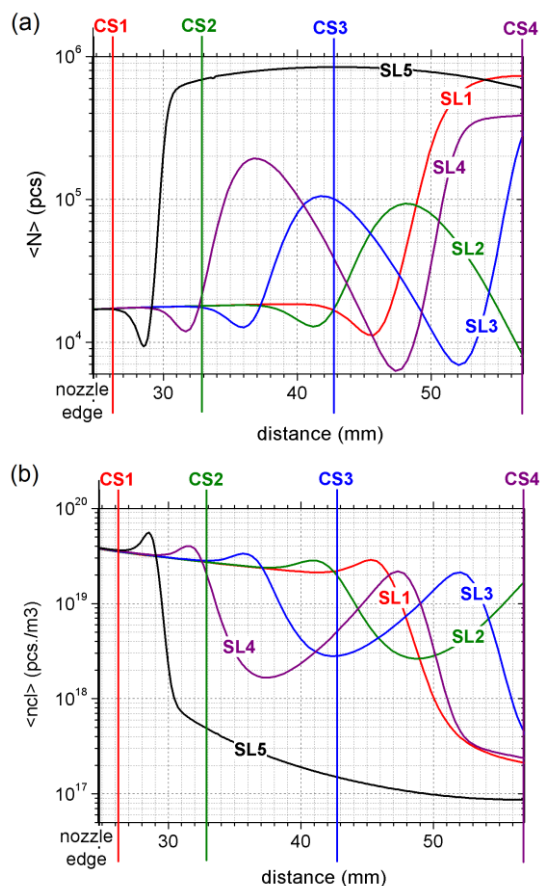


**Fig. 2.** Distributions of (a) mean cluster size $<N>$ and (b) mean cluster concentration $<n_{cl}>$, along five stream lines (SL1-SL5) as a function of the distance from the nozzle throat.

The graphs shown on Fig. 1,2 clearly demonstrate that the distance from the nozzle throat is an important parameter which defines the properties of the gas-cluster jet. We suggest that this fact can be effectively used for efficient control over X-ray and THz emission yields produced from argon gas-cluster jet under irradiation with high-intense laser pulses.

In our experiments on laser-cluster interaction we used the setup described in details in our previous paper [4], which was modified to provide a possibility of focusing the laser beam into the gas-cluster jet at various distances below the output edge of conical supersonic nozzle. The focus point was located at the axis of symmetry of the nozzle and could be positioned discretely in the range between 1.5 mm to 32.3 mm below the nozzle edge that corresponds to the locations of CS1-CS4. Our laser system provided pulses with energy up to 30 mJ at 10 Hz repetition rate, central wavelength was 810 nm, the pulse duration could be tuned in the range of 50–600 fs by chirping the laser pulse in a vacuum grating compressor.
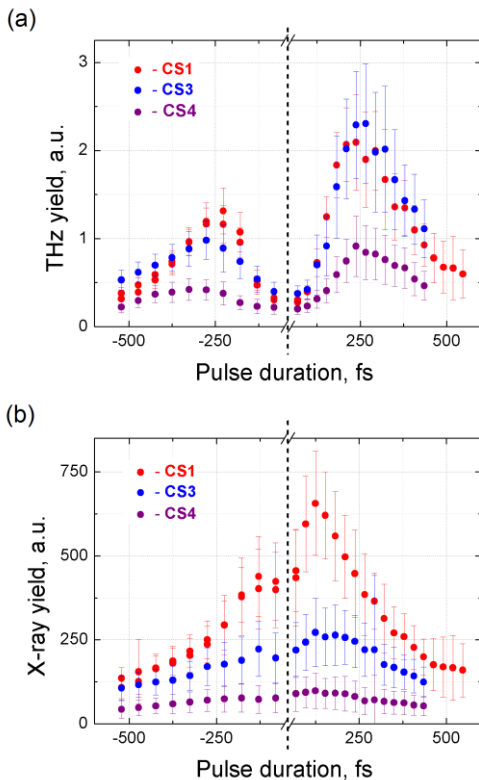


**Fig. 3.** X-Ray (a) and THz (b) yields from an Ar gas-clusters jet as a function of the temporal duration of the excitation laser pulses recorded at the cross-sections of CS1 (red dots), CS3 (blue dots), and CS4 (purple dots). The vertical dotted line in the center represents the pulse duration for a Fourier limited pulse.

Let us consider the experimental results. THz and X-Ray yields from Ar gas-clusters jet as a function of temporal duration of exciting laser pulse are presented on Fig. 3. Measurements have been performed for both positively (right side) and negatively (left side) chirped optical pulses. Pulse duration of around 55fs corresponds to Fourier-limited pulse and is indicated by related vertical line on Fig. 3. The symbols of dif-

ferent colors depict experimental data measured for three cases of position of laser beam focus relatively to the nozzle, and correspond to CS1, CS3 and CS4 cross-sections.

It can be seen from Fig. 3 that THz yield strongly decreases in the region of minimum pulse durations whereas X-Ray emission intensity demonstrates maximum values under these conditions. Maximal value X-ray signal monotonously decreases as the distance between excitation area and the nozzle throat increases from CS1 to CS4. In contrast with this behavior, THz signal demonstrate roughly equal values in the CS1 and CS3, but it decreases in the CS4 position. As it can be seen from Fig. 1,2 there are mainly small-size clusters fractions are contained in cross-section CS1, and predominantly large-size clusters are in cross-section CS4.

In conclusion, we carried out numerical simulations of the cluster formation process in a supersonic jet of Ar. We have shown that the distance from the nozzle output edge is an important parameter describing the properties of the gas-cluster target, which should be taken into account when developing the effective sources of THz and X-ray radiation based on cluster nanoplasma.

**References**

1. *Krainov V., and Smirnov M.* Cluster beams in the super-intense femtosecond laser pulse // Phys. Rep. 2002. V. 370, P. 237-331.

2. *Nagashima T., Hirayama H., Shibuya K., Hangyo M., Hashida M., Tokita S., and Sakabe S.* Terahertz pulse radiation from argon clusters irradiated with intense femtosecond laser pulses // Opt. Expess 2009 V. 17, P. 8907

3. *Alexeev I., Antonsen T.M., Kim K.Y., and Milchberg H.M.* Self-focusing of intense laser pulses in a clustered gas // Phys. Rev. Lett. 2003 V. 90, P. 103402

4. *Balakin A.V., Dzhidzhoev M.S., Gordienko V.M., Esaulkov M.N., Zhvaniya I.A., Ivanov K.A., Kotelnikov I.A., Kuzechkin N.A., Ozheredov I.A., Panchenko V.Y., Savel'ev A.B., Smirnov M.B., Solyankin P.M., Shkurinov A.P.* IEEE Trans. Terahertz Sci. Technol. 2017 V. 7, P. 70-79

# Terahertz generation from single and multiple filaments in air

O. Kosareva[1,2,3], N. Panov[1,2], D. Shipilo[1,2], V. Andreeva[1,4], T.-J. Wang[5], Y. Chen[6], W. Liu[3], A. Savel'ev[1], and A. Shkurinov[1]

[1]Lomonosov Moscow State University, 1/2 Leninskie gori, Moscow, Russia, kosareva@physics.msu.ru
[2]Lebedev Physical Institute of Russian Academy of Sciences, Moscow, Russia
[3]Institute of Modern Optics, Nankai University, Tianjin, China
[4]School of Mathematics, University of Minnesota, Minneapolis, Minnesota, USA
[5]Shanghai Institute of Optics and Fine Mechanics, Chinese Academy of Sciences, Shanghai, China
[6]Shanghai Jiao Tong University, Shanghai, China

Terahertz (THz) photonics is entering an era of strong electromagnetic fields in the THz frequency range [1]. Optical breakdown plasma takes a specific place among THz sources. With the appearance of compact commercial terawatt laser systems and the actualization of remote sensing tasks, two-color optical breakdown in air has turned into a powerful mechanism of broadband THz generation at the observation point [2]. There are several problems associated with THz remote sensing applications. First, the directional diagram of emitted THz radiation usually has a conical structure [3]. Nevertheless, as the filament length increases, the divergence angle decreases [4]. Second, the limitation of air-breakdown THz applications to remote-sensing tasks is due to low signal-to-noise ratio in the amplitude analysis of THz radiation reflected from the object under study. Therefore, one can use polarization analysis of useful signals whose effective application requires thorough control of the state of polarization of THz radiation. Third, further optimization of the THz yield from two-color filaments is required to approach the signal level obtained from optical rectification in crystals [1]. Control over the relative temporal (and spatial) properties of the optical pump fields, e.g. via the pulse chirp, offers an important means to control and optimize the optical-to-THz conversion process. With increasing pulse peak power and transition to multiple filamentation more overall THz energy is generated however the proper regularization of the high-peak-power beam is needed to provide for the maximum THz yield in the narrow angle.

In this paper we present a series of studies for the control and optimization of THz directionality, polarization and energy yield.

We observe linear-to-elliptical transformation of THz radiation through independent control of initially linear polarization directions of $\omega$ and $2\omega$ beams. Strongly elliptical THz radiation appears abruptly at the threshold angle of ~85° between the $\omega$ and $2\omega$ light fields. The physical reason for THz beam ellipticity was identified by us as the nonlinear response of the birefringent medium induced by an 800 nm pump. We found THz ellipticity and energy yield using a vectorial nonparaxial propagation equation (Fig. 1).

We have demonstrated and justified the mechanism which dictates the optimum chirp to maximize the THz yield from a two-color filament. We have experimentally measured the THz energy yield using 800-nm pulses in a single filament regime, being chirped from 35 fs up to 250 fs both positively and

negatively. We found that the positively chirped pulse proves to be a more advantageous choice since the $\omega$–$2\omega$ pulse overlap is larger by ~15 fs as compared with the transform-limited pulse (Fig. 2).
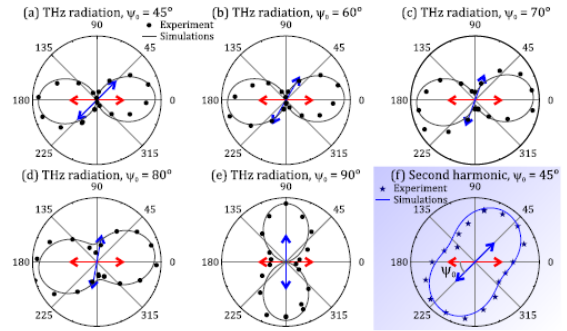


Fig. 1 (a)–(e) THz energy after transmission through THz analyzer, in dependence on its rotation angle, for different angles $\psi_0$, for different angles $\psi_0$ between polarization directions of the 800 nm ($\omega$) and 400 nm ($2\omega$) beams. (f) Second-harmonic energy after its transmission through polarization analyzer. Red (blue) arrow indicates the incident polarization of the $\omega$ ($2\omega$) beam.
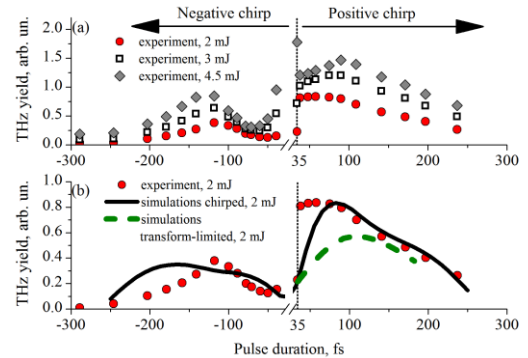


Fig. 2 (a) The experimentally measured dependence of the THz energy on the pump (800 nm) chirped pulse duration. The pump energy is fixed for each chirped pulse duration variation in the range from –300 fs (FWHM, negatively chirped) to +250 fs (FWHM, positively chirped). (b) The experimental vs. simulated dependence of the THz energy on the 800-nm 2-mJ chirped pulse duration. Green dashed curve shows simulated THz yield for the transform-limited pulse.

We have shown that a $2D$ array of multiple plasma filaments in atmospheric density gases leads to the efficient increase of terahertz radiation emitted in the forward direction. As the number of filaments in an $N \times N$ array is augmented, the THz energy increase per unit polar angle in the central cone exceeds the standard gain factor $N^2$ [4,5]. The two-dimensional multiple filament array can be produced from an actu-

al non-ideal elliptical beam using a phase plate to introduce a phase barrier and block the interaction between the neighboring filaments. Such regularized structure of plasma channels is used to control the directional diagram of THz radiation from a sub-terawatt-peak-power $800\ nm + 400\ nm$ femtosecond laser pulse.
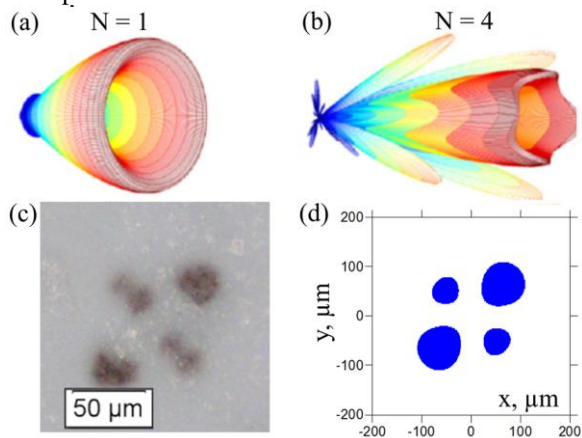


Fig. 3. (a, b) Full 3D angular THz intensity distribution from an array of $N$ multiple filaments with the length $L = 1$ cm. (c) Single-laser-shot burnt photo paper images after the geometrical focus of 1.1-mJ 35-fs 800 nm + 400 nm elliptical beam transported through a phase mask in air. The reproduction of the plasma channels in $3D$+time carrier resolved simulations is given in (d).

### References

1. *X.-C. Zhang, A. Shkurinov, and Y. Zhang.* Extreme terahertz science // Nat. Photonics 2017. V. 11, p. 16.

2. *T.-J. Wang, S. Yuan, Y. Chen, J.-F. Daigle, C. Marceau, F. Théberge, M. Châteauneuf, J. Dubois, and S. L. Chin.* Toward remote high energy terahertz generation // Appl. Phys. Lett. 2010. V. 97, p. 111108.

3. *V. Andreeva, O. Kosareva, N. Panov, D. Shipilo, P. Solyankin, M. Esaulkov, P. G. de Alaiza Martínez, A. Shkurinov, V. Makarov, L. Bergé, and S. L. Chin.* Ultrabroad terahertz spectrum generation from an air-based filament plasma // Phys. Rev. Lett. 116, 063902 (2016).

4. *N. Panov, V. Andreeva, O. Kosareva, A. Shkurinov, V. A. Makarov, L. Bergé and S. L. Chin.* Directionality of terahertz radiation emitted from an array of femtosecond filaments in gases // Laser Phys. Lett. 2014. V. 11, p. 125401.

5. *S. I. Mitryukovskiy, Y. Liu, B. Prade, A. Houard, and A. Mysyrowicz.* Coherent synthesis of terahertz radiation from femtosecond laser filaments in air // Appl. Phys. Lett. 2013. V. 102, p. 221107.

# Laser-plasma generation of tunable ultrashort pulses in terahertz and mid-infrared ranges

A. A. Silaev[1,2], V. A. Kostin[1,2], I. D. Laryushin[1,2], N. V. Vvedenskii[1,2]

[1]Institute of Applied Physics, Russian Academy of Sciences, Nizhny Novgorod, Russia, silaev@appl.sci-nnov.ru
[2]University of Nizhny Novgorod, Nizhny Novgorod, Russia

The generation of tunable ultrashort pulses in the terahertz (THz) and mid-infrared (mid-IR) ranges is an important problem of both fundamental interest and for many applications. In particular, such sources are required for the observation of ultrafast electronic and vibrational dynamics in a wide class of materials [1]. Such sources are also of interest because of the possibilities of spectroscopy and diagnostics of various media [2]. Apart from this, the use of intense ultrashort pulses in the mid-IR range with controlled phase for the generation of high harmonics makes it possible to reach the short-wave region of the soft X-ray range and to obtain ultrashort attosecond pulses [3].

In this paper we report on analytical and numerical investigation of generation of tunable ultrashort pulses in THz and mid-IR ranges based on the ionization-induced multiwave mixing of fields of intense two-color femtosecond pulses. If the ratio of the frequencies $\omega_{1,2}$ of quasi-monochromatic components of the two-color ionizing field is close to an irreducible rational fraction $\omega_2 : \omega_1 = a : b$, where $a + b$ is a not too large odd integer, the ionization-induced multiwave mixing in the produced plasma can result in the efficient excitation of the current of free electrons at a low (compared to the frequencies of the ionizing field) combination frequency responsible for generation of tunable ultrashort pulses in THz and mid-IR ranges [4, 5]. A strong dependence of the ionization rate on the field strength is responsible for a very short duration of generated pulses, which is determined by the ionization duration (characteristic time of increase in the plasma density). As a result, the generated pulses can be few-cycle or even subcycle, and the phase difference between the carrier and envelope in these pulses is determined by the phase shift between single-color components in the ionizing field.

As the most important and practically interesting example of ionization-induced generation of ultrashort pulses in the mid-IR range, we consider here the two-color ionizing pulses containing quasi-monochromatic components whose frequency ratio $\omega_2 : \omega_1$ is close to 2. Such two-color pulses usually consist of the pump field and an additional field, which is obtained using either frequency doubling crystals and frequency-selective elements creating detuning frequency [6] or an optical parametric amplifier generating radiation near half the frequency [7]. We assume that the time-dependent linearly polarized two-color ionizing field is given by

$$\mathbf{E}(t) = [F_1(t)\cos(\omega_1 t) + F_2(t)\cos(\omega_2 t + \varphi)]\mathbf{x}_0, \quad (1)$$

where $F_{1,2}(t)$ are the slow envelopes of single-color quasimonochromatic components, $\varphi$ is the phase shift, and $\mathbf{x}_0$ is the unit vector. We consider Gaussian envelopes $F_{1,2} = (8\pi I_{1,2}/c)^{1/2} \exp(-t^2/2\tau^2)$ with the maximum intensities $I_{1,2}$, where $\tau = \tau_p/(4\ln 2)^{1/2}$, $\tau_p$ is the intensity full width at half-maximum, and $c$ is the speed of light. Let $\omega_1$ be the lowest of two frequencies, $\omega_2 = 2\omega_1 + \Delta\omega$, and $|\Delta\omega| << \omega_1$. We also assume that the duration of the generated pulse is much smaller than the characteristic time of current relaxation in plasma and the period of plasma natural oscillations. As a result, the field (1) can be considered as given and all dissipative terms in equations for low-frequency (at frequencies much lower than $\omega_1$) current density $\mathbf{j}_{LF}$ can be neglected.

The performed *ab initio* simulations of the excitation of the electron current are based on the solution of the three-dimensional time-dependent Schrödinger equation (3D TDSE) [4, 5]. This equation allows describing all stages of the dynamics of the electron wavefunction $\psi(\mathbf{r}, t)$ of the hydrogen atom in a strong external field $\mathbf{E}(t)$ The initial condition corresponds to the ground ($1s$) state. The time derivative of the electron current density is expressed in terms of as

$$\frac{\partial \mathbf{j}}{\partial t} = \frac{e^2 N_m}{m}\left[\mathbf{E} + \left\langle \psi \mid \frac{e\mathbf{r}}{r^3} \mid \psi \right\rangle\right], \quad (3)$$

where $N_m$ is the density of neutral atoms before the ionization, $e$ and $m$ are electron charge and mass, respectively. The temporal profile of $\partial \mathbf{j}_{LF}/\partial t$ is obtained from $\partial \mathbf{j}/\partial t$ by means of the ideal low-pass filter (the cutoff frequency of the filter corresponds to the lowest frequency above $|\Delta\omega|$ at which the spectral density $\partial \mathbf{j}/\partial t$ reaches a local minimum).

Spectra and time profiles of $\partial \mathbf{j}_{LF}/\partial t$ calculated from the numerical solution of Eqs. (2) and (3) are shown in Figs. 1 and 2, respectively, for various values of the detuning frequency $\Delta f = \Delta\omega/2\pi$. As is seen in Fig. 1, the spectrum contains a pronounced bell-shaped peak near $\Delta f$. The width of the peak is much larger than the widths of the spectra of quasi-monochromatic components of the ionizing field and depends only slightly on $\Delta f$, whereas the height of the peak depends on both the magnitude and sign of $\Delta f$. Pulses generated at negative detuning are more intense than those generated at positive detuning.

This asymmetry with respect to the sign of detuning can be very large, and the spectral peak at positive detuning can be an order of magnitude lower than the peak at negative detuning. The peaks have
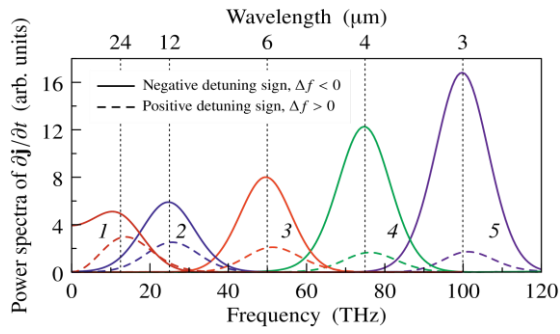
**Fig. 1**. Power spectra of $\partial \mathbf{j}/\partial t$ found from the numerical solution of the 3D TDSE (2) for the two-color ionizing field (1) at various (dashed lines) positive and (solid lines) negative detuning frequencies $\Delta f = \Delta\omega/2\pi = (1) \pm12.5$, (2) $\pm25$, (3) $\pm50$, (4) $\pm75$, and (5) $\pm100$ THz. The frequency $\omega_1$ corresponds to the wavelength 800 nm, components intensities $I_1 = 2\cdot10^{14}$ W/cm$^2$, $I_2 = I_1/10$, pulse duration $\tau_p = 100$ fs, and phase shift $\varphi = 0$.

smooth flanks, and the corresponding time dependences also have fairly smooth envelopes, as is seen in Fig. 2 plotted for two values of the phase shift. Changing $\varphi$ by $\pi/2$ results in a phase shift of $\pi/2$ in the generated pulse. The durations of pulses at different detuning values are approximately equal and are much smaller than the duration of the initial ionizing field, which corresponds to the generation of few-cycle or subcycle pulses (depending on the detuning frequency).

For the interpretation of the results of quantum-mechanical simulation, we use an analytical approach based on the equation for the plasma density $N(t)$ and the classical equation for the current density $\mathbf{j}(t)$ of free electrons in a cold collisionless plasma with a varying number of particles

$$\frac{\partial N}{\partial t} = (N_m - N)w(E), \qquad \frac{\partial \mathbf{j}}{\partial t} = \frac{e^2 N}{m}\mathbf{E} \qquad (4)$$

with the initial condition $N = 0$ (at $t \to -\infty$) [4, 5, 7]. Here, $w(E)$ is the probability of tunnel ionization per unit time, and it is assumed that the ponderomotive energy of the electron in this field is much higher than the ionization energy. The use of perturbation theory with respect to the corresponding weak field ($F_1$ or $F_2$) allows to obtain closed-form analytical expression for $\partial \mathbf{j}_{LF}/\partial t$ and explain the origin of the asymmetry and other characteristic features of the excitation of low-frequency current. Particularly, it is shown that the duration of the excited current is determined by the ionization duration $\tau_i$ (the characteristic time of plasma formation), which is much shorter than the duration of the ionizing field because of the steep dependence of the ionization rate on the field strength. At quite large detuning frequencies, $|\Delta f|\tau_i \geq 1$, a pulse is generated at the frequency $\Delta f$, and its phase is determined by $\varphi$. At smaller detunings $|\Delta f|\tau_i < 1$, a subcycle pulse is generated, and $\varphi$ affects both the phase and amplitude of the generated pulse. The central frequency of the generated pulse is about $1/\tau_i$, and this value specifies the lower limit of the possible frequency tuning range. In this case, a significant residual current density, i.e., a static component (zeroth harmonic) of $\partial \mathbf{j}_{LF}/\partial t$
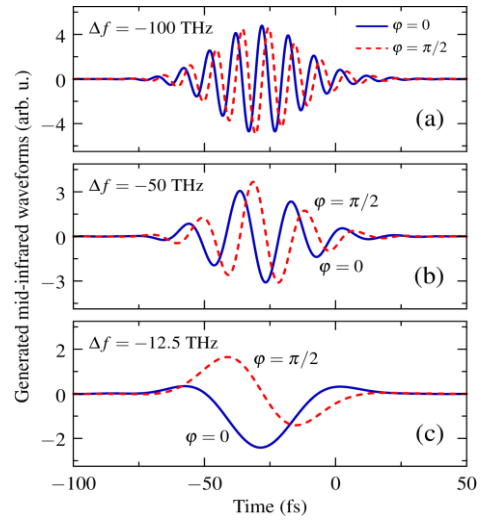


Waveforms of generated pulses of the low-frequency current $\mathbf{x}_0\cdot(-\partial \mathbf{j}_{LF}/\partial t)$ found from the numerical solution of 3D TDSE at the same parameters as in Fig. 1, but at two phase shifts $\varphi = 0$ and $\pi/2$ and three negative detuning frequencies $\Delta f =$ (a) $-100$, (b) $-50$, and (c) $-12.5$ THz.

depending on $\varphi$ can be excited. The presence of this component can be seen in the results of numerical calculations presented in Fig. 1 (solid line 1) and in Fig. 2c. This residual current density is responsible for the generation of THz radiation [4, 6, 7], and Eqs. (10)–(12) determine the high-frequency part of the spectrum of this THz radiation, which extends to frequencies about $1/\tau_i$.

### References

1. *Krausz, F, Stockman M. I.* Attosecond metrology: from electron capture to future signal processing // Nature Photonics. 2014. V.8. P.205.

2. *Cossel, K.C. et al.* Gas-phase broadband spectroscopy using active sources: progress, status, and applications // J. Opt. Soc. Am. B. 2017. V.34. P. 104-129.

3. *Zenghu, C., Corkum, P.B., Leone, S.R.* Attosecond optics and technology: progress to date and future prospects // J. Opt. Soc. Am. B. 2016. V. 33. P. 1081-1097.

4. *Kostin, V. A., Laryushin, I. D., Silaev, A. A., Vvedenskii, N. V.* Ionization-induced multiwave mixing: terahertz generation with two-color laser pulses of various frequency ratios // Phys. Rev. Lett. 2016. V. 117, No. 3. P. 035003.

5. *Silaev, A. A., Kostin, V. A., Laryushin, I. D., Vvedenskii, N. V.* Ionization mechanism of the generation of tunable ultrashort pulses in the mid-infrared range // JETP Letters. 2018. V. 107, No. 3. P.151-156.

6. *Theberge, F. et al.* Generation of tunable and broadband far-infrared laser pulses during two-color filamentation // Phys. Rev. A 2010. V. 81, No.3. P. 033821.

7. *Vvedenskii, N. V., et al.* Two-color laser-plasma generation of terahertz radiation using a frequency-tunable half harmonic of a femtosecond pulse // Phys. Rev. Lett. 2014. 112, No.5. P. 055004.

# Quantum-mechanical simulations of low-frequency current excitation during ionization of many-electron atoms by intense laser pulses

A. A. Silaev[1,2], A. A. Romanov[1,2], N. V. Vvedenskii[1,2]

[1]Institute of Applied Physics, Russian Academy of Sciences, Nizhny Novgorod, Russia, silaev@appl.sci-nnov.ru
[2]University of Nizhny Novgorod, Nizhny Novgorod, Russia

Great progress in computer technology opens up the possibility for *ab initio* numerical study of various ionization-stimulated phenomena arising from the interaction of atoms and molecules with intense laser pulses. These include the excitation of a low-frequency current (with frequencies much lower than the optical one) in a plasma created by a laser pulse. The interest to this phenomenon is associated with the possibility of its use for the generation of coherent and broadband radiation in the terahertz and mid-infrared ranges and possibility of tuning the spectrum of generated radiation [1-11]. The low-frequency current density is excited effitiently under the asymmetry of ionizing pulses [1-10] or ionized molecules [11]. Among the various methods of generating low-frequency current, the most well-known one is based on the use of two-color ionizing laser pulses [1-8]. The low-frequency current is generated at some combination frequency of two-component laser pulse for a whole set of ratios between component frequencies [5-8].

The efficient excitation of high-power terahertz and mid-infrared radiation is associated with the need to use of high-intensity laser pulses, which produce fast ionization of a gas medium and accelerate the freed electrons up to high energies [2, 5, 7, 9, 10]. The action of such intense pulses on atoms or molecules (most of which are multielectron quantum systems) may be accompanied by a dynamic response of various electron orbitals, which was not taken into account in previous similar studies. This response can significantly influence the magnitude and waveform of the low-frequency current.

This paper is devoted to direct numerical simulations of ionization-induced excitation of low-frequency electron current density in multielectron atoms of noble gases. Our approach is based on the time-dependent density functional theory (TDDFT), which has recently been increasingly used in atomic, molecular, and strong-field physics [12]. The basis of this approach is the system of time-dependent Kohn-Sham (TDKS) equations, which takes into account the interaction of electrons with the atomic nucleus and the external electric field of the laser pulse, as well as the electron-electron interaction. In the atomic system of units (in which $|e| = \hbar = m_{\mathrm{e}} = 1$, where $\hbar$ is the reduced Planck constant, $e = -|e|$ is the charge and $m_{\mathrm{e}}$ is the mass of the electron) these equations are:

$$i\frac{\partial}{\partial t}\psi_n(\mathbf{r},t) = \hat{H}\psi_n(\mathbf{r},t), \quad n = 1,...,N,$$
$$\hat{H} = -\frac{1}{2}\nabla^2 - \frac{Z}{r} + \mathbf{r}\mathbf{E}(t) + V_{\mathrm{ee}}[\rho(\mathbf{r},t)].$$

(1)

Here, $\psi_n$ is the wave function of the *n*-th TDKS orbital, $Z$ is the nuclear charge, $N$ is the number of electrons, $\rho(\mathbf{r},t)$ is the electron density, and $V_{ee}[\rho(\mathbf{r},t)]$ is the potential of electron-electron interaction. The initial Kohn-Sham orbitals correspond to electronic configuration of the unperturbed atom. For considered noble-gas atoms, the atomic orbitals are initially occupied by the pairs of electrons with opposite spin. Due to the weak influence of the magnetic field, the zero spin polarization is conserved during interaction with the laser pulse. The electron density is related to TDKS orbitals by equality

$$\rho(\mathbf{r},t) = \sum_{n=1}^{N}|\psi_n(\mathbf{r},t)|^2.$$

(2)

The electron-electron interaction potential consists of the Hartree potential $V_{\mathrm{H}}[\rho(\mathbf{r},t)] = \int d^3 r' \rho(\mathbf{r}')/|\mathbf{r} - \mathbf{r}'|$, describing the electron repulsion in the framework of the mean field and the exchange-correlation potential for which the spin unpolarized form of LB94 approximation [12] is used.

Using TDKS orbitals and Ehrenfest's theorem we find the time-dependent dipole acceleration of the atomic system:

$$\mathbf{a}(t) = -N\mathbf{E}(t) - \int d^3 r \frac{Z\mathbf{r}}{r^3}\rho(\mathbf{r},t).$$

(3)

The obtained dipole acceleration is proportional to the time derivative of macroscopic electron current density,

$$\frac{\partial \mathbf{j}(t)}{\partial t} = -N_m \mathbf{a}(t)$$

(4)

where $N_m$ is the gas density before the start of the ionization process.

Based on the developed computer code for solving the 3D TDKS, we calculate the current density $\mathbf{j}(t)$ excited by two-color laser pulses containing the main and second harmonics in a wide range of intensities and durations of the laser-pulse components. The found electron current density $\mathbf{j}(t)$ has a very wide frequency spectrum. Besides the low-frequency part, it contains a large component at the frequency of the ionizing laser pulse and its low-order harmonics. Also it contains a wide plateau ending with a pronounced cutoff in the frequency region, which corresponds to the extreme UV or soft-x-ray radiation [13]. We extract the low-frequency component from the full current density and study differences in its excitation for different noble-gas atoms. The results obtained on the basis of TDDFT are compared with the calculations of the single-active electron (SAE) approximation. In the framework of SAE approximation all orbitals except highest-occupied orbital are "frozen", and the field of

the parent ion is described by a static potential well. It is shown that taking into account the dynamics of all the electrons can lead to a change in the optimal relative phase between the components of the two-color laser pulse and in the corresponding maximum low-frequency current. Based on the results obtained, the range of applicability of SAE approximation is determined.

## References

1. *Clough B., Dai J., Zhang, X.-C.* Laser air photonics: beyond the terahertz gap // Mater. Today. 2012. V. 15, No.1-2. P. 50-58.

2. *Vvedenskii, N. V., et al*. Two-color laser-plasma generation of terahertz radiation using a frequency-tunable half harmonic of a femtosecond pulse // Phys. Rev. Lett. 2014. 112, No.5. P. 055004.

3. *Balčiūnas, T. D. et al.* CEP-stable tunable THz-emission originating from laser-waveform-controlled sub-cycle plasma-electron bursts // Opt. Express. 2015. V. 23, No. 12. P. 15278-15289.

4. *Theberge, F. et al.* Generation of tunable and broadband far-infrared laser pulses during two-color filamentation // Phys. Rev. A 2010. V. 81, No.3. P. 033821.

5. *Kostin, V. A., Laryushin, I. D., Silaev, A. A., Vvedenskii, N. V.* Ionization-induced multiwave mixing: terahertz generation with two-color laser pulses of various frequency ratios // Phys. Rev. Lett. 2016. V. 117, No. 3. P. 035003.

6. *Zhang, L.-L. et al.* Observation of terahertz radiation via the two-color laser scheme with uncommon frequency ratios // Phys. Rev. Lett. 2017. V.119, No. 23. P. 235001.

7. *Silaev, A. A., Kostin, V. A., Laryushin, I. D., Vvedenskii, N. V.* Ionization mechanism of the generation of tunable ultrashort pulses in the mid-infrared range // JETP Letters. 2018. V. 107, No. 3. P.151-156.

8. *Kostin V.A., Vvedenskii N.V.* Generation of Few- and Subcycle Radiation in Midinfrared-to-Deep-Ultraviolet Range During Plasma Production by Multicolor Femtosecond Pulses // Phys. Rev. Lett. V. 120, No. 6. P. 065002.

9. *Silaev, A.A., Vvedenskii, N. V.* Residual-current excitation in plasmas produced by few-cycle laser pulses // Phys. Rev. Lett. 2009. V. 102, No. 11. P. 115005.

10. *Silaev, A. A., Vvedenskii N. V.* Analytical description of generation of the residual current density in the plasma produced by a few-cycle laser pulse // Phys. Plasmas. 2015. V. 22, No. 5. P. 053103.

11. *Alexandrov, L. N., Emelin, M. Yu., Ryabikin M. Yu.* Unidirectional current excitation in tunneling ionization of asymmetric molecules // Phys. Rev. A. 2013. V. 87, No. 1. P. 013414.

12. *Ullrich, C. A.* Time-dependent density-functional theory: concepts and applications // Oxford University Press. 2012.

13. *Krausz, F., Ivanov, M.* Attosecond physics // Rev. Mod. Phys. 2009. V. 81, No. 1. P. 163.